Analysis and Modeling of Air-Flow Specific Lung Sounds for Non-Invasive Detection of Airway Status

by

January Elizabeth Gnitecki

A Thesis submitted to the Faculty of Graduate Studies of

The University of Manitoba

in partial fulfilment of the requirements of the degree of

DOCTOR OF PHILOSOPHY

Department of Electrical and Computer Engineering

University of Manitoba

Winnipeg

THE UNIVERSITY OF MANITOBA

FACULTY OF GRADUATE STUDIES

*****

COPYRIGHT PERMISSION

Analysis and Modeling of Air-Flow Specific Lung Sounds for

Non-Invasive Detection of Airway Status

BY

January Elizabeth Gnitecki

A Thesis/Practicum submitted to the Faculty of Graduate Studies of The University of

Manitoba in partial fulfillment of the requirement of the degree

DOCTOR OF PHILOSOPHY

ACKNOWLEDGEMENTS

I have confined my acknowledgements to those who have played the most major roles in my life during graduate school.

To my advisor, Prof. Zahra Moussavi, and my co-advisor, Prof. Hans Pasterkamp: Thank you for all of your guidance, patience, advice, and time. I learned a great deal from each of you and I feel fortunate to have worked with both of you.

Many thanks to the following providers of funding:

Children's Hospital Foundation of Manitoba, Inc.; Manitoba Institute of Child Health and the Biology of Breathing Group; Canadian Asthma Foundation; University of Manitoba Graduate Fellowship; University of Manitoba Faculties of Engineering and Graduate Studies; Elizabeth Anne Hogan Memorial Scholarship; Edward R. Toporeck Graduate Fellowship in Engineering; Natural Sciences and Engineering Research Council of Canada; University of Manitoba Students' Union, Graduate Students' Association, and Alumni Association.

And finally, thank you to my parents, my BFF and my SP for being genuine and kind.

ABSTRACT

Analysis of recorded lung sounds provides objective and non-invasive tools for the diagnosis of respiratory health status. Relating lung sound signals to their underlying physiology via a model would provide further information regarding the respiratory system, and possibly alleviate the necessity for reference recordings. The thesis work contributes to the current state of lung sound research through extensive experimental findings pertaining to characteristics of lung sounds in health and disease, along with a novel approach to modeling lung sounds. Though several research studies contributed to the thesis work, including adaptive filtering of heart sounds from lung sounds and waveform fractal dimension analysis, the thesis focuses mainly on two research paths. Geometrical and dynamical state space parameters were studied to provide information pertinent to inductive modeling, with focus on the effects of air flow and lung sound sensor location in healthy subjects, and induced bronchial constriction in patients. This work presents a novel approach, as the exploration of state space analysis in respiratory acoustic research is a recent development. A deductive model was achieved using equations describing acoustical fluid flow and motion of a mass-spring chain, representing generation and transmission of lung sounds respectively. The Pareto distribution was incorporated in order to allow modification of elements in the transmission model to represent many tissue-air compositions in the mass-spring analogy of the parenchyma, rather than a constant tissue-air ratio as in past work. Also unlike other work in lung sound modeling, adaptive tuning was achieved via a genetic algorithm. Model parameters were optimized so as to match, based on mean square error (MSE), selected frequency domain features of the model output with those of lung sounds recorded over the

right lower lung lobes of healthy children and children with asthma and/or airway hyper-responsiveness. The optimization resulted in MSE values that were less than five percent, and a significant difference in one model parameter was found between the healthy and asthmatic children. The signal processing analyses as well as the modeling provided insight into changes in lung sounds with respiratory condition, and the findings are promising for diagnostic application of lung sounds.

TABLE OF CONTENTS

LIST OF TABLES

LIST OF FIGURES

LIST OF COPYRIGHTED MATERIAL FOR WHICH PERMISSION WAS OBTAINED

The following list provides the title of each copyrighted item, its source, and the page on which it appears in the thesis.

LIST OF ABBREVIATIONS

AHR	Airway hyper-responsiveness
ANC	Adaptive noise cancellation
BD	Bronchodilator
BDR	Bronchodilator response
ERV	Expiratory reserve volume
fBm	Fractional Brownian motion
FD	Fractal dimension
FEF_{50}	Forced expiratory flow at 50% of FVC
FEV_1	Forced expiratory volume in one second
FRC	Functional residual capacity
FVC	Forced vital capacity
IC	Inspiratory capacity
ILSA	International Lung Sounds Association
IRV	Inspiratory reserve volume
KFD	Katz fractal dimension
KSFD	Katz-Sevcik fractal dimension
MCh	Methacholine challenge
PEF	Peak expiratory flow
PFT	Pulmonary function testing
PSD	Power spectral density
RLL	Right lower lobe
RLS	Recursive least squares
RV	Residual volume
TLC	Total lung capacity
TV	Tidal volume
VC	Vital capacity
VFD	Variance fractal dimension

Note: Italicized abbreviations denote physiological measurements.

CHAPTER 1

Introduction

"Improvements on the classical acoustical stethoscope, such as compact electronic stethoscopes using transistors, when used in combination with that excellent instrument the ear, hold much promise for the future." [McKu58]

1.1 Respiratory Sounds: History and Applications

1.1.1 Brief History and General Information

Respiratory sounds serve as useful tools in the assessment of respiratory disease [McKu58]. The numerous efforts put forth into the evolution of the stethoscope over nearly 200 years are testament to this (Fig. 1.1). The invention of the stethoscope, a term that literally means "chest-seeing device," was borne out of necessity to listen to a patient's lung sounds by a physician, Dr. René T. H. Laënnec [Gedd05], [McKu58] (depicted in Fig. 1.1). Though no longer monaural, as it was originally designed [Gedd05], the common (analog) stethoscope has other limitations, such as bandwidth, in some cases attenuating sounds above frequencies as low as 112 Hz [PaKW97]. Electronic stethoscopes have the capability to measure a wider range of frequencies, typically up to 500 Hz [Melb01]. However, the frequency content of lung sounds can extend to around 1000 Hz [PaKW97], depending on air flow during breathing, sensor location, and respiratory condition (which will be elaborated on in subsequent chapters of the thesis). In addition, stethoscopes provide mainly subjective, point-of-care assessment, without reference to air flow of breaths other than in a general sense, i.e. tidal or deep (unless interfacing an electronic stethoscope with external media, such as a pneumotachograph).

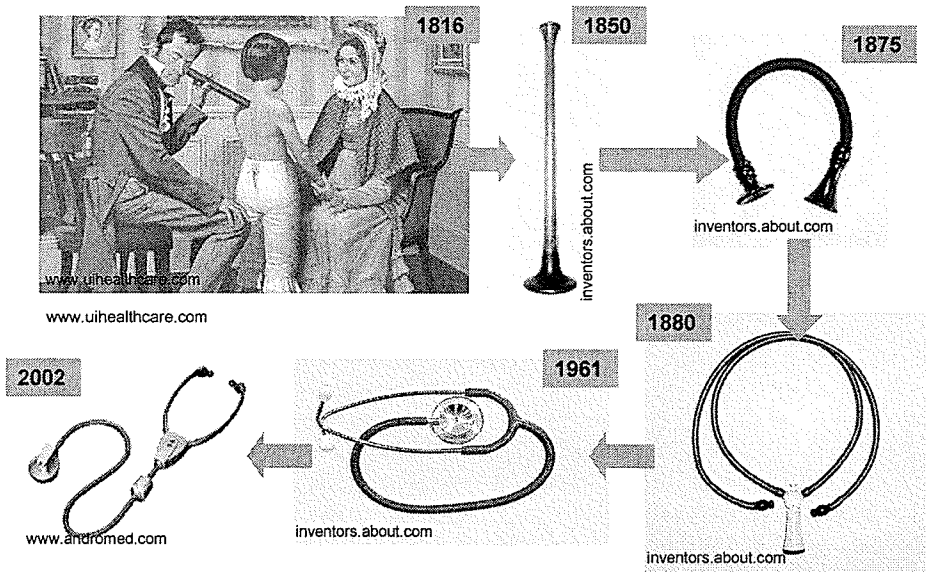

Fig. 1.1: Pictorial history of the stethoscope.

It is believed that the first objective method for evaluating sounds emerging from the chest involved time-frequency analysis, via spectrogram, and it was presented by Dr. Victor McKusick in 1958 [McKu58]. It was not until the 1970's that research into technologically advancing the assessment of lung sounds (using computers) started gaining significant popularity, and the International Lung Sounds Association (ILSA) was formed in 1976 as a result [Melb01]. Since that time, the introduction of increasingly sensitive, sophisticated, and objective methods for recording and analyzing both lung and tracheal sounds via computer has created several research pathways into various aspects of these sounds and their relation to respiratory disease. For the most part, computerized respiratory sound analysis is confined to a respiratory acoustics laboratory setting [EaCh00b].

1.1.2 Respiratory Sounds and Pulmonary Function

Recorded respiratory sounds have been studied as potential replacements for air flow measurement [QKDK02], [STPD04], [YaMo06], focusing mainly on tracheal

sounds. Both tracheal and lung sounds have shown promise as tools for augmenting standard methods of pulmonary function testing (PFT) in children [BDMM92], [MaSS94], [NCSB91], [PBKM97], [PCOH97], [SAWT93], [WBPS95]. Traditional PFT, e.g., spirometry and whole-body plethysmography (described further in Chapter 2), require forced respiratory maneuvers and/or a high degree of subject cooperation, which may pose insurmountable difficulty for very young or ill patients. The forced oscillation method of PFT is relatively simple, and it has been found promising as a method of deciphering normal airways from asthmatic ones [QKOM01], but it has proven useless in children during bronchial provocation [WBPS95]. For these reasons, it is desirable to reliably incorporate objective auscultation in clinical PFT, which is noninvasive and generally does not require coordinated, complicated maneuvers.

In past studies, several aspects of respiratory sounds have been examined in conjunction with pediatric lung function. These include adventitious sounds such as cough in children with asthma [LLZW03], [RiRP99], [SGPU00]. However, cough has been found to be of low diagnostic value to assess airway obstruction or asthma when used on its own [RiRP99], [SGPU00].

Wheeze is another adventitious sound, somewhat resembling that of a harmonica when many notes are played at once. Some studies have found wheeze to be a positive sign of airway obstruction when measured over the lung [BDMM92], [SGPU00] and/or trachea [NCSB91], [SGPU00]. However, others have shown wheeze to be an insensitive marker for bronchial narrowing in children [MaSS94], [PBKM97], [PCOH97], [SAWT93], [SGLG96].

Unlike cough and wheeze, decrease in intensity of lung sounds emerging only from movement of air in airways has been found to consistently accompany bronchial constriction via bronchial provocation testing (described in Chapter 2) [BHCP04], [GnMP04], [PBKM97], [PCOH97]. To prove that such a change in intensity has occurred, reference lung sounds must also be acquired either before bronchial provocation (i.e., at baseline) or after a return to baseline from the state that bronchial provocation had induced. One alternative is to develop a theoretical model, with parameters specific to respiratory state; this is addressed in the thesis.

1.2 Thesis Objectives

The thesis work was geared towards a few main objectives. It was focused on inspiratory lung sounds that are free from adventitious sounds. Both signal processing of lung sounds (inductive analysis), and modeling the generation and transmission of these sounds (deductive analysis), were employed to develop noninvasive measurement techniques of airway status in asthma or airway hyper-responsiveness using objective auscultation. The first step was to assess several aspects of lung sounds using signal processing, including lung sound and air flow relationships; variability; changes with respiratory condition, including bronchial dilation and constriction; fractality; and heart sounds, with an adaptive filter developed for their cancellation from lung sounds. It is important to account for heart sounds because they contaminate lung sounds in terms of both timing and frequency range. The signal analysis work that has been published elsewhere will not be presented at length in the thesis; see Appendix A for the publication list. Appendix B presents studies of variability and changes in lung sound intensity in healthy subjects and patients undergoing bronchial provocation testing (respectively).

The above-noted characteristics of lung sounds provide information on the signal features as they relate to identified conditions such as flow or bronchial constriction. Knowing more about the factors that contribute to producing lung sound signals would further enhance the usefulness of objective lung sounds analysis for clinical diagnostic or monitoring purposes. State space analysis was applied to lung sound signals to elucidate the geometrical and dynamical parameters of the dynamical system that governs the processes producing the signals under investigation, such as the number of differential equations required to represent the system. This type of analysis has been applied to lung sounds from healthy subjects and patients. Theoretically state space parameters would differ between health and disease, which is useful in terms of diagnostic application and the desire to use only one lung sound recording for this purpose.

A deductive lung sound model could also potentially alleviate the need for reference lung sound recordings, and enhance what is known about lung sound generation and transmission. Equations describing acoustical fluid flow and motion of a mass-spring chain, representing generation and transmission of lung sounds respectively, provided grounds upon which to investigate the potential of such a model. Combining theory of sound generation by vortical flow in airways with transmission of this sound through the thorax is a novel approach to modeling lung sounds.

1.3 Outline of Chapters

The first three chapters present background information pertaining to lung function, structure, and sounds. Chapter 2 contains detail on the former two topics, and also a section outlining definitions and methods of diagnosing asthma and airway hyper-responsiveness. Chapter 3 incorporates experimental findings pertaining to the relations

of lung sound to air flow and frequency, and also covers non-respiratory sounds that may interfere with the analysis of lung sounds such as heart sounds. The fourth chapter is devoted to features of lung sounds pertaining to fractal and chaos analyses, and presents background information on these methods. The fifth and sixth chapters present details of the design and verification of the lung sound generation and transmission model that was developed in the thesis work. Conclusions and recommendations are drawn in Chapter 7, the final chapter. As mentioned above, Appendix A contains a list of publications and Appendix B outlines work in variability and changes in lung sound features with airway status. Appendix C provides copyright permission forms for figures used in the thesis and Appendix D contains algorithms.

Note that several studies are presented throughout the following chapters, and selected pertinent studies have been placed in an appendix (for the sake of the flow of the thesis). Ethics approval for each study was obtained from the University of Manitoba Human Research Ethics Board. The author of this thesis was an active member of the teams involved in the data acquisition. The roles of the author in each study included setting up hardware and preparing software for data acquisitions; placing sensors on subjects; explaining consent forms to subjects (and their guardians as necessary); guiding subjects through each protocol; ensuring data storage; and analyzing data.

CHAPTER 2

Lung Structure and Function

"The simplest and still most widely invoked anatomically based model of pulmonary mechanics is that consisting of a single homogeneously ventilated alveolar compartment served by a single conduit."
[BaLu05]

2.1 Introduction

The lungs are complex organs without which the body could not survive. One could live having lost limbs or eyes, for instance, but at least one lung is absolutely essential. This chapter provides detail with regard to lung structure and function, and measuring lung function in both health and disease, with focus on asthma and airway hyper-responsiveness (AHR).

2.2 Overview of Basic Lung Structure

During embryonic development, the human lung begins as a single airway comprised of endodermal tissue that bulges out from the primitive foregut [Gilb89], and branches dichotomously into surrounding mesodermal tissue, initiating the formation of the right and left lung lobes [Weib84]. From these two branches, several new airways form continuously throughout gestation, with the branching scheme roughly resembling that of an oak tree. Airway dimensions decrease in each successive generation of branches. By birth, there are 24 generations of airways, separated into two functional zones, seven categories (i.e., trachea, bronchi, bronchioles, etc., Fig. 2.1), two left lung lobes, and three lobes on the right [Weib84]. Figure 2.1 shows a rough outline of the lung airways and zones [Weib63]; Fig. 2.2 presents a cast of the airways of an adult lung

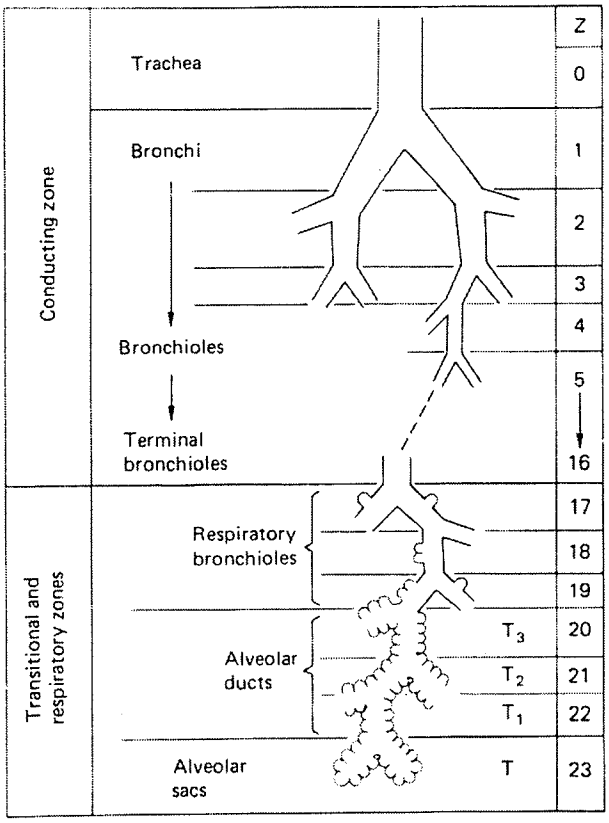

Fig. 2.1: Human lung branching. Beyond generation $z = 2$, branching within one lobe is shown. Ridges along airways in zones beyond $z = 16$ develop into alveoli postnatally [Weib63]. (*Reprinted with kind permission of Springer Science and Business Media; see Appendix C.*)

[Weib84]; and Fig. 2.3 is an anatomical transverse diagram of the thoracic cavity [Gray74].

The airways in the conducting zone (Fig. 2.1) are comprised of smooth muscle tissue with rings of cartilage spaced along the airways of the first four generations, and an inner wall lining of epithelium consisting of ciliated cells and cells that secrete mucus and surfactant [Weib84]. The epithelium is corrugated along the length of each airway [SeWP00], [WHDK97]. In human subjects with healthy airways, it has been shown that the inner airway walls are smooth [BPPM05]. Past work using mathematical modeling of mucosal folding in airways has suggested that healthy airways actually contain many longitudinal corrugations that are closely spaced, and thus on the whole are less

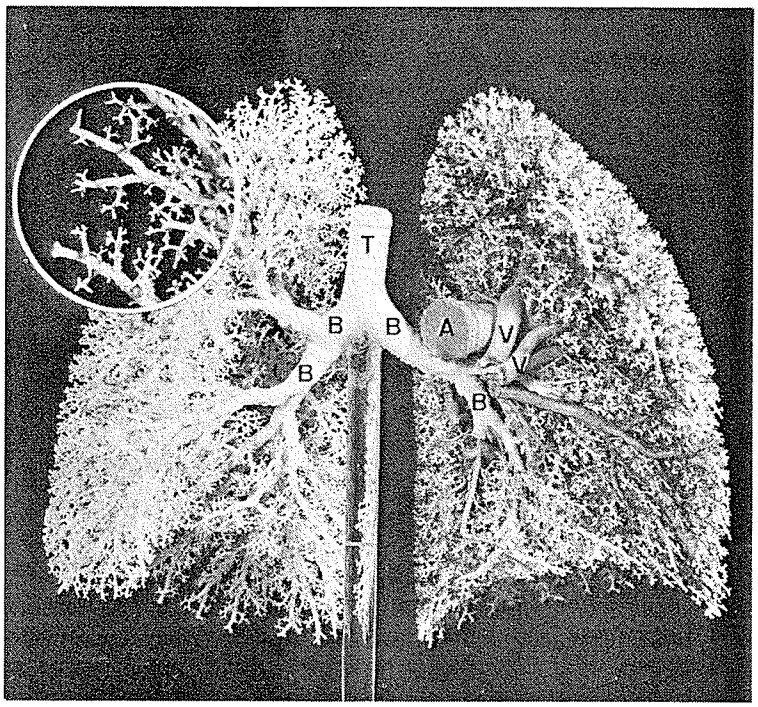

Fig. 2.2: Resin cast of adult human lung, with trachea (T), bronchi (B), artery (A), and veins (V) labeled. Inset shows a close-up of peripheral airway branching [Weib84]. (*Reprinted by permission of the publisher from THE PATHWAY FOR OXYGEN: STRUCTURE AND FUNCTION IN THE MAMMALIAN RESPIRATORY SYSTEM by Ewald R. Weibel, p. 273, Cambridge, Mass.: Harvard University Press, Copyright © 1984 by the President and Fellows of Harvard College; see Appendix C.*)

prominent than those of the airways of fatal and non-fatal asthmatic patients [CPKH00], [SeWP00]. When there is a contraction force such as that during bronchial constriction in an asthma attack, the corrugations may "bulge into" the airway [SeWP00]. The presence of corrugations adds complexity to understanding lung function and the dynamical properties of flow in lung airways (especially asthmatic airways).

The transitional and respiratory zones of the lungs (Fig. 2.1) contain smaller airways with walls that are comprised of less smooth muscle tissue than those of the conducting zone, along with alveoli, which are honeycomb-like air pockets [Weib84]. The alveoli and alveolar ducts are densely packed within the lung lobes (Fig. 2.1). There are approximately 170 alveoli within each cubic millimeter of lung parenchyma

[ONJK04], which also consists of collagen, elastin, surfactant, and the interstitium (mainly connective tissue fibers) [Weib84], as well as capillaries (discussed in Section 2.3.1), larger veins and arteries, and blood [WoWh86]. In fact, nearly half the mass of a lung is made up of blood circulating in vessels, which has an average composition that is similar to that of parenchyma in health [WoWh86]. In disease, water content varies in the parenchyma [WoWh86].

In vivo, the lung airways and parenchyma are enveloped in a membrane – the pulmonary pleura [Gray74] (Fig. 2.3, *Pleura Pulmonalis*). The internal surface of the thoracic cavity is also lined with a membrane, called the parietal pleura [Gray74] (Fig. 2.3, *Pleura Costolis*). Between the pulmonary and parietal pleura there are a few

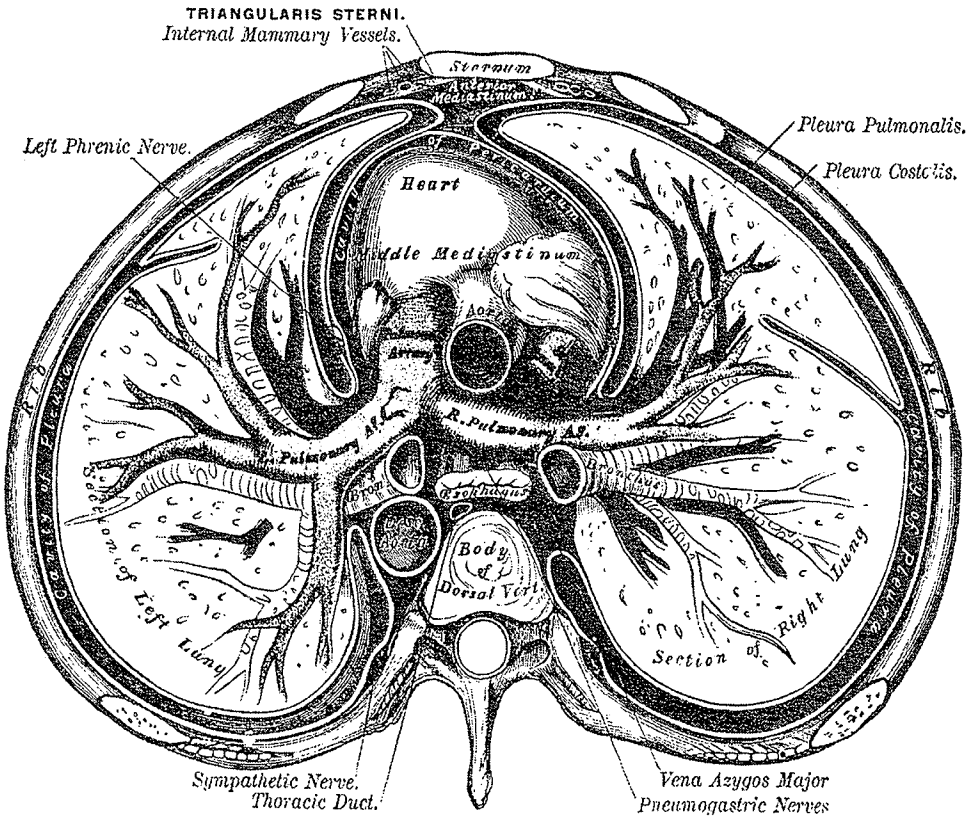

Fig. 2.3: Transverse section of the human thorax [Gray74]. (*Reprinted with kind permission from the Perseus Books Group, Cambridge, MA; see Appendix C.*)

micrometers of space, known as the pleural cavity, which is filled with a fluid to accommodate the movement of the lung and thoracic cavity during breathing [Fung90].

2.3 Lung Mechanics

2.3.1 Basic Lung Mechanics

The lungs serve to facilitate the human body's need to consume oxygen (O_2) and expel carbon dioxide (CO_2) [Weib84]. Tiny veins and arteries approximately 8 μm in diameter [Weib91], known as capillaries, line the alveoli in a web-like manner and the thin tissue barrier between these sacs and capillaries allows for exchange (via diffusion) of O_2 and CO_2, which begins shortly after birth [Weib84]. In a study of excised human lungs [WeGo62], inflated to three-fourths of total lung volume, of five subjects aged between eight and 74 years, the average number of alveoli was found to be $296 \times 10^6 \pm 3.9\%$ with an average number of capillaries of $277 \times 10^9 \pm 8\%$. Together the alveoli and capillaries form a surface area for gas exchange that measures approximately 130 m^2 [Weib91].

The neurological control of breathing involves negative feedback: an increase in the level of CO_2 in the blood will cause ventilation to increase, which will result in a decrease in CO_2, allowing ventilation to also decrease, bringing on an increase in CO_2 once again, and so on the cycle goes [GlMa88]. Mechanically, the difference between the pressure at the mouth – atmospheric pressure – and pressure in the alveoli is basically what governs the movement of air in lung airways [Fung90]. The right and left diaphragms, which together form a large dome-shaped muscle beneath the lungs and ribcage spanning the thoracic cavity, move downward during inspiration in sync with an

outward movement of the chest, and during expiration the diaphragms relax upward [West74]. The volume of air moved into and out of the lungs at rest is called the tidal volume (*TV*), and it is approximately 10% of the total lung capacity (*TLC*) [West74]. Figure 2.4 shows a rough breakdown of these and other lung volumes.

2.3.2 Heterogeneity in Breathing and Bronchial Constriction

In general, the dimensions of airways through which air flows are not necessarily consistent between breaths [SASL98], [SBHP94]. Furthermore, during breathing at rest, fundamental respiratory variables including *TV* and respiratory frequency, as well as levels of O_2 and CO_2 in alveoli, continuously vary around mean values [DPAD66]. In asthmatic subjects, it has been found that there may be considerable variability in the pattern in which asthmatic airways constrict [LuGi97]. These phenomena may be tied to

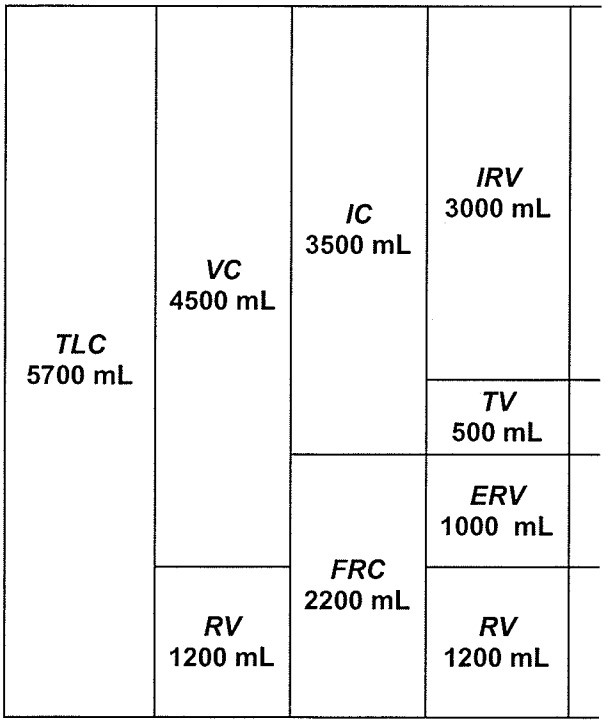

Fig. 2.4: Lung volumes, approximate for a healthy adult male (values vary with individual size and gender) [West74]. Values shown: Total lung capacity (*TLC*); inspiratory reserve volume (*IRV*); tidal volume (*TV*); expiratory reserve volume (*ERV*); residual volume (*RV*); inspiratory capacity (*IC*); functional residual capacity (*FRC*); and vital capacity (*VC*).

the notion that the cost of, or work involved in, operation of physiological systems tends towards a minimum [Murr26]. Since the work required for air to flow through constricted airways is greater than when airways are not constricted [Conr77], it is conceivable that there is adaptability in the lung in terms of airway recruitment which would contribute to inhomogeneity in breathing and airway constriction. Adaptability is the ability of a biological system to cope with unexpected disturbances of its environment [Conr77].

2.4 Measuring Lung Function

2.4.1 Overview of Lung Function Measurements

There are numerous methods that may be used to measure lung function. In fact, the most powerful tool in asthma diagnosis is *spirometry* [Mack99], described below, and as will be discussed in Section 2.5, the primary definition of asthma is in terms of disorder of function (i.e., resistance to air flow in airways) [Scad83]. Thus, it is prudent to provide an overview of common pulmonary function testing (PFT) methods and measurements, as well as implications.

Spirometry is the most widely performed test of respiratory mechanics [Prid99]. It involves a maximum-effort forced expiratory maneuver, which requires an inspiration of a volume of air to reach *TLC* (i.e. full inflation of the lungs per Fig. 2.4), a short pause, and a forceful expiration of this lung volume that should be continued until flow ceases (leaving only the *RV* in the lungs per Fig. 2.4). Subjects performing spirometry wear nose clips and exhale through a mouthpiece into a spirometer, which is a device that calculates a curve representing expired volume versus time. This curve, known as a spirogram, provides measurements such as the forced expiratory volume in one second (FEV_1) and the forced vital capacity (*FVC*). Forced expiratory flow at 50% of *FVC* (FEF_{50}) and peak

expiratory flow (*PEF*) may also be obtained from spirometry via the maximum expiratory flow-volume curve, a plot of expiratory flow (in liters per second, L/s) versus expired volume (in L) [Prid99].

Reference values based on healthy subjects that account for gender, anthropometrics, and race are available for each of the aforementioned spirometric measurements [Prid99]. It is important to account for these variables because there is considerable variation in maximum expiratory flow between individuals.

Another piece of equipment used in PFT, a body plethysmograph, can be used to provide not only the spirometric measurements mentioned above, but also total airway resistance and absolute lung volumes [Prid99]. During *body plethysmography*, a subject sits in a closed, airtight chamber, and breathes through a large caliber mouthpiece and pneumotachograph. For airway resistance measurement, the test begins by having the subject breathe tidally as changes in the pressure of the chamber, ΔP, are plotted against changes in the subject's air flow, $\Delta \dot{V}$. The slope $\Delta P/\Delta \dot{V}$ is generally measured around zero flow [Prid99]. Then, the subject pants shallowly and the pathway between the mouthpiece and pneumotachograph is occluded. During this procedure pressure at the mouth may be equated with alveolar pressure, P_{alv}, and when plotted against pressure in the chamber, the slope $\Delta P_{alv}/\Delta P$ may be obtained. Airway resistance may then be calculated by multiplying the two aforementioned slopes, because pressure drop through the airways is proportional to air flow.

Both spirometry and body plethysmography require comprehension and cooperation from subjects undergoing the tests. Unlike spirometry, airway resistance measurements do not require maximal forced maneuvers. However, reference values for

airway resistance are relatively underdeveloped [Prid99]. As well, a body plethysmograph is more bulky and expensive than a spirometer. Thus, spirometry is generally used more widely than body plethysmography.

Resistance to flow may be determined using other methods, such as the *esophageal balloon technique*, *air flow interruption*, and *forced oscillation* [Prid99]. The esophageal balloon technique is invasive, as it involves inserting a catheter with a small inflatable sac on its end (the "balloon") into a subject's esophagus. A differential pressure transducer measures the difference between esophageal pressure (considered to reflect lung elastic recoil pressure) and pressure at the mouth as a subject breathes through a pneumotachograph (for flow measurement). Plotting pressure as a function of flow provides resistance. The technique is subject to noise such as cardiac artifact. Few laboratories use this routinely [Prid99]. The second method listed, air flow interruption, is less sensitive and tends to underestimate resistance relative to body plethysmography, and it is not widely used. Basically, this method involves cessation of tidal breathing for a brief period of time, i.e. less than one second, and measuring the pressure at the mouth before and after this interruption of air flow, which reflects alveolar pressure at the moment of cessation [Prid99]. As with body plethysmography, the ratio between differences in pressure and flow provides resistance.

Unlike the two methods just described, measurement of resistance to flow by forced oscillation is gaining popularity [Prid99]. When it was first introduced in the 1950's its technical requirements were quite demanding, but recent advances in, for instance, pressure transducer technology, have made its use more convenient. As its name implies, sinusoidal oscillations are superimposed on a subject's breathing pattern by

introducing a low-frequency sinusoidal pressure wave at a subject's mouth (generally around 4-6 Hz) [QKOM01]. The ratio of pressure at the mouth to air flow as the subject breathes tidally is measured per cycle of the sinusoidal input, and this instantaneous relationship is the respiratory impedance, Z_{rs} [QKOM01]. Impedance encompasses resistance and reactance as real and imaginary parts respectively [Prid99], the latter being comprised of elastic and inertial resistances to flow [QKOM01]. In asthma, increasing severity of airway obstruction results in increased resistance to flow, and hence higher measurements of Z_{rs} would be expected relative to reference values for healthy subjects [QKOM01]. Though this method has been found promising in deciphering healthy from asthmatic adults [QKOM01], it is important to note that forced oscillation has proven useless in children during bronchial provocation [WBPS95] (as indicated in Chapter 1).

2.4.2 Measuring Airway Hyper-responsiveness (AHR)

To measure AHR, an enhanced tendency to narrowing that is another physiological abnormality associated with asthma (as will be discussed below), airway constriction (i.e. obstruction) may be induced using a provocative stimulus such as methacholine [InPr99]. Methacholine is a commonly used direct-acting agent and it is usually nebulized and delivered through a facemask while a subject breathes tidally for two minutes. It is administered in increasing concentrations, with lung function measurement obtained between inhalation of each dose (generally via spirometry). This test for AHR is known as the *methacholine challenge* (MCh). The test stops when a maximal dose is reached, or when a subject exhibits a decrease in FEV_1 that is greater than 20% relative to the baseline value (before or when the maximal dose has been reached). The latter condition results in AHR diagnosis. Though AHR is not exclusive to

asthma, nor does it necessarily exclude asthma in patients who fail to demonstrate AHR, MCh is nonetheless a widely used method to diagnose asthma [InPr99].

Rather than inducing airway constriction, determining whether inhalation of a bronchodilator drug improves lung function is another method of assessing AHR [InPr99]. The bronchodilator response (BDR) is relatively simple to measure: it involves PFT, followed by inhalation of nebulized β_2-agonist; allowing an interval of time for the bronchodilator agent to reach full effect (approximately 15 minutes for salbutamol); and obtaining another lung function measurement. The best way of expressing BDR is as the absolute change in FEV_1 between pre- and post-bronchodilator measurements, normalized by the percent predicted FEV_1. A BDR, or improvement in FEV_1, of greater than 15% is considered large and indicative of AHR and potentially asthma [InPr99]. Both BDR and MCh will be referred to later in the thesis.

2.4.3 Variability in Lung Function Measurements

PFT measurements are prone to both intra- and intersubject variability [Prid99]. Measurements such as the FEV_1, FVC, FEF_{50}, and PEF require maximal, forced efforts, and intrasubject variability in these values may result from submaximal performance by the subject undergoing PFT [Prid99]. Acknowledging this type of variability, most experts suggest that subjects repeat PFT to provide at least three satisfactory measurements of the aforementioned parameters. However, having subjects repeat the tests too many times may induce bronchial constriction in a few asthmatics; thus, there exists a trade off between establishing reproducibility and minimizing unwanted disturbance of the system under study.

2.5 Asthma and Airway Hyper-responsiveness

2.5.1 Definitions and General Information

Asthma is a complex disease with many possible phenotypes [KWWC06], and without a universally agreed upon definition [SWAD06]. The literal meaning of the word asthma is "different breathing" [ChCh83]; indeed, it is primarily characterized by wide variations over short periods of time in resistance to air flow in lung airways [Scad83]. It is difficult to precisely define asthma partly because different physicians observe different aspects of the disease [Hogg78], and also due to lack of agreement amongst physicians [Scad83]. Its diagnosis is based on a combination of features such as respiratory symptoms; variable air flow obstruction; airway pathology; and physiological abnormalities such as AHR (mentioned in the preceding section) [SWAD06]. The combination of exposure to risk factors and genetic predisposition is generally recognized as the cause of asthma [ChBe06]. The primary risk factor for asthma is airway inflammation, which is a result of injury or death of tissues [PaHa00].

Worldwide, approximately 300 million people are affected by asthma, and this figure is expected to rise by 100 million by the year 2025 [PFDR06]. The increasing prevalence is occurring in both industrialized and developing countries [ChBe06]. It has been suggested that in Canada and non-English speaking regions of Europe, asthma prevalence on average is decreasing, having peaked at around 8-12% (grouping adults and children) [voHa05].

Recent data indicate that asthma causes approximately 239,000 deaths per year worldwide, which amounts to approximately 0.4% of all deaths due to disease [PFDR06]. Most asthma deaths, between 80%-85%, occur in patients with poorly controlled severe

asthma [PFDR06]. Approximately 20% of severe asthma cases are poorly controlled [PFDR06]. Asthma results in a similar number of "disability-adjusted life years" to osteoarthritis, cirrhosis, diabetes, and schizophrenia, and causes a large burden of disability [PFDR06].

2.5.2 Diagnosis

A. Symptoms and Predictive Factors

Examination of symptoms is an indirect method of gauging the presence and severity of AHR and asthma [PaHa00]. A patient's perception of their asthma symptoms as well as presence of certain prognostic factors may be assessed using a questionnaire, such as that of the Wythenshawe Community Asthma Project (WYCAP) based in South Manchester, UK [HSTF01]. Classification of the questionnaire responses via a neural network provided a method of identifying individuals who likely have asthma, which may reduce the number of cases of undiagnosed asthma, or allow for prioritizing a population for PFT where resources for diagnosis are limited [HSTF01]. However, questionnaires are inherently subjective and may be open to interpretation if not designed properly. Rigid questionnaires may cause an inaccurate skew in responses.

As mentioned above, a predictor of doctor-diagnosed asthma is AHR, which (obtained via MCh) was found to have a sensitivity of 84.6% and a specificity of 80.5% [SWAD06]. Adding it to other symptoms tended to decrease their sensitivity and increase specificity, though wheezing with AHR was the best predictor [SWAD06].

Wheeze is a musical sound containing tones at various frequencies ranging from 80-2000 Hz, which can emerge from narrowed airways during breathing, and is often associated with asthma [Boha00]. Though many patients suffering from asthma may wheeze, it is non-specific because patients who wheeze do not necessarily have asthma

[ChCh83] – those with chronic obstructive pulmonary disease (COPD), cystic fibrosis, or bronchiolitis, for instance, may also wheeze [Boha00]. In addition, wheeze does not always accompany airway narrowing during an asthma attack, even in severe cases [Boha00], which indicates that it lacks sensitivity.

Another change in respiratory sound, decrease in lung sound intensity, has also been shown to correlate with bronchial constriction [BHCP04], [Boha00], [PCOH97], and more consistently than wheeze [BHCP04]. A retrospective study of the observations made by two respiratory therapists of the lung sounds of 490 children before and after bronchial provocation via MCh indicated that decrease in lung sound intensity was present in 100% of children who experienced severe bronchial constriction, whereas wheeze over the lung occurred in only 39% of these children [BHCP04]. Change in lung sounds with airway condition will be examined further in later chapters of the thesis.

B. Techniques

As mentioned above, standard methods in asthma assessment involve measuring AHR through administration of bronchoconstrictor or bronchodilator agents, in conjunction with PFT performed before and after ingestion of these agents [KWWC06]. Induced bronchoconstriction, e.g. via MCh, is more risky and causes more distress to a patient relative to bronchodilation, and it also may be less feasible [KWWC06].

In infancy, evidence on preferred methods for evaluating lung function and airway obstruction is limited [LBBA06]. In general, noninvasive tests are preferable to those that are invasive, given that they provide the same information and accuracy [PaHa00]. A noninvasive test should not adversely affect the tissues of the body via breakage, infection, or dissipation of energy [PaHa00]. Several efforts to develop noninvasive measurements of airway inflammation in children have been made

[HeHe06]. Table 2.1 summarizes both noninvasive and invasive methods of asthma diagnosis other than those noted above.

Table 2.1
Methods of Asthma Diagnosis

Method	Premise	Positives (+) and Negatives (-)
Exhaled nitric oxide, eNO [PaHa00]	Level of eosinophils, elevated in asthmatics [PFDR06]	+ simple, relatively inexpensive [PaHa00] + noninvasive [PaHa00] - non-specific; eNO may be high in airway conditions associated with inflammation other than asthma [BPKE00] - requires inhalation to *TLC* and immediate exhalation through a resistance [BPKE00] (i.e. subject cooperation required)
Sputum examination [PaHa00]	Level of eosinophils [PFDR06]	- requires induction by inhalation of hypertonic saline for several minutes which can result in airway constriction [PaHa00] - non-specific (see above) +/- noninvasive [PaHa00], unless constriction occurs
Fibreoptic bronchoscopy [PaHa00]	Level of eosinophils [PFDR06]; assessment of airway wall remodeling via cellular constituents [dMPC05]	+ provides indication of airway wall remodeling - inconvenient: requires sedation [PaHa00] - invasive [PaHa00] +/- generally safe, except in patients with AHR [PaHa00]
Blood test [PFDR06]	Level of immunoglobulin E, elevated in asthmatics [PFDR06]	+ simple - not 100% reliable [PFDR06] - invasive
Raised volume rapid thoraco-abdominal compression technique (RVRTC) [LBBA06]	Spirometric measurements, e.g. forced expiratory volume in 0.5 s, *FVC*, *TV* [LBBA06]	+ can be used on infants - requires sedation - lung volume raised using pneumotachograph and then thorax compressed via inflated jacket to induce forced expiration - no international recommendation or standardization - custom-built equipment [LBBA06]
Transcutaneous oxygen ($P_{tc}O_2$) [LBBA06]	Electrode on skin provides information on gas exchange and reflects integrated output of respiratory and vascular systems [LBBA06]	+ sensitive to detect induced airway obstruction during MCh [LBBA06] - may not be useful at baseline [LBBA06]
Positron emission tomography (PET) [MuVe05]	Provides three-dimensional image of radioactivity that is proportional to the concentration of an ingested radioisotope [MuVe05]	+ use of a radioisotope that is delivered to poorly ventilated regions through the bloodstream can quantify hypoventilation and gas-trapping which occur during asthma [MuVe05] - high cost and difficult to produce radioisotopes [MuVe05] - requires a brief apnea [MuVe05]
High resolution computed tomography (HRCT) [Hans00]	Measurement of airway wall thickening, indicative of asthma [dTEM05]	+ provides image of the lung in vivo - requires breath hold at full inspiration [dTEM05] or other suspension of breathing [Hans00] - exposes subjects to radiation [dMPC05] - very sensitive to motion [dMPC05]

2.6 Summary

This chapter outlined lung structure and function in health and disease. Asthma and airway hyper-responsiveness (AHR) were also covered, in terms of several aspects. Many methods for diagnosis of asthma and AHR were presented. Each method consists of downsides, such as invasiveness; the need for bulky and expensive equipment, such as for body plethysmography or HRCT; and the need for subject cooperation, which is especially concerning when children are to undergo testing, and in fact sedation is often required. Thus, there exists opportunity for new diagnostic techniques. As outlined in Chapter 1, lung sounds offer a basis upon which monitoring and diagnostic methods can be developed. Recording lung sounds is not an invasive procedure, and does not involve bulky or extremely costly equipment. Changes in airway status are reflected by changes in lung sounds, and digital signal processing allows for elucidating such changes, as will be highlighted in other chapters in the thesis. A lung sound model could potentially allow for the use of one lung sound recording in diagnosis and would also provide more insight into lung sound generation and transmission in different respiratory conditions. This will be elaborated on in later chapters.

CHAPTER 3

Lung Sounds: Genesis, Recording, and Analysis

"Although respiratory sound analysis by computer has seen major innovations over the past 30 years it has not, as yet, found a major place in clinical medicine. It is self-evident that modern technology offers immense advantages with respect to the capture, storage, analysis and communication of sounds that are normally heard through a stethoscope, but it remains to be conclusively established how these facilities can routinely and effectively be employed to aid the day-to-day diagnosis and management of patients with respiratory diseases." [EaCh00b]

3.1 Introduction

As indicated in Chapter 1, lung sounds provide useful information in the assessment of respiratory disease, and hence, tools for auscultation have existed for nearly two centuries. In order to improve upon existing technology and develop new methods to listen to, record, and analyze lung sounds, the theory of sound as well as the generation and transmission of lung sounds must be understood. This chapter provides an overview of these topics, along with aspects of recording and analyzing lung sounds, and characteristics of recorded lung sounds in health.

3.2 Overview of Lung Sound Generation

Any relative motion between two fluids (or two solids), or between a fluid and a solid, may emit sound [Blak86]. Successions of positive and negative changes in pressure in an unsteady region of fluid give rise to small density fluctuations that propagate as sound at a particular velocity [MoIn68], [Pran52].

Lung sounds are produced within lung airways during inspiration and expiration of air. Lung sounds recorded on the chest wall represent not only sound generated by flow in lung airways, but also the effects of thoracic tissues and sound sensor

characteristics on sound transmitted from the lungs to a data acquisition system, and non-respiratory contaminating sounds (see Sections 3.4 and 3.5).

Flow of gas volume, $\dot{V}$, in respiratory airways may be laminar or turbulent, or in a transitional phase between these two states. Turbulence is defined as flow with random fluctuations in velocity, whereas laminar flow does not have these random fluctuations [West77]. Fluid motion in nature is almost always inherently unstable, and therefore laminar flow exists as an exception, unless a fluid's viscosity is high, which is not the case for air [Davi04].

Turbulent flow, and any flow incident on an airway bifurcation, aside from causing resistance to increase, result in vortical air flow, which is considered to be the mechanism by which lung sounds are produced [Blak86], [HaPa79]. Vortices, or locally rotating fluid motions, are essential to the production of sound by flow [Blak86]. Vortices have been employed in modeling lung sounds, outlined in Chapter 5.

It is important to note that inspiratory lung sounds are the main focus of research in this thesis, because expiratory lung sounds are often of low amplitude [GaPA81], [GNRC95] and thus reveal relatively less information about the underlying airway status (when they do not contain adventitious sounds). As well, inspiratory lung sounds are produced in peripheral airways more so than expiratory sounds [KrWa90], and may provide more regional information on airway status. Chapter 5 outlines further aspects of breathing pertinent to the generation of sound.

3.3 Overview of Lung Sound Transmission

Though lung sounds exist near the lower threshold of human audibility between approximately 20 and 1000 Hz [PaKW97], the human ear can detect respiratory sounds either by listening closely to the body or through a stethoscope, discussed in Chapter 1. The excitation of sound by air flow in airways and resulting acoustic radiation to the chest wall involves four basic factors: the damping in the structure through which sound must travel; the mass of the structure; the speed of vibration wave propagation in the structure relative to the acoustic wave propagation in the fluid; and the wavelength of the structural vibration compared with the vortex size of the exciting-fluid stresses [Blak86]. The former three topics are outlined briefly in this section and will be discussed in more detail in Chapter 5, along with the latter topic.

Damping can occur via two main mechanisms: geometric damping and viscous forces in a biological material [JLBK89]. Geometric damping is the dissipation of wave energy with distance from a source, which occurs as wave fronts encounter a greater volume of the material through which they are traveling as they propagate from the source [JLBK89]. From the inner airways to the chest wall, the materials through which respiratory sounds are transduced with increasing radial distance include airway walls; parenchyma; fluid within the interstitium and the pleural cavity; rib cage (ribs and intercostal muscles); muscular-fatty tissue; and skin [VoGO95] (see Fig. 2.3 in Chapter 2). Properties of these materials pertaining to sound propagation have been presented and verified in some cases in past work [HKPW01], [Rice85], [Veva84], [VoGO95] and are shown in Chapter 5 (Table 5.1).

Parenchyma and bone are considered dispersive tissues, and the velocity of sound measured in these tissues depends on the measurement technique and method of data

analysis [Duck90]. Dispersion in the lung is more significant for sound at higher frequencies [Duck90], and it has been shown experimentally that higher frequency sounds travel faster than lower frequency sounds; they are also attenuated more than those at lower frequencies as gas-volume increases (and density decreases) based on excised sheep lungs [BSRW05]. This phenomenon explains in part the characteristic shape of the power spectral density (PSD) of lung sounds, presented later in this chapter. That is, sound power is highest at low frequencies and decreases as frequency increases. It has also been shown in human subjects that the tissues between lung airways and the chest wall act as low pass filters [MDKP97]. Note that the low pass filter effect of only the airway wall would be minimal due to the thinness of the wall relative to the wavelengths of the sound produced in lung airways (discussed in Chapter 5).

Transmission of sound through the human thorax has been studied using finite element or finite difference analyses, though not extensively [MHMO99], [NWKG04]. These studies used either sinusoidal inputs with frequencies in the range of lung sound spectra up to 1500 Hz [NWKG04] or wavefronts between 1.6 and 3.0 MHz [MHMO99]. In this thesis a more in-depth assessment of sounds produced in airways, and transmitted through the airways in conditions of health and disease, is an objective, through both signal analysis and modeling, as presented in Chapters 4-6. Further details pertaining to both lung sound generation and transmission are provided in Chapters 5 and 6.

3.4 Lung Sounds: Recording and Flow-Specific Characteristics

Currently, universal standards for recording lung (and tracheal) sounds, in terms of sound sensors and signal processing hardware and software, do not exist [EaCh00a],

[PaKW97]. Methods and equipment employed in various studies in lung sounds research have been reviewed and standardizations have been suggested [EaCh00a], [Muss92], [PaKW97], but to date a consensus among investigators in the field has not been reached. The methods employed to record lung sounds used in the thesis, outlined in this section, are specific to the laboratory through which lung sounds were acquired, namely the Respiratory Acoustics Laboratory in the Manitoba Institute of Child Health, Winnipeg, Manitoba, Canada.

3.4.1 Data Acquisition Methods Relevant to the Thesis

A piezoelectric contact accelerometer (Siemens EMT25C) was used for all lung sound recordings involved in the thesis work. Sounds were amplified with a gain of 200, and filtered using custom-designed eighth order Butterworth band pass filters with passband 7.5-2500 Hz, unless otherwise noted. Flow was always recorded simultaneously with respiratory sounds, via a Fleisch no. 3 pneumotachograph (again, unless otherwise indicated). A National Instruments™ analog to digital conversion card, model DACard-1200, digitized data at 10240 Hz and 12 bits.

Other studies have employed electret microphones [PaKW97] and laser Doppler vibrometry [QWLA04], for instance; each type of sensor has its own advantages and disadvantages, and it is not an objective of this thesis to determine or develop an optimal respiratory sound-sensing device. This has been studied in [PKDW93] and has been the focus of recent research on a BioAcoustic Transducer Testing ("BATT") device [KPPW06]. Lung sounds manifest as vibrations of the tissue of the chest, and measurement of this vibration is generally complicated and difficult [Veva84]. It has been suggested, for example, that the presence of a transducer for recording lung sounds leads to the conversion of longitudinal waves into surface waves [VoGO95]. The

displacement of the chest wall during breathing is less than 10 μm, and it is easily affected by the method used to measure it [LoMu84]. In modeling (Chapter 6), consideration is given to the effects on lung sound measurement by the accelerometer that has been used; its effect has been examined relative to lightweight and relatively heavy contact sensors by others [Veva84].

3.4.2 Relationships of Lung Sounds to Frequency and Flow

Recorded lung sounds exhibit a PSD that is broadband with decreasing power as frequency increases [GaPA81]. The amplitude of lung sounds in healthy subjects, void of any adventitious sounds, has been shown to have a linear $\log_{10}$-$\log_{10}$ relationship with frequency [GaPA81]. Inspiratory and expiratory lung sounds differ in terms of both amplitude and frequency range. At comparable flows, inspiratory lung sounds will exhibit greater intensity than expiratory sounds [GNRC95], [MDKP97]. The peak frequency of expiratory sounds has been shown to exceed that of inspiratory sounds when measured with an esophageal stethoscope [MDKP97]. This is likely because expiratory sounds have been found to be produced in central airways whereas inspiratory sounds are produced more peripherally, as noted above [KrWa90]. Indeed, measurements over one posterior and three anterior chest locations indicated that expiratory sounds have lower peak frequency than inspiratory sounds [GNRC95]. As mentioned above, the thesis work involves analysis and modeling of inspiratory lung sounds.

In addition to considering breath phase, i.e. inspiration/expiration, a minimum flow must exist in order for lung sounds to surpass a signal to noise ratio (SNR) of 3 dB, which is frequency-dependent [CIGP97], [GSTP03], [YaMo05]. The SNR is generally calculated as the ratio between sounds acquired during breathing and those acquired during breath hold, which provides indication of ambient, heart and muscle noise. The

latter two sounds will be discussed further in Section 3.5. Lung sound SNR can exceed 3 dB when flow is near zero, i.e. at transitions between respiratory phases, which is likely due to the effects of heart and muscle sounds. One study [YaMo05] showed that when the effect of heart sounds is cancelled, the required minimum flow decreased for lung sounds at frequencies below 450 Hz recorded over the right upper lobe (RUL) anteriorly. Indeed, phase transition ambiguity occurs below 300 Hz more so than above, and also depends on sensor location [GSTP03]. Lung sounds acquired at the anterior site resulted in significantly more ambiguity at phase transitions than those acquired posteriorly ($5 \pm 8\%$ vs. $28 \pm 29\%$ anteriorly, $p < 0.01$, paired t-test) [GSTP03].

For calculation of PSD, and all other features discussed in subsequent chapters of the thesis, the signals must be portioned into segments that may be considered wide-sense stationary [Cohe86]. If respiratory flow, measured at the mouth in most studies, has been acquired simultaneously with respiratory sounds, signals may be sectioned according to target or plateau regions of the flow signal [GaCu96], as illustrated in Fig. 3.1. The sounds within these segments are further sectioned into windows for frequency domain conversion.

In Fig. 3.1, the PSD of inspiratory lung sounds and breath hold were calculated using fast Fourier transform in 100 ms Hanning windows, overlapped by 50 ms, and averaged across all breaths within the target flow range (or at zero flow for breath hold). The sounds were recorded from a child over the posterior right lower lung lobe (RLL) [GMBP04], [GnMP04]; the data set containing these lung and breath hold sounds will be presented in Chapter 4. As mentioned above, lung sounds of healthy subjects generally have broad band and sloped spectra [GaPA81].

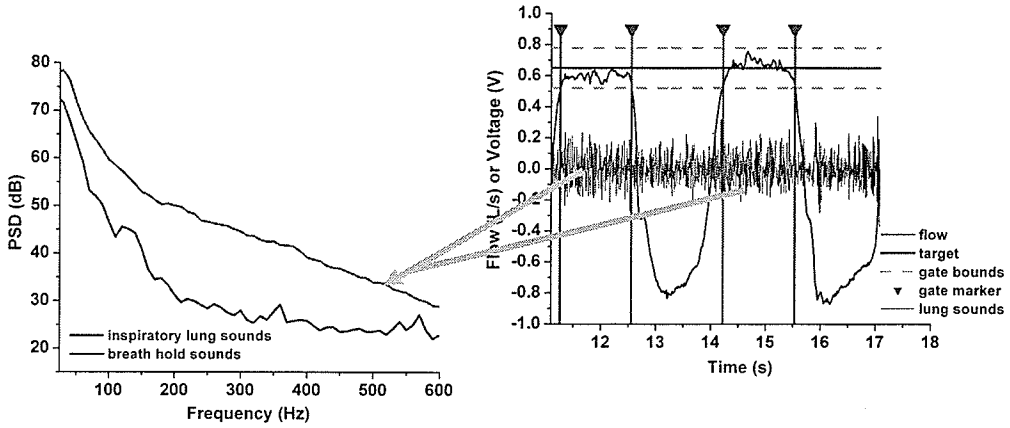

Fig. 3.1: Illustration of technique for calculating a lung sound spectrum (lung sounds measured over posterior RLL). (Lung sound and breath hold power referenced to $1x10^{-8}$ W.)

In general, as air flow in lung airways increases, sound intensity and frequency range increase, and several mathematical relations between air flow and lung sounds recorded on the chest have been proposed [GaCu96], [HoMo02], [KrWa90], though not one is widely agreed upon. Interestingly, it has been shown that route of breathing [KPKT98] and breathing apparatus used to measure air flow [PaGM03] do not have an appreciable effect on lung sounds [PaGM03].

In order to illustrate changes in intensity of lung sounds with changes in air flow, Fig. 3.2 shows characteristics of lung sounds recorded from six healthy subjects (three males), ages 10-26 years with body-mass indices ranging from 17.6-24.7 kg/m^2 [GHPM05]. Lung sounds over the RUL anteriorly and RLL posteriorly, and air flow at the mouth, were measured while subjects breathed at 7.5, 15, and 22.5 mL/s/kg (low, medium, and high flow respectively), one recording per flow. Each recording consisted of target breathing for 50 s followed by a 10 s breath hold. Subjects maintained target flow levels by monitoring and modifying their breathing according to a LabVIEW™ (National Instruments) virtual instrument (VI) user interface, which instructed subjects to breathe so that one full breath occurred per approximately two seconds. Subjects breathed

through a three inch cardboard mouthpiece (one inch diameter) and wore nose clips. These lung sounds were obtained in order to study methods of reducing heart sounds from lung sounds, which will be outlined in Section 3.5. Lung sounds in portions of the recordings free of heart sounds were extracted in an automated manner using ECG, presented in [GHPM05]. Average SNR per recordings grouped by flow was determined across the subjects, and mean values of SNR (± standard error, SE) are shown in Fig. 3.2 for each recording location. From this figure, it is clear that SNR, i.e., lung sound intensity, increases with flow; that sound intensity is quite frequency-dependent; and that sensor location affects lung sound intensity. These experimental observations emphasize what has been discussed above.

3.5 Non-Respiratory Sounds in Recorded Lung Sounds

Aside from frequency and flow, non-respiratory sounds such as heart sounds, mentioned above, are important considerations when analyzing lung sounds. The effect of non-respiratory sounds in lung sound recordings may be prominent in both time- and

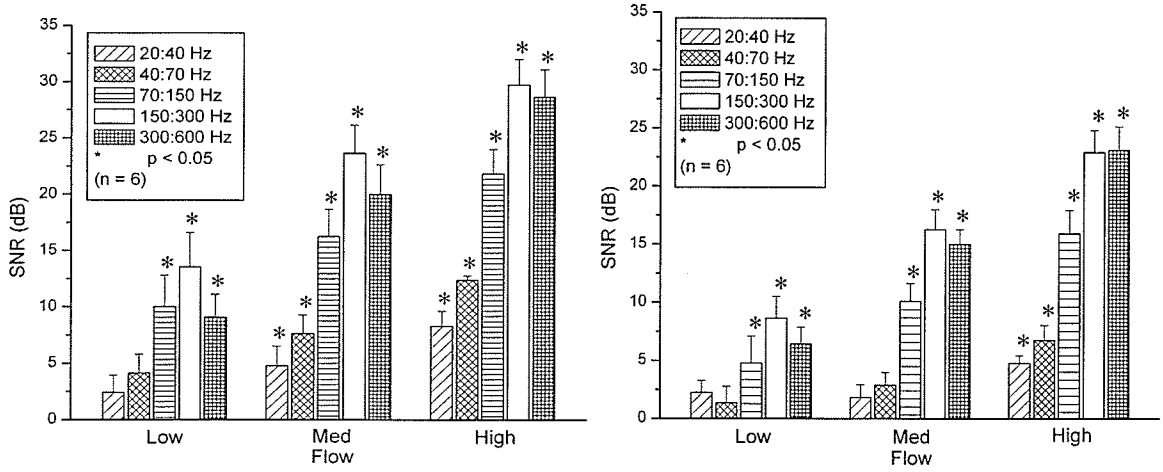

Fig. 3.2: SNR for lung sounds acquired over right upper anterior (left graph) and lower posterior lung lobes.

frequency-domains. This section deals with non-respiratory sounds from both biological and non-biological sources and their impact on lung sounds.

3.5.1 Heart Sounds

Depending on frequency range and sensor location, heart sounds may figure prominently in recorded lung sound signals. The first heart sound results when blood is pumped from the heart to the rest of the body, during the latter half of the cardiac cycle, and it is comprised of sounds resulting from the rise and release of pressure within the left ventricle along with the increase in ascending aortic pressure [Luis64]. After blood leaves the ventricles, the simultaneous closing of the semilunar valves, which connect the ventricles with the aorta and pulmonary arteries, causes the second heart sound [Sher01]. The first and second heart sounds in healthy subjects were the primary foci of the thesis work, and it is therefore beyond the scope of this work to present detail with respect to other heart sounds.

Both lung and heart sounds overlap in time and frequency, with each having most of their energy below 300 Hz, which poses quite a challenge to the application of any signal processing technique for filtering heart sounds from lung sounds. Our studies [GHPM05], [GnMP03] have shown that there are significant differences between the average power of anterior RUL lung sound segments with and without heart sounds in low and medium flow recordings up to 150 Hz, based on frequency bands 20-40 Hz, 40-70 Hz, and 70-150 Hz. At high flow, however, this difference is significant only below 70 Hz. Figure 3.3 shows these results.

A component of the thesis work was to develop an adaptive noise cancellation (ANC) method based on recursive least squares (RLS) filtering not only for cancellation but also localization of heart sounds in recorded lung sounds; a few publications cover

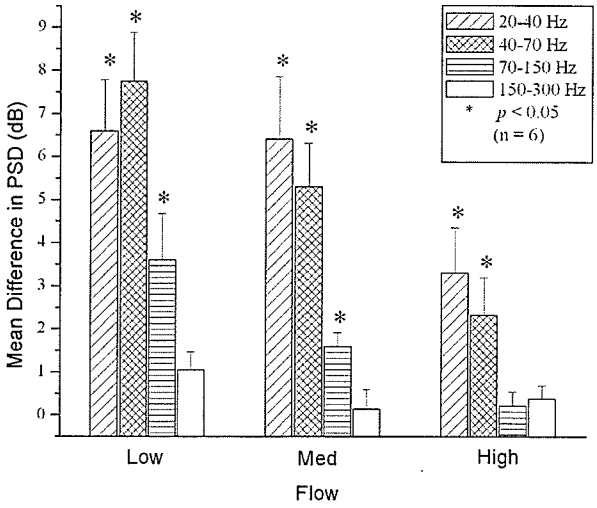

Fig. 3.3: Differences between PSD calculated for lung sounds including and excluding heart sounds, RUL, flows 7.5 mL/s/kg (low), 15 mL/s/kg (medium), and 22.5 mL/s/kg (high), 6 subjects [GnMP03]. Error bars depict mean standard error.

this work in detail [GHPM05], [GnMo07], [GnMP03]. Though the RLS algorithm performed well in reducing heart sounds [GHPM05], [GnMP03], it had been applied to signals acquired from healthy subjects with no known cardio-respiratory condition (outlined above). In fact, none of the previous studies dealing with heart sound reduction [ChAG97], [ChAz96], [HaPa97], [HaPa98], [HMAA00], [HoMo03], [IRFP86], [KoRu92], [LuLQ88], [MoFT04], [PoMT03], [YiZh01] presented results based on subjects who were not healthy, and some researchers chose to use fabricated signals [ChAG97], [ChAz96]. Until techniques are evaluated for their robustness using a wide range of heart sounds, e.g. those including variable split of the second heart sound or audible sounds other than only first and second heart sounds, the use of heart sound reducing algorithms will remain an object of experimentation. It was therefore not an objective of the thesis to incorporate heart sound removal into further analysis and modeling of lung sounds, as presented in subsequent chapters.

3.5.2 Muscle Sounds

Muscle sounds, though useful for measuring localized muscular activity, generally pose a nuisance to respiratory sound research. For instance, it has been shown that low frequency muscle sounds are of higher amplitude than higher frequency lung sounds, and that muscle sounds may figure prominently up to around 200 Hz in lung sounds recorded over the right upper and lower lung lobes anteriorly [Kram83]. The presence of chest-wall muscle sounds in recorded lung sounds was studied in depth in a thesis that presented a piezoelectric sensor design made of polyvinylidene difluoride film to record and study chest-wall muscle and lung sounds during breathing [Gros89]. The PSD of chest-wall muscle sounds recorded while subjects maintained static, open-glottis inspiratory pressure at different lung volumes was found to peak at 6-11 Hz, but also to extend into the 75-250 Hz range [Gros89].

During inspiratory breathing, the muscles responsible for chest-wall muscle sounds include intercostals and parasternal intercartilaginous muscles, which increase the diameter of the chest by elevating the ribs [Gros89]. Elevation of the first and second ribs is also accomplished by accessory muscles for inspiration, the scalenes, and the sternocleidomastoid, another accessory muscle, elevates the sternum [Gros89]. The right and left diaphragms per se likely do not have a great effect on lung sounds measured on the chest. Other muscles, such as pectorals, might affect lung sounds, depending on sound sensor location. Muscle sound in general results from the summation of sounds produced over many muscle fibers during muscle fiber contraction. Experimentally it was shown that muscle sound power was quadratically related to force output on effort. Thus, the contribution of muscle sounds to lung sounds would be higher for deep breathing than tidal breathing.

Lung sounds recorded while subjects prolonged inspiratory and expiratory breath phases at constant target flows for approximately three seconds (i.e., high-volume breathing) exhibited the typical rumbling of muscle sounds near the end of breath phases [GSTP03]. This resulted in ambiguity of onset of breath phases based on spectral envelope of lung sounds within 75-150 Hz and 150-300 Hz, which suggests that increased sound at low frequencies due to muscle rumble may provide indication of respiratory effort. Rumblings at the end of inspiration persisted through the transition between breath phases into the expiratory phase; prolonged expiration did not result in muscle rumblings of the same caliber.

3.5.3 Other Non-Respiratory Sounds

Artifacts in recorded lung sounds can emerge from both respiratory and non-respiratory sources. The former type comprise sounds such as wheezes and crackles, which have been studied as diagnostic indicators in past work but were not a focus of the thesis, as indicated in Chapter 1. The latter noises include heart and muscle sounds discussed above, but may also emerge as a result of several other factors. For instance, any coarse hair touching the sensor would introduce crackling or tapping noises, and sensor locations must therefore be shaved. Air bubbles between a sensor and the double-sided tape that is used to adhere it to the chest may also cause crackle-like sounds as the chest wall moves during breathing. Poor adherence between the tape and the body would result in the sound of the tape ripping off of the skin as a subject breathed, which would be a lot louder than lung sounds. Properly cleaning the sensor location with alcohol prior to adhering it would alleviate this problem.

Manual marking of artifacts, achieved by listening to recorded sounds and examining their spectrograms, was considered the most reliable way of accounting for

artifacts within each signal in the thesis, since a standard automated signal processing technique has not been established for this purpose. Artifacts may figure prominently in PSD analysis, and may in turn provide a false indication of the extent of a lung sound signal's PSD. Figure 3.4 depicts PSD before and after artifact exclusion, for both lung sounds (top PSD curves) and breath hold (using a recording from the RLS-ANC data set).

The cable of the Siemens EMT25C accelerometer sensor is of major concern in terms of its potential to cause noise. It is a very thin coaxial cable (approximately 1.5 mm diameter) and any slight contact with it causes rubbing or clicking sounds in recorded data. The cable must be prevented from touching anything, which can be achieved by hanging it such that enough slack exists to allow it to move freely, or by taping it to the body and equipment using loops of tape.

Accelerometer sensors in general introduce another manner in which recorded lung sounds may be altered, in that their weight plays a major role in their ability to accurately detect the movement of the chest that represents lung sounds [Veva84], which

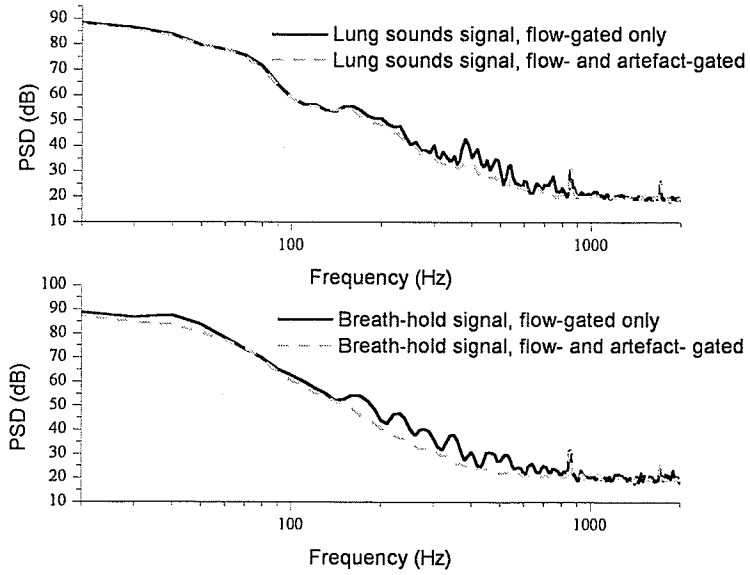

Fig. 3.4: Comparing flow-gated lung sounds and breath hold signals before and after artifact-gating; RUL, low flow, subject 6 [GnMP03].

is less than 10 μm as mentioned above. Sensitivity and sound quality have been shown to be lower for heavier accelerometers [PKDW93]. Though the use of microphones alleviates this issue, a microphone must be separated from the body surface by an air cavity since it measures changes in air pressure. The shape, depth and width of the cavity that separates the microphone from the body may pose other possible sources of contamination to recorded lung sounds due to resonances [KWOP95], [WKZP94]. It has been shown that microphones may attenuate low frequency sounds up to 300 Hz and be more sensitive to sounds at high frequencies relative to contact accelerometers [PKDW93]. Recent work using a BioAcoustic Transducer Testing (BATT) System [KPPW06] has elucidated the relative performance of several sensors used in lung sounds research.

3.6 Summary

This chapter was meant to provide an introduction to lung sounds in terms of their generation, transmission, recording, and aspects of their analysis. The segmentation of lung sounds based on flow, shown in Fig. 3.1, and the aspects of recording lung sounds outlined in Section 3.4, were employed in all lung sound studies presented in the thesis. Analysis of time series data in general is directed at discovering characteristics of the underlying process, which is referred to as an inverse problem [PoMi99], or inductive modeling [Marm04]. It is important to point out that signal featuring contributes to but does not stand alone in overall decision-making based on lung sounds (or biological waveforms in general); without observations other than the signals per se, the range and depth of possible characterization of a system and development of a diagnostic tool are

limited [Coat02]. Without a priori information regarding physiological and environmental factors, it is also more difficult to select the appropriate approach for the analysis of time series, which is complicated further when the mathematical background of the underlying process is unknown [PoMi99].

CHAPTER 4

Fractal and Chaos Analyses of Lung Sounds

"... fractal models have been used extensively and with an increasing success in physical research during the last 10-15 years. Fractal models are not only applicable to exploring in more detail previously described processes and structures (e.g. random walks, linear polymeric molecules) but they also provide a deeper insight into phenomena which it would be impossible to comprehend and quantify using traditional methods." [ZoLy95]

4.1 Introduction

The following sections discuss the use of fractal dimensions in a few lung sound applications, and nonlinear tools for measuring aspects of lung sounds not provided by more traditional analyses in lung sounds research such as power spectral density (PSD). As mentioned in Chapters 3 and 5, respiratory sounds are produced by fluid flow energy that is transformed into sound by nonlinear processes. Therefore, the use of nonlinear signal processing techniques seems appropriate for analysis of respiratory sound signals.

4.2 Fractal Analysis

4.2.1 Background

A fractal object or process possesses self-similarity [PeJS92]. A self-similar process is a stochastic process that is invariant to scaling in time and space [EmMa02]. Mathematically, a d-dimensional real-valued stochastic process $\{X(t),\ t \geq 0\}$ is self-similar if for any $a > 0$, there exists $b > 0$ such that [EmMa02]:

$$\{X(at)\} \overset{d}{=} \{bX(t)\} \tag{4.1}$$

The value of b can be expressed as $b = a^H$, where H is unique and $H \geq 0$ [EmMa02]. This value is known as the Hurst exponent, and it will be referred to in Section 4.2.2.

A fractal dimension (FD) is a non-integer dimension that exceeds the Euclidean dimension of a natural object or process that is self-similar, or in other words whose smaller parts are reduced-size copies of its larger parts [Kins94]. Waveform FD values indicate the quantity of information embodied in a waveform in terms of morphology, entropy, spectra or variance [Kins94]. In general, a FD may be determined by counting the number, N, of measurements of size r that is needed to outline or cover an object or process. This procedure is repeated for n different measurement sizes, which change by some scaling factor. After at least $n = 3$ measurement sizes, a relationship should emerge between the logarithm of N and the logarithm of r. If the relationship is inverse linear, then the slope of this inverse line, i.e. the exponent of the power law, provides the dimension of the object or process (non-integer for fractals) [Kins94], [PeJS92].

Considering morphological properties of lung sound signals, it appears that these signals will possess valid FD values, i.e., values greater than the Euclidean dimension of a line (one) but less than that of a surface (two). In physical systems, the property of self-similarity in pure fractal objects is not strict but is probabilistic, and there are minimum and maximum scaling limits [Kins94]. This is known as self-affinity. Realistically, an object occurring in nature, such as a physiological signal, that exactly duplicates itself over several scales does not exist. Thus, if lung sounds or portions of lung sounds possess fractal properties it would be in the self-affine sense.

Fractal analysis has proven useful for extraction of certain lung sound characteristics [GnMo03], [HaRe03]. Both variance and morphology-based FD techniques have been employed in the thesis research thus far, as outlined in Section 4.2.3. These waveform FD techniques are described in the following section.

4.2.2 Calculation of Waveform Fractal Dimensions

A. Brief Overview of Fractional Brownian Motion

One approach in the study of waveforms as fractal processes is to model waveforms using properties of fractional Brownian motion (fBm), which is a known self-similar process (waveform) with independent and stationary increments [EmMa02]. It is also a unique Gaussian process, which has a mean of zero and the following covariance function [EmMa02]:

$$c(t,s) = \frac{1}{2}\left(|t|^{2H} + |s|^{2H} - |t-s|^{2H}\right). \tag{4.2}$$

In a discrete formulation, t ranges from one to some sample limit N, and $s = t{:}N$ for every value of t. The value of H is the Hurst exponent, as mentioned above, and $0 < H \leq 1$ for fBm [EmMa02].

A method of fBm synthesis is the Cholesky technique [Duec03], [EmMa02]. Cholesky fBm is labeled as such because Cholesky factorization is involved in its synthesis [EmMa02]. With this type of factorization, an upper-triangular matrix is obtained from the covariance of fBm (4.2), which is multiplied by a vector of Gaussian random variables to form the Cholesky fBm. This type of fBm simulation will be referred to in work describing lung sound modeling in Chapter 5.

B. Variance Fractal Dimension (VFD)

A precursor to the valid calculation of VFD for signals is that the PSD of the process under investigation must be broadband and sloped. Lung sound waveforms exhibit this quality, discussed in Chapter 3. This attribute provides evidence of fBm [Kins94] (discussed above), as does the non-self-crossing character of lung sound waveforms recorded on the chest surface. Furthermore, the waveforms exhibit

quasiperiodicity because they emerge from a natural biological process that is approximately periodic (i.e., respiration), which implies that they are not purely random [Kins94], also compliant with the nature of fBm.

The VFD is determined using H [Kins94], defined above. The calculation is based on the variance of the amplitude increments of a waveform, $B(t)$, over a time increment $\Delta t = |t_2 - t_1|$, with $B(t_2)$ - $B(t_1)$ denoted as $(\Delta B)_{\Delta t}$. Using this variance, a power law is defined as, $Var[(\Delta B)_{\Delta t}] \sim \Delta t^{2H}$, and the Hurst exponent is therefore

$$H = \lim_{\Delta t \to 0} \left[\frac{1}{2} \frac{\log_b [Var(\Delta B)_{\Delta t}]}{\log_b (\Delta t)} \right], \tag{4.3}$$

with $b = 2$ for this study. Using (4.3), the VFD for a process with embedding Euclidean dimension, E (equal to one for waveforms), is determined by

$$VFD = E + 1 - H. \tag{4.4}$$

Practically, the technique for calculating H and VFD begins by choosing a window size of N_T-increments, based on the known characteristics of lung sounds. A range of integers, k, is chosen such that each window of size N_T, shown in Fig. 4.1, contains a number, N_k = int(N_T/n_k), of smaller windows of size $n_k = 2^k$, that is greater than 30 per variance calculation (for statistical significance) [Kins94]. For instance, in a study on fractality of lung sounds (mentioned in Section 4.2.3), k ranged from five to eight, regardless of window size [GnMo05]. The variance is calculated in each window per stage k in a single pass, shown in previous work [GnMo03]. The values $X_k = \log_2(n_k)$ and $Y_k = \log_2[Var(\Delta B)_k]$ are then stored for the window of N_T-samples per step k, and the least-squares fit for points in X_k and Y_k is determined after going through all divisions of N_T, obtaining a slope, s, for the $\log_2$-$\log_2$ plot for these values. The value of H is computed as 0.5*s, and the VFD for this window as per (4.4).

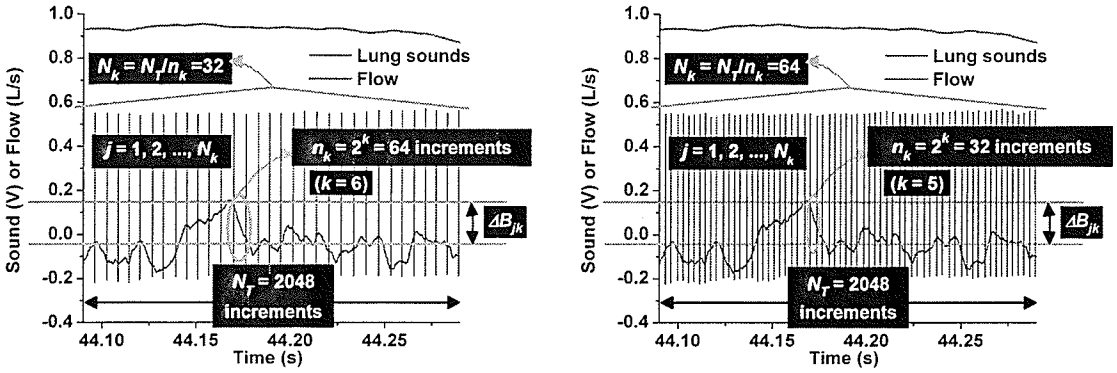

Fig. 4.1: Example of parameters necessary for VFD calculation, for two window sizes.

C. Katz Fractal Dimension (KFD)

The Katz algorithm [Katz88] for obtaining a waveform FD is based mainly on morphology, and is calculated as:

$$KFD = \frac{\log_{10}(n)}{\log_{10}(n) + \log_{10}(d/L)}, \tag{4.5}$$

where n is the number of increments between samples of the waveform over which KFD is calculated; L is the sum of all of the distances between successive increments; and d is the value of the maximum distance measured from the beginning of the first increment. Figure 4.2 depicts the variables involved in (4.5) based on a 200 ms portion of a lung sound recording (corresponding to flow at plateau).

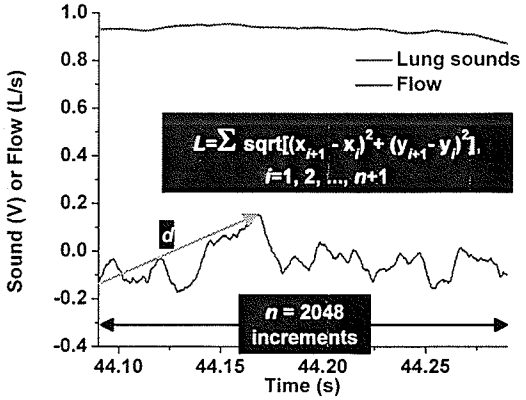

Fig. 4.2: Illustrating variables involved in KFD calculation.

D. Katz-Sevcik Fractal Dimension (KSFD)

In 1998, Carlos Sevcik [Sevc98] presented a variation of the KFD method, termed the Katz-Sevcik FD (KSFD) for the purpose of this thesis, which involves normalization along the y- and x-axes before calculation of FD:

$$x_i^* = \frac{x_i}{x_{\max}}, \text{ and} \tag{4.6}$$

$$y_i^* = \frac{y_i - y_{\max}}{y_{\max} - y_{\min}} \tag{4.7}$$

where x_i and y_i denote the coordinates of the i^{th} sample of the window; x_{max} and y_{max} are the maximum values within the window and are not necessarily corresponding coordinates; and y_{min} is the minimum y-value per window. From these values, the length, L, of the signal within the window of N samples is determined as mentioned above for the KFD. Then,

$$KSFD = 1 + \frac{\ln(L) + \ln(2)}{\ln(2N')} \tag{4.8}$$

where $N' = N$-1. Sevcik found that his method offered results that were closer than KFD to previously reported data on the signals under test [Sevc98].

4.2.3 Brief Overview of Applications of FD Analyses

The waveform FD calculation techniques outlined in Sections 4.2.2-B, -C, and -D were applied to one lung sounds data set in order to examine the fractal nature of lung sounds by comparing results from these three waveform FD techniques. This work was published in [GnMo05]. It was shown that proving the fractality of lung sounds seems to be dependent on the technique used to calculate their FD, and also on the scaling

parameters applied to the waveforms. Changes in lung sound amplitude (and/or frequency) with flow resulted in changes in FD values.

Using the data that had been employed in the heart sound RLS-filtering study discussed in Chapter 3, it was found that the VFD was a useful tool for localizing heart sounds in lung sounds recorded at low and medium flows, with VFD values decreasing at points corresponding to the onset of first and second heart sounds [GnMo03]. The use of VFD and morphology-based KFD values in a one-nearest neighbor (NN) classification scheme to distinguish lung sounds from children pre- and post-bronchial constriction showed that the KFD may improve classification in a NN classifier relative to using lung sound intensity alone [GnMP04].

As a pilot study to determine the potential in developing a model to distinguish lung sounds of healthy subjects from those with lung function at 80% or lower relative to healthy reference values (i.e. poor lung function) and/or asthma, RMS-SNR and KFD features of these sounds were statistically compared between these groups [GnMP05b]. The linear relationships between these features and inspiratory air flow were determined for each recording. KFD and RMS-SNR were plotted with respect to average flow per window, which was normalized by both weight and height.

In [GnMP05b], SNR did not offer prominent trends in any comparison. This further validates that SNR is not necessarily useful across the whole lung sounds spectrum, as shown in past work [GnMP04], but is a useful parameter when averaged across certain frequency ranges, such as octave bands, as discussed in Appendix B. It is true that respiratory therapists were able to observe changes in sound intensity via observations with a stethoscope (see Chapter 2), i.e., without filtering lung sounds into

octave bands; however, as mentioned in Chapter 1, most stethoscopes reduce the intensity of lung sounds above 500 Hz. Thus, such auscultation effectively provides lung sounds that are band-limited within the lower frequency range of these sounds.

The percentages of significantly different intercepts resulting from the KFD curves between subjects with poor lung function and/or asthma and healthy subjects [GnMP05b] indicated that KFD is sensitive to subtle changes in lung sounds and provide promise in the use of one lung sound recording to distinguish respiratory health from disease. It would be ideal to develop a diagnostic technique that would not require comparison of lung sounds recorded before and after an induced change in respiratory state. This notion will be revisited in Chapters 5 and 6, which present a lung sounds model that incorporates the KFD as a feature used to tune the model.

4.3 State Space Analysis

The underlying nature of the processes producing lung sounds, i.e., whether stochastic or deterministic, is not yet established. From material presented in Chapter 3, it seems logical to attempt to develop deterministic differential equations governing the dynamical system responsible for lung sound generation: properties of the "input," i.e. air flow, and "output," i.e. sound, are known; it is the matter of combining the characteristics of the individual components of the system that is a focus of the thesis. The fact that relations exist between respiratory flow measured at the mouth (input) and sound measured over the chest (output) suggests that it may be possible to predict conditions of the respiratory system from lung sounds. However, more parameters besides those

relating to air flow would likely be required, such as patient anthropometric data and properties of the respiratory flow itself.

If the evolution of a deterministic system's differential equations gives rise to random behavior, the system may be defined as chaotic [Casd90], [PaCh87]. A chaotic system is one that is sensitive to initial conditions, which means that relatively small changes in variable values (e.g., 0.01% [Kins94]) will lead to system outputs that differ in an unpredictable manner [PaCh87]. When time series solutions of individual system equations are plotted with respect to one another, creating a multi-dimensional state space, the resulting graph will appear as a complex geometrical object that has a FD [ABST93]. In fact, the corresponding points of the time series solutions when plotted will exhibit orbit-like behavior: the points will fall into certain regions collectively forming a trajectory in the state space, and if the time series is long enough the geometrical object will emerge without the trajectory having crossed itself [Kins94]. This is what is known as an "attractor" [Kins94]. Conceptually its effect is similar to that of a magnetic field in certain regions of the state space, pulling polarized particles of the time series into the field. In this manner the state space exhibits regularity (though the particles will not be pulled into the "field" in the same configuration twice). Thus, a chaotic dynamical system is one which is both unpredictable, and contains order.

A well-known example of a deterministic system that results in chaotic behavior is the Chua circuit [Kins94]. The equations governing this circuit are as follows:

$$\begin{aligned} \frac{dx}{dt} &= \alpha\left(y - h(x)\right) \\ \frac{dy}{dt} &= x - y + z \\ \frac{dz}{dt} &= \beta y \end{aligned} \quad , \tag{4.9}$$

where x represents voltage V_{C1} across circuit capacitor C_1; y represents voltage V_{C2} across circuit capacitor C_2; and z represents current i_L through circuit inductor L divided by conductance G. The other parameters are indicated in the algorithm used to solve the circuit system which is shown in Appendix D. The system has been evaluated using the Runge-Kutta formula for solving differential equations (also shown in the algorithm). The voltage time series' (V_{C1} and V_{C2}) are shown in Fig. 4.3, along with the two-dimensional attractor obtained by plotting these outputs with respect to one another.

Analysis of recorded lung sounds can provide characteristics of the dynamical system producing lung sounds, which constitutes an inverse approach [PoMi99] or inductive modeling [Marm04]. If the equations governing a nonlinear deterministic and potentially chaotic system are not available, an estimation of the number of differential equations required, also known as the system dimension, M, may be obtained by computation of Lyapunov exponents, λ_i, based on the time series output of the system

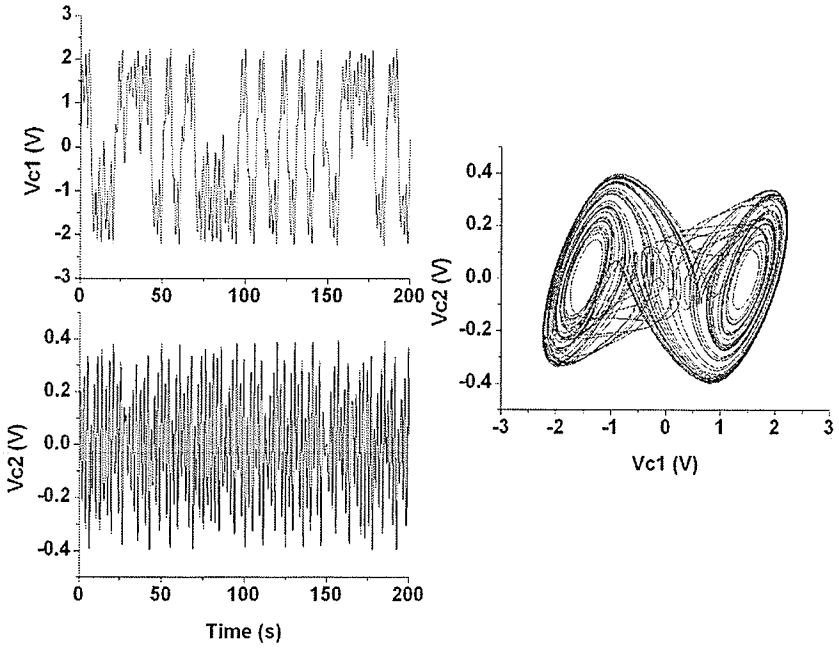

Fig. 4.3: Chua circuit output and attractor.

[Casd90]. Lyapunov exponents were originally developed in classical mechanics to examine a system's stability [ZbZS02], and the sign of exponents, i.e. positive or negative, provide indication of divergence or convergence (respectively) of a system's energy [BaUM97], [Onys03]. The presence of both positive and negative Lyapunov exponents provides evidence for existence of chaos, though a positive exponent may also mean the presence of a singularity [CVFG04]. The sum of Lyapunov exponents must be negative because the system dynamics must be dissipative overall [RoCD93]. In order to calculate Lyapunov exponents based on time series data, parameters obtained from a few essential data operations are required [BaMM99], [BaUM97], which are outlined in the following section.

4.3.1 Geometrical State Space Parameters

The first step in nonlinear analysis is to define, from a single time series measurement, the m-dimensional trajectory that comprises the system [BaMM99], [ChTo92]. The value of m is called the embedding dimension, and it dictates the number of dimensions required to reconstruct a system's state space, or attractor [BaMM99], [ChTo92].

The state space, when deterministic dynamical equations are not available, is basically a collection of vectors obtained from the reconstructed trajectory matrix, created using Takens method of delays. From a time series of length N (number of samples in the signal), i.e. $x = x_0, x_1, x_2, \ldots, x_N$, the trajectory matrix is formed as:

$$\mathbf{X} = \begin{pmatrix} x_0 & x_\tau & x_{2\tau} & \cdots & x_{(m-1)\tau} \\ x_1 & x_{\tau+1} & x_{2\tau+1} & \cdots & x_{(m-1)\tau+1} \\ x_2 & x_{\tau+2} & x_{2\tau+2} & \cdots & x_{(m-1)\tau+2} \\ & & \vdots & & \end{pmatrix} \tag{4.10}$$

The relation between m, which may be determined as discussed in the following paragraph, and system dimension M is such that $m \geq 2M + 1$ [BaMM99], [ChTo92]. Careful choice of m and of the delay, τ, should result in an attractor containing no areas where state-space vectors, $\mathbf{X}_j$ (i.e., rows of the matrix (4.10)), $j = 1, 2, \ldots, B$, $B = (N-(m-1)\tau)$ intersect [RoCD93]. An approximation for the delay may be obtained by the autocorrelation of the time series, whereby the lag at which the autocorrelation drops to $(1-1/e)$ of its maximum value provides an approximation of τ.

Calculating the nearest neighbors between state space vectors provides estimates of m described as follows [AbMo04], [ABST93]: Minimum Euclidean distances, say $w_m(i)$, are determined between a reference vector $\mathbf{X}_i$ and every other vector in state space, $\mathbf{X}_{\hat{j}}$, $\hat{j} = 1, 2, \ldots, B$, $\hat{j} \neq i$. The value of m is then increased by one, and minimum distances for this new dimension, $w_{m+1}(i)$, are compared with $w_m(i)$. Increasing the dimension by one results in increasing the number of columns in the trajectory matrix (4.10), and increasing displacement of the state space trajectory from the identity line is optimal. Thus, it is conceivable that a greater number of nearest neighbors found for embedding dimension m than for dimension $m + 1$ will be "false:" the state space plot is too far from its "true" representation in the former case. To quantitatively determine the value of m that reduces the number of false neighbors, the distances between nearest neighbors from the final column of the trajectory matrix (4.10) for embedding dimension $m + 1$ (per row) are compared with the nearest neighbor distances $w_m(i)$ from embedding dimension m by taking the ratio between them. Values that surpass a particular threshold may be considered false neighbors. Embedding dimensions are increased until the number of false neighbors diminishes to zero. The threshold was chosen as two, which is

the minimum value that may be chosen, since it implies that the new distance for $m + 1$is at least twice the value of the distance for m [ABST93].

Once a value of m has been approximated, a method of determining an appropriate lag other than the autocorrelation technique may be used, which involves finding the average displacement of the state space trajectories from the identity line [RoCD94] (i.e., the state space obtained when $\tau = 0$). This distance is calculated as,

$$\langle S_m(\tau)\rangle = \frac{1}{B}\sum_{i=1}^{B}\left\|\mathbf{x}_i^{\tau} - \mathbf{x}_i^{0}\right\|, \tag{4.11}$$

with $\|\ \|$ indicating Euclidean distance [RoCD94]. As τ increases, the displacement $\langle S_m(\tau)\rangle$ increases also, and the relationship is linear until the plot of $\langle S_m(\tau)\rangle$ versus τ begins to plateau [RoCD94]. The value of τ for the data that were used to test the algorithm [RoCD94] corresponds to the point at which slope of the plateau is approximately 40% of the slope of the linear increase. Since these data were created based on systems of differential equations known to be chaotic, it is not known how well the $\langle S_m(\tau)\rangle$ curves would follow a similar characteristic shape, i.e. linear increase followed by plateau, for time series from systems for which governing equations are not known. Some examples of curves for lung sounds are shown in Section 4.4.

4.3.2 Dynamical State Space Parameters

Determining Lyapunov exponents from time series data is very much dependent upon the reconstructed state space, and can be quite difficult [ABST93]. A method for determining Lyapunov exponents from time a series [BaUM97] has been used successfully on speech signals [BaMM99], and has been applied to lung sounds in this study. After determining the Takens matrix based on optimal m and τ values as described

above, a number of nearest neighbor rows $\mathbf{X}_k$ is determined for each row $\mathbf{X}_j$. The neighbors are ordered according to Euclidean distance in an ascending manner. Each neighbor row is then labeled γ_c, $c = 1, 2, \ldots$ with $c = 1$ corresponding to the closest row [BaUM97]. Forty neighbors were used, arranged as:

$$\mathbf{Y}_z = \begin{pmatrix} (\gamma_1 - \gamma_{b+1}) + (\gamma_{2b+1} - \gamma_{3b+1}) + \cdots + (\gamma_{6b+1} - \gamma_{7b+1}) \\ (\gamma_2 - \gamma_{b+2}) + (\gamma_{2b+2} - \gamma_{3b+2}) + \cdots + (\gamma_{6b+2} - \gamma_{7b+2}) \\ \vdots \\ (\gamma_b - \gamma_{b+b}) + (\gamma_{2b+b} - \gamma_{3b+b}) + \cdots + (\gamma_{6b+b} - \gamma_{7b+b}) \end{pmatrix}, \tag{4.12}$$

where $b = 5$, and represents the number of subgroups of the neighborhood of rows. Past findings [BaUM97] and also constraints of data length determined b and the number of neighbor rows. With $\mathbf{Y}_z$, $\mathbf{T} = \mathbf{Y}_z{}^{\mathrm{T}}\mathbf{Y}_{z+1}$ is calculated, where $\mathbf{Y}_{z+1}$ is a matrix formed by setting $\gamma_c = \mathbf{X}_{k+1}$. **QR**-decomposition is performed on **T**, and Lyapunov exponents, λ_i, are calculated based on the **R**-matrix as follows:

$$\lambda_i = \lim_{n\to\infty} \frac{1}{n} \sum_{j=1}^{n} \log\left(\mathbf{R}_j\right)_i, \tag{4.13}$$

where, in reality, $n = B$-1, since there is not an infinite amount of data. The number of Lyapunov exponents is equivalent to the value of m, hence $i = 1, 2, \ldots, m$.

4.4 Factors Affecting Changes in State Space Parameters of Lung Sounds

Geometrical and dynamical state space parameters have been determined for lung sounds in healthy subjects in very few studies [AJHA06], [CVFG04], [GnMP05a]. The state space analyses described in the preceding section were applied to lung sounds of healthy subjects and subjects with symptoms of asthma undergoing induced

bronchoconstriction via methacholine challenge (MCh). The main objective was to elucidate the diagnostic potential of these parameters. Differences in parameters between healthy subjects and patients, and between patients pre-MCh, post-MCh, and post-bronchodilator (BD) were examined. Effects of flow and sensor location were assessed for healthy subjects [GnMP05a]. The impact of presence of heart sounds on state space parameters was examined for both groups of subjects.

4.4.1 Data Recording and Protocol

Lung sounds recorded for previous studies from six healthy subjects (three males) ages 10-26 years [GHPM05] and eight children (five males) undergoing MCh [GnMP04] were analyzed. Lung sounds from the healthy subjects were acquired over the right upper lung lobe (RUL) anteriorly and lower lobe (RLL) posteriorly. Air flow was measured while these subjects breathed at targets of 7.5, 15, and 22.5 mL/s/kg (± 20%) through a mouthpiece and pneumotach with a nose clip in place. Further details with regard to these lung sounds were presented in Chapter 3 in conjunction with the RLS-ANC heart sound reduction study. Sound intensity (SNR) values for the lung sounds of healthy subjects were shown in Fig. 3.3.

Appendix B and [GnMP04] present information with regard to the patients undergoing MCh. SNR values for the patients before and after MCh are shown in Fig. B.4 in Appendix B. Subjects breathed through a facemask and pneumotach at tidal flows. Flows targeted for analysis that adequately captured breaths during tidal breathing were 15 mL/s/kg for the four responders to MCh and two of the non-responders to MCh, and 7.5 mL/s/kg for the other two non-responders. All lung sound recordings were 50 s long and were followed by a 5 s breath hold. Lung sounds were recorded over the RLL.

For the work in state space parameters, the lung sounds that were used were not only the lung sounds recorded pre- and post-MCh, but also those obtained post-BD (salbutamol inhalation following MCh) for the four subjects who responded to MCh with significant bronchial narrowing (responders), indicated by a greater than 20% change (decrease) in FEV_1 (ΔFEV_1) [GnMP04].

Lung sounds corresponding to inspiratory plateau flow were used. It is important to point out that the signals undergoing nonlinear analysis should be stationary [Casd90], and therefore lung sound recordings have been analyzed only in sections corresponding to plateau regions of flow. Note that the patients were not asked to breathe tidally and hence not at any target level, and only breaths within the chosen ranges noted above were used. All data were analyzed with heart sounds included and also manually excluded (located on a spectrogram and via listening, corroborated by ECG information for healthy subjects [GHMP05]).

4.4.2 Results

Table 4.1 shows mean and standard deviation (SD) values across the six healthy subjects for target flow (maximum values per breath), embedding dimension (m), time delay (τ) (in samples) based on $\langle S_m(\tau) \rangle$, and percentage of breaths with positive Lyapunov exponents (λ_i). For healthy RUL and RLL lung sounds, whether including or excluding heart sounds, values of τ decreased with increasing flow (and thus with increasing intensity). Embedding dimensions did not vary much in any case. Figure 4.4 provides examples of graphs used in finding m, τ, and positive λ_i values for one breath at medium flow from one healthy subject, comparing between RUL and RLL lung sounds and also with lung sounds of one patient pre-MCh.

Table 4.1

Mean ± SD of Flow, m, τ from $\langle S_m(\tau) \rangle$, and % of Breaths with Positive λ_i and of Total Positive λ_i - Healthy Subjects

	Including heart sounds			Excluding heart sounds			
Flow (L/s)	m	τ (samples)	% breaths with pos. λ_i	m	τ (samples)	% breaths with pos. λ_i	% total pos. λ_i
			RUL				
0.64 ± 0.13	9.07 ± 2.64	49.1 ± 25.2	83.4 ± 17.7	9.35 ± 2.23	47.3 ± 21.9	61.7 ± 14.5	18.9 ± 6.03
1.09 ± 0.26	9.25 ± 2.34	33.4 ± 19.0	85.7 ± 11.8	8.94 ± 2.00	31.9 ± 22.2	78.5 ± 18.5	26.4 ± 9.42
1.65 ± 0.32	9.07 ± 1.50	20.3 ± 14.4	96.1 ± 4.99	9.00 ± 1.53	22.9 ± 15.0	91.0 ± 12.5	33.3 ± 10.0
			RLL				
0.64 ± 0.13	8.04 ± 1.81	39.9 ± 20.1	78.8 ± 18.2	8.80 ± 1.91	36.6 ± 15.5	65.3 ± 6.23	21.3 ± 4.95
1.12 ± 0.25	8.37 ± 1.50	34.4 ± 16.4	88.3 ± 13.4	8.91 ± 1.58	30.5 ± 13.1	84.6 ± 19.9	26.8 ± 7.57
1.63 ± 0.34	8.54 ± 1.60	21.4 ± 15.7	91.5 ± 13.6	9.92 ± 1.97	19.7 ± 11.6	76.4 ± 9.67	21.8 ± 6.52

As shown in Table 4.1, the percentage of breaths with positive λ_i was lowest at low flow for each sensor location, and also decreased with exclusion of heart sounds for every flow and location. High flow RUL lung sounds exhibited the highest percentage of breaths with positive λ_i including and excluding heart sounds. The total percentage of positive relative to negative λ_i, also presented in Table 4.1 for lung sounds excluding heart sounds, increased with flow for RUL lung sounds and did not vary much between flows for RLL lung sounds. On average at least two-thirds of λ_i were negative for both

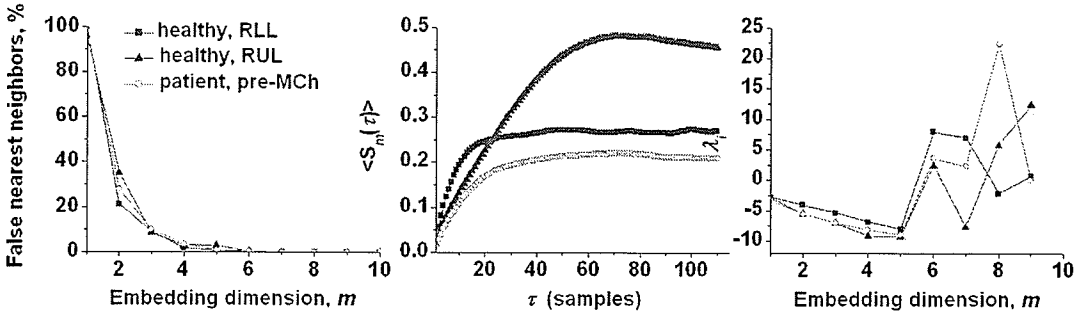

Fig. 4.4: State space measures for one healthy subject, RUL and RLL, and one patient pre-MCh, based on one breath each (flow at 15 mL/s/kg, heart sounds excluded).

healthy subjects and patients.

Noteworthy trends were exhibited for state space parameters of lung sounds acquired pre- and post-MCh and post-BD from responders, shown in Table 4.2. Percentage of breaths with positive λ_i and of total positive λ_i decreased post-MCh, and returned to near-pre-MCh values post-BD. The τ behaved similarly, except it increased post-MCh rather than decreased. As found for healthy subjects, m did not change appreciably.

Since lung sounds from the non-responders did not all match in terms of flow (i.e., two were acquired at 7.5 mL/s/kg while the others were acquired at 15 mL/s/kg as mentioned in Section 4.4.1), state space parameters were not averaged across these subjects. Only the mean percentages of total positive λ_i, having been found to not change appreciably with flow for RLL lung sounds of healthy subjects (Table 4.1), were determined, and were found to be 27.56 ± 5.09% pre-MCh and 22.98 ± 6.13% post-MCh. Values of m and τ for non-responders were not outside of the ranges found for other subjects (Tables 4.1 and 4.2).

Interestingly, the percentage of total positive λ_i per responder and non-responder as a function of ΔFEV_1, shown in Fig. 4.5, falls by at least 10% post-MCh for subjects with ΔFEV_1 greater than or equal to 15% (magnitude), and does not appreciably change

Table 4.2
Mean ± SD of Flow, m, τ from $\langle S_m(\tau) \rangle$, and % of Breaths with Positive λ_i and of Total Positive λ_i - MCh Responders

	m	τ (samples)	% breaths with pos. λ_i	% total pos. λ_i
Pre-MCh	9.22 ± 1.53	25.0 ± 7.42	96.4 ± 4.75	35.6 ± 2.66
Post-MCh	8.37 ± 1.31	31.7 ± 11.0	63.1 ± 27.6	18.7 ± 7.55
Post-BD	9.14 ± 1.27	24.0 ± 8.21	87.2 ± 7.55	32.3 ± 2.97

for non-responders with lower ΔFEV_1. It is important to note that though the non-responders did not exhibit a ΔFEV_1 that would warrant diagnosis of airway hyperreactivity (and potential diagnosis of asthma), they cannot be considered healthy, or even as control subjects for the responders to MCh, because they were referred by a physician for MCh as a result of respiratory distress.

Figure 4.6 compares state space plots for the subjects used in Fig. 4.4. Embedding dimension vectors one and three, labeled $\mathbf{X}_1$ and $\mathbf{X}_3$, were used; since it is possible to plot at maximum only three dimensions, whereas there are m dimensions per breath, several combinations of trajectories may be plotted with respect to one another, and trajectories $\mathbf{X}_1$ and $\mathbf{X}_3$ were thus chosen arbitrarily. The state space parameters describe the state space in detail, and provide more information than what can be manually observed; these graphs are shown only as typical examples of attractors.

4.4.3 Discussion

Mean values of the embedding dimension, m, changed little between flows for lung

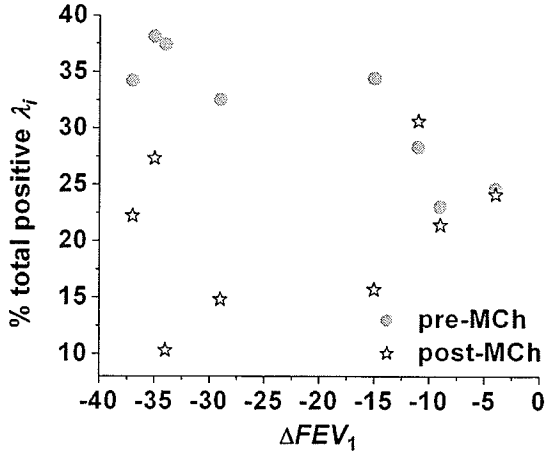

Fig. 4.5: Percentage of total positive λ_i as a function of ΔFEV_1 for all patients (lung sounds of the two subjects with ΔFEV_1 of -4% and -9% corresponded to flow of 7.5 mL/s/kg; others breathed at 15 mL/s/kg).

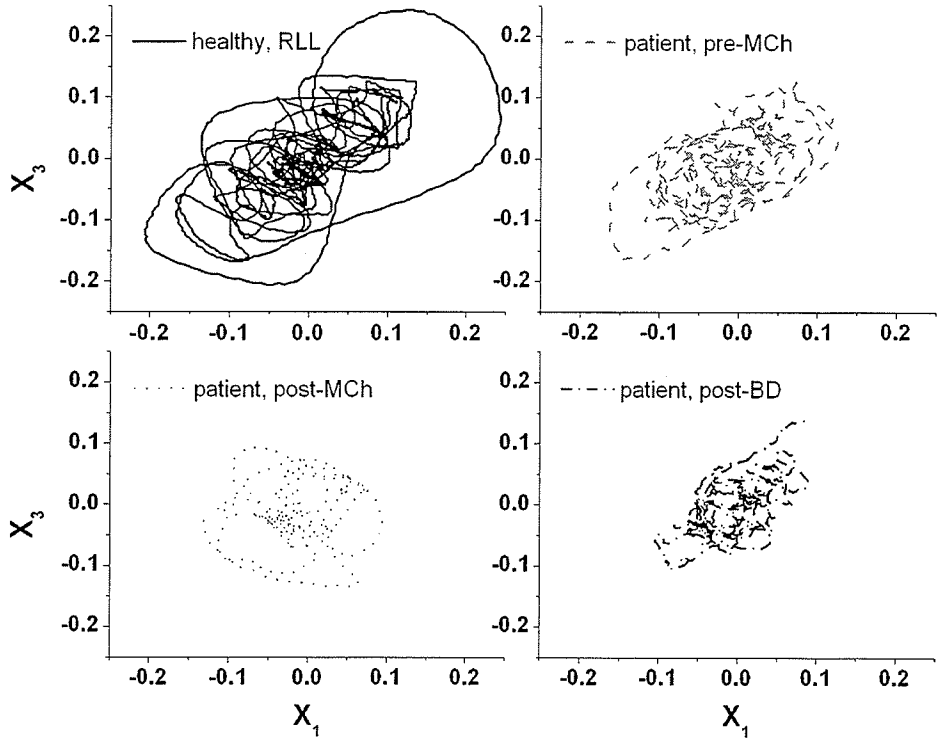

Fig. 4.6: Examples of state space trajectories for one healthy subject and one patient pre-MCh, post-MCh, and post-BD (RLL, 15 mL/s/kg, heart sounds excluded).

sounds of healthy subjects. Values ranged between approximately six and 12; past work found values near both the lower [AJHA06] and upper [CVFG04] bounds of this range based on lung sounds recorded over the left [AJHA06] and right and left [CVFG04] upper lung lobes anteriorly. Lung sounds in each of those studies were acquired with an electronic stethoscope and digitized at 44.1 kHz. Subjects breathed at about 15 mL/s/kg and lung sounds were analyzed within inspiratory flow at plateau in [AJHA06]. The values of m presented in [CVFG04] were not calculated but chosen and lung sounds were analyzed across both inspiration and expiration whole phases at tidal flow. The chosen values were said to be high in order to account for the possible presence of noise [CVFG04], which was inevitable due to the analysis of whole breaths.

Percent of breaths with positive λ_i and values of τ varied with flow in healthy subjects. The changes, particularly the high number of breaths with positive λ_i at high flows for RUL lung sounds with and without heart sounds, may represent the increase in turbulence that accompanies increase in flow according to the Reynolds number [Blak86], especially considering the proximity of the anterior RUL location to large airways, i.e. bronchi and trachea. Turbulence in itself has been shown to be chaotic [RuTa71], which may be borne out by lung sounds at higher flows. Thus, fewer occurrences of positive λ_i may indicate bronchial constriction, since decrease in airway diameter results in decrease in Reynolds number and hence turbulence [Blak86]. Indeed, this result was found for the lung sounds of patients: percentages of breaths with positive λ_i and total percentage of positive λ_i substantially decreased post-MCh in responders, and were restored to near-pre-MCh values post-BD (Table 4.2). Though there are changes that occur in the lungs with bronchoconstriction that could affect transmission of sound from airways to the chest wall, such as increased stiffness of airway walls and possible air trapping or hyperinflation, it is not clear which components of sound would be impacted by these factors.

Excluding heart sounds from lung sounds of healthy subjects also had an impact on percentages of breaths with positive λ_i for all flows and sensor locations – the percentages decreased. The results of state space analysis of heart sounds using the recurrence statistic reported in [ALHA05] complement the finding of our study. The recurrence statistic is related to the distance between state space vectors, and it was found to be lower for regions of lung sound recordings outside of heart sounds [ALHA05]. Decrease in this distance would theoretically be akin to increase in convergence of the

attractor, which is represented by negative λ_i as mentioned in Section 4.3.

It is possible that the removal of heart sound segments, rather than removal of heart sounds per se, could have caused the jumpy behavior of the percentage features (Table 4.1) and high standard deviations in all cases. Another contributing factor to both of these phenomena could be that the data are not of infinite length, which is an ideal requirement of the Takens matrix [ABST93], though the method we used to calculate λ_i was developed for short time series [BaUM97]. Using a higher sampling rate could have improved results [ZbDZ02]. Increasing the number of subjects in each group would likely reduce the standard deviations. These are important considerations for future work with state space parameters.

The percentages of total positive λ_i for all cases indicate that there are many more negative than positive λ_i values, which is realistic since overall energy dissipation, represented by negative λ_i, is to be expected [AJHA06], [BaUM97]. With heart sounds excluded, percentages of breaths with positive λ_i and of total positive λ_i for lung sounds of patients pre-MCh and post-BD were within the range of these percentages for lung sounds of healthy subjects for corresponding sensor location and flow (i.e., RLL and 15 mL/s/kg). This indicates that state space parameters may not be able to distinguish healthy lung sounds from lung sounds of subjects with hyper-responsive airways and possibly asthma. However, as mentioned above, it is encouraging that changes were exhibited in the state space parameters of patients' lung sounds between baseline and bronchial narrowing: percentages of positive λ_i decreased for all responders and one non-responder (who exhibited high ΔFEV_1) post-MCh (Fig. 4.5). Work of breathing increases with airway narrowing, partly due to hyperinflation, which causes an increase in pressure

needed to generate flow, and partly because the diaphragms flatten, resulting in greater respiratory muscle effort [PKMR02]. Hence, energy dissipation in the respiratory system increases, and such energy behavior corresponds with negative λ_i values as indicated in section 4.3, thus providing further justification for the λ_i results. Note that differing views exist on whether positive λ_i values for lung sound signals provide indication of chaotic dynamics [AJHA06] or singularities [CVFG04]; it is not an objective of the thesis work to resolve this issue.

Values of τ for healthy subjects decreased with increase in flow for each sensor location whether heart sounds were present or not. These values did not change substantially with exclusion of heart sounds. On average, values of τ for the patients' lung sounds pre-MCh were slightly lower than those for corresponding healthy lung sounds, and increased post-MCh. This result is rather counter-intuitive to the observed decrease in percentages of positive λ_i discussed above. However, an explanation may be provided by examining Fig. 4.6 – whereas the surface area occupied by the trajectory appears to be more compact in the post-MCh example relative to pre-MCh, thus justifying the λ_i results suggestive of convergence, the points in the trajectory in this smaller space appear to be further apart, which would increase the distance measure in the method for finding τ [BaUM07], [GnMP05a] and hence increase τ. It is important to recall, though, that the state space parameters account for all dimensions whereas any graphical presentation may display at most three.

Vortical and/or turbulent air flow of air in ducts such as human airways produces sound (discussed in Chapters 3 and 5), and equations governing this phenomenon in general are known [Blak86]. Lung sounds are modified versions of this sound, as a result

of the passage of sound waves through the chest. Although highly complex, it is possible that as a whole the system producing lung sounds may be mathematically modeled [KWAW01]. The results of this study suggest that τ and λ_i values may prove constructive in modeling lung sounds. The consistency of m indicates that the number of differential equations involved in a system model would not change with conditions, e.g. air flow or respiratory status, implying that only model parameters would differ. As well, changes in both τ and λ_i may prove useful in classification of respiratory status, especially considering that the τ and percentages of λ_i values returned to pre-MCh values post-BD in responders to MCh. Unlike past analysis of state space parameters of lung sounds [AJHA06], [CVFG04], this work examined lung sounds acquired at different flows from healthy subjects and also lung sounds recorded from patients undergoing MCh. Further study with a more congruent and larger group of subjects is required to verify the potential of state space parameters in lung sound analysis.

In spite of all of the possible connections between state space parameters of lung sounds and flow dynamics presented above, it is important to point out that the changes in percent of breaths with positive λ_i and values of τ with flow for healthy subjects could have been a result of changes in sound intensity and/or bandwidth that occur with flow. As discussed in Chapter 3, lung sounds increase in intensity and frequency as air flow increases. In order to determine the extent to which the state space parameters found in this study were affected by sound intensity and by flow dynamics, more information pertaining to the latter would be required. Since it is not possible to visualize air flow within airways as a subject breathes, a physical model would help to elucidate how the parameters relate to sound intensity and flow.

Another important consideration is noise in data. It has been suggested that state space analysis applied to data containing stochastic noise may result in parameters indicative of chaos when the data itself may not in fact be chaotic [CKIC97]. Separating the signals representing lung sounds from additive noise (which can result from a myriad of potential factors) would not be possible for the data employed in this work, because reference recordings of sound within the hardware or other sources were not acquired. This is a recommendation for future study. Simply applying the state space analyses to a generated white (or colored) Gaussian noise signal in order to estimate the effects of broad-band noise could provide misleading results, since it would not be possible to know how well the generated noise matched with noise in the data. It would comprise a whole study in and of itself and it was not employed in the thesis but is also recommended for future work (see Chapter 7).

Though filtering data reduces noise to an extent, filtering should be avoided in state space analysis as it could alter the dynamics in the time series [ZbDZ02]. However, filtering is generally a necessity in order to satisfy the Nyquist criterion. Indeed, lung sounds in relevant past work [AJHA06], [CVFG04] have been filtered prior to analysis. Note that a sensor may in itself effectively filter data due to its particular frequency response. One way in which filtering could have affected findings is in terms of positive λ_i and hence divergence of the state space – it has been shown that filtering may attenuate divergence, and further that sampling (decimation) can cause results to show no divergence in data known to otherwise exhibit positive exponents [ZbDZ02]. The latter finding indicates that sampling of data should occur at as high a rate as possible, even surpassing that dictated by the Nyquist criterion if necessary [ZbDZ02].

4.5 Summary

Fractal dimensions and state space parameters introduce potentially useful tools in the study of lung sounds in health and disease. This chapter presented studies that have implemented these features in the assessment of changes in lung sounds with changes in the airways, and with different recording conditions such as sensor location and air flow. In Chapters 5 and 6, fractal dimensions have been used as features to compare model with recorded lung sounds.

CHAPTER 5

Development of a Lung Sound Generation and Transmission Model

"... most physiological systems exhibit significant and essential dynamic nonlinearities. This problem is compounded by the fact that physiological systems are also often nonstationary (i.e., their functional characteristics vary with time) necessitating models whose parameters also change with time." [Marm04]

5.1 Introduction

The generation and transmission of lung sounds, in a strict quantifiable and hence reproducible sense, are not completely understood. Since sound at the chest may be measured (sound transmission characteristics of thoracic materials between airways and the chest wall have been published and presented later in this chapter in Table 5.1), and equations governing sound pressure produced by fluid flow are known [Blak86], it is conceivable that the lung sound generation and transmission system may be mapped mathematically. Such a model could bring forth further understanding of lung physiology and pave the way for new diagnostic techniques for airway diseases, such as airway hyper-responsiveness (AHR) and asthma. It could also allow prediction of airway status based on a single recording of lung sounds. This chapter outlines the development of a lung sounds model incorporating both generation and transmission.

5.2 Past Attempts at Modeling Lung Sounds

Lung sound models have been presented in relatively few studies conducted in respiratory sound research. Of those that have attempted modeling, most have focused on sound transmission, employing a white noise input signal to simulate flow-generated

sound, and approximating the airways using circuit models [WADS92], [WSGS90], or applying more mechanically-based estimations for properties of the thoracic cavity [Veva84], [VoGO95], [VoZK94].

Though a considerable amount of work has been done on modeling flow patterns through respiratory airways [LiSZ03], [PeSS71], [vaHP04], [WiDe97], respiratory sound resulting from flow vortices or turbulence has rarely been studied. Hardin and Patterson [HaPa79] proposed vortices as theoretically the major mechanism for generation of lung sounds. That study presented several useful insights into lung sound generation in airways, and also equations for predicting sound frequency based on airway characteristics and flow. Their validation was based on a glass model of four airway generations. As well, their theory was based on steady flow but incorporated time-dependence; this issue will be addressed further in Chapter 6.

One study has attempted to model both generation and transmission of lung sounds using computational fluid dynamics to generate sound in a three-dimensional image of three generations of pig airways, and modeling sound propagation through a thorax from the Visible Human project [KWAW01]. Vortex flow in airways was the mechanism by which sounds were generated [KWAW01], supporting the work in [HaPa79]. It was suggested that lung sounds recorded from pigs be used to validate the model [KWAW01], even though sound transmission was based on a human thorax, and recorded sounds wouldn't allow validation of the generated sound but only the generated sound that was transmitted. The model necessitates high-resolution x-ray computed tomography images of the lung airways and also a supercomputer.

Focusing on sound transmission, another group modeled the human thorax as a set of five concentric cylindrical layers, each with distinct physical properties representing the tracheal wall, parenchyma, ribs together with intercostal muscle, fat, and skin [VoGO95]. Sound generation on inspiration was assumed to occur only in the trachea, a notion that did not take into account earlier findings to the contrary [KrWa90]. The transfer function of acceleration of the thorax produced by the model followed a typical spectrum of lung sounds acquired from a healthy subject, i.e., it was broad band over approximately 20-1000 Hz with intensity inversely proportional to frequency. Formal validation with sound recorded from human subjects was not presented. The authors also found that the presence of the accelerometer resulted in conversion of longitudinal waves to surface waves leading to distortion of the transmitted lung sound signal, which they suggested can be minimized with lightweight sensors (also determined in past work examining optimal sensors for recording heart sound vibrations [Veva84]).

Others have attempted to approximate transmission characteristics using an acoustic circuit [WSGC89]. As in [VoGO95], sound was simplified to be generated mainly in the trachea, and the parenchyma was approximated as a mixture of gas bubbles in water. Each of seven T-networks of the circuit model was comprised of electrical components with values analogous to acoustical parameters of the vocal tract, tracheal, and bronchial walls. The interconnected T-networks formed an effective tube, which was concentrically surrounded by the air-bubbles-in-water representation of the parenchyma mentioned above. A pressure perturbation input to the circuit resulted in a cylindrical wave, and its transmission through the pseudo-parenchyma was measured at four sites in the model. Validation was achieved using transmitted sound measured at corresponding

sites (thoracic and tracheal) from four healthy adult male subjects, using band-limited white noise as input at their mouths while subjects did not breathe but maintained an open glottis. Power spectra of model and experimental acceleration were in reasonable qualitative agreement. (This model will be referred to in more detail later in this chapter.)

Lung sound simulation was achieved by another group [KoRu97] using white noise filtered by an all-pole infinite impulse response filter with coefficients that were averaged estimates of autoregressive (AR) parameters of real lung sounds (per previously published work). Eight sets of coefficients were used per breath phase, producing sequences of segments that were each 150 ms for inspiration and 350 ms for expiration, though these and other aspects of the model were flexible (such as the option of incorporating simulated adventitious sounds). The simulation was found to produce realistic lung sounds qualitatively, as judged via auscultation by a panel of physicians comparing the simulated sounds with teaching tapes of real lung sounds. Though this type of lung sound model does not offer in-depth insight into theoretical mechanisms of lung sound generation and transmission, the authors suggested that it presents potential for use in a diagnostic setting, allowing for "fitting" the simulated sounds to real lung sounds and examining differences in characteristics of the simulation (e.g. coefficient values) between respiratory states (e.g. healthy and asthmatic).

Using a fractal tree (a modified Cantor set) to approximate the airway branching network of the lungs up to 23 generations, two related studies [deBF04], [FadB05] proposed that sound was generated by air flow in each airway at a distinct pitch (consistent across one generation), inversely proportional to the airway radius. Fluid-fluid and fluid-tissue interactions were incorporated as mechanisms for sound production by

air flow in airways, theorizing that air "particles" experience "shocks" via the interactions, which can be summed within one branch. The intensity of sound pressure generated in this manner was considered to be proportional to the number of shocks. The resulting sound was evaluated in terms of its spectrum, resulting from the combination of sound across all airways of the branching tree. A finding of particular interest was that sounds within a low frequency range, 75-160 Hz, were produced mainly by fluid-fluid interaction, whereas fluid-tissue interaction was responsible for sounds within 160-1000 Hz. The authors claimed the spectrum resulting from the model was both quantitatively and qualitatively in "perfect accordance" with that expected of real lung sounds (in health, as noted above) found in past work. Formal validation using recorded lung sounds was not presented.

In my thesis work I attempted to address limitations of the aforementioned models, as well as their application mainly to healthy respiratory states, by modeling lung sounds in a way that may aid in acoustic prediction of AHR mentioned above. Specifically, equations describing sound production by fluid flow and motion of a mass-spring chain were used to model lung sounds based on both their generation and transmission. This chapter presents the methods involved in this work, and Chapter 6 presents model validation and results.

5.3 Modeling Considerations

A number of key parameters and functional properties, including *system bandwidth*, *memory*, *dynamic range*, *linearity*, *stationarity*, and *ergodicity* need to be considered when developing a physiological model [Marm04]. The *bandwidth* of a

system is the range of input frequencies over which the system generates a significant output response [Marm04]. It can be elucidated by using broad band noise as input and measuring the frequency above which the output power spectral density (PSD) falls below the noise floor [Marm04]. Experimental studies of sound transmission from the mouth to various locations on the chest wall and trachea have been performed [PoSY01], [Rice83], [WSGS90], as have studies on the transmission of sound through excised lungs [BSRW05]. Consistently, it has been shown that the attenuation of sound increases with frequency and with volume of air in the lungs [BSRW05], [PoSY01], [WSGS90]. In vivo, one study showed that frequency domain intensity of transmitted white noise (limited to 50-680 Hz) measured over right anterior upper and posterior lower locations of seven healthy men decreased (rolled-off) by approximately 32 dB and 41 dB, respectively, between 50 and 450 Hz [PoSY01]. Maximum attenuation for these locations occurred at 387.3 ± 34.3 Hz anteriorly and at 436.1 ± 41.0 Hz for the posterior site. Attenuations corresponding to these frequencies were 21.5 ± 4.8 dB and 18.2 ± 2.4 dB respectively, averaged across measurements at four volumes between 24% and 80% total lung capacity (*TLC*). Higher volume resulted in higher attenuation for every subject and recording location. Attenuation was measured with respect to sound over the extrathoracic trachea, which was a technique also used in another study involving a more broad band range of input frequencies, i.e. 100-1000 Hz [WSGS90]. That study examined the maximum output frequency of sound transmitted to the posterior right lower lungs of eight healthy men, which was found to be approximately 650 Hz [WSGS90].

Aside from intensity (or attenuation), speed of transmitted sound is also frequency- [LuDW95], [KrWa90] and volume- [PVSM03] dependent. Sound

transmission speed is related to system *memory*, in that both parameters can be estimated via the maximum lag of the cross-correlation between a broad band input and the corresponding system output [Marm04]. For white noise within 300-1600 Hz that was input at the mouths of 11 healthy adult male subjects, it was shown that near the high end of this range sound transmission to the right posterior chest wall (corresponding to the right lower lung lobe, RLL) was nearly three times faster than that of the lower frequency sounds [LuDW95]. Transmission times between high and low frequencies ranged approximately linearly from 1 ms to 3 ms, respectively. Subjects held their breath with their glottis open to maintain lung volume at functional residual capacity (*FRC*). A similar, earlier study by researchers of the same laboratory (as [LuDW95]) using a noise input of 100-600 Hz at the mouths of eight healthy adult males (maintaining *FRC*) suggested that sound energy at higher frequencies travels along the trachea further into the lung than sound energy at lower frequencies, which is coupled from the trachea [WADS92]. That group further postulated that transmission at low frequencies, below around 300 Hz, could be used to provide information concerning the trachea and parenchyma, whereas transmission of higher frequency sound could be used to study smaller airways.

It is important to point out that propagation time, or phase delay, may be greater than one period of the signal being transmitted, which introduces ambiguity in measurement of transmission time, especially at high frequencies [WADS92]. The phase delay may be considered unambiguous at frequencies less than or equal to 100 Hz, where the period is greater than or equal to 10 ms, because the maximum propagation time of sound through the lung has been found to be 10 ms [WADS92]. In addition, just as

bandwidth has been shown to be volume-dependent as discussed above, so too has phase delay. For example, injecting low-frequency polyphonic sound within 70-140 Hz into a subject's supraclavicular space, rather than through the mouth, resulted in transit times that were at maximum, about 13 ms for the posterior RLL region across 21 healthy subjects (adults and children), which decreased to a minimum of approximately 9 ms when lung volume increased to vital capacity [PVSM03].

The studies dealing with lung sound transmission parameters discussed thus far were focused mainly on sound output relative to frequency and lung volume, and did not experiment with varying amplitude of the input sound. The input amplitude range that a physiological system is expected to experience over its natural course of operation is often how the system's *dynamic range* is defined [Marm04]. Dynamic range for lung sounds should be considered in terms of a range of air flows, rather than levels of sound within the lungs per se, because flow within airways produces lung sound [KrWa90]. The absolute lower bound of this range is the flow above which the ratio between lung and background sounds (i.e., signal-to-noise ratio, SNR) is greater than 3 dB [CIGP97], [YaMo05]. Finding this threshold flow may be achieved by plotting lung sound SNR with respect to air flow. The upper bound of the air flow range depends on the particular experimental purpose. It could be defined as a target flow value with a certain tolerance added to it, in experiments involving targeted breathing, or as a subject's tidal flow if breathing at rest is required. Its absolute maximum would be dictated by a subject's anthropometrics (and lung volume) and/or their respiratory state.

Air flow is also involved in defining the *linearity* of the system from which lung sounds emerge. Linearity exists if the superposition principle holds, which most

physiological systems do not strictly obey [Marm04]. However, many can be approximated fairly well by linear models under certain operating conditions. A linear relationship exists between the average power of inspiratory lung sounds and flow within particular flow ranges [Kram84] (overall, the relationship is piecewise linear). Thus, a limited range of flow, for instance a target flow with a certain tolerance gate (e.g., ± 20%), provides a linear operating region, provided that flow ranges are within physiologic, submaximal flows (e.g., tidal flow).

Stationarity and *ergodicity*, like linearity, are also functional parameters that, realistically, need to be examined within particular conditions of operation [Marm04]. Testing for stationarity requires repetition of identical experiments with the same experimental setup preparation at different times; the observed outputs should have matching second-order statistics. Lung sounds are nonstationary as whole signals, but are piecewise stationary within time segments of 100-200 ms [OhPa93]. Ergodicity, on the other hand, is seldom acknowledged in practice and does not usually hold, because it requires perfect invariance of functional properties across many signals obtained under a constant operating condition [Marm04], which would be impossible to achieve with biological data (a stationary process can be non-ergodic [Cohe86]). In terms of stationarity, to comply with past work a window of 100 ms is used for calculation of all features of real and model lung sounds involved in this modeling study.

To summarize, a lung sound model should: cover an adequate bandwidth; take into account frequency- and volume-dependent attenuation; generate a signal of length that exceeds the minimum memory by at least 10 times [Marm04], and that corresponds with requirements for stationarity; and be based on a flow that is within a limited range

and sufficient to produce lung sounds. Each of these physiological parameters and functional properties was taken into account in model development.

5.4 Lung Sound Generation Model

5.4.1 Model Structure

In this study a lung sound generation model was developed using two-dimensional finite element analysis. One airway within the first bifurcation of the RLL, labeled RS6 [vaHP04], was the airway upon which the finite element analysis was based, because velocity profiles for air flow within this airway have been experimentally determined in [vaHP04]. This airway is within the fourth generation of lung airways (counting the trachea as generation zero) [vaHP04] with diameter 0.45 cm and length 1.27 cm [Fung90]. Figure 5.1 shows airway RS6 and its "mother" and "sister" airways along with its velocity profiles, discussed further in Section 5.4.2. A circle was used to model the cross-section, because the velocity profiles found in [vaHP04] were based on rigid-walled cylinders. A circular cross-section does theoretically correspond to that of a healthy subject as discussed in Chapter 2.

5.4.2 Velocity Profiles

Due to the asymmetry of the pattern formed by the airway tree in the lungs, velocity profiles of air flow may be quite complex [vaHP04]. In addition, airways branching from a bifurcation often curve, and branches may be short in length relative to their diameter [vaHP04]. Velocity profiles have been modeled using computational fluid dynamics based on the Navier-Stokes equation for the first seven generations of airways, shown in Fig. 5.1A [vaHP04]. The work of this thesis in modeling lung sounds is focused

on airway RS6, as mentioned above. This airway is the first daughter branch of the RLL [vaHP04]. The branching angle is approximately 60° [vaHP04]. This particular airway was chosen because theoretically it was the most proximal airway to the location from which the lung sounds that were used in the testing and validation of the model were recorded. As well, since RS6 is within the first bifurcation of the RLL, the value of flow within this airway could be calculated using half of the percentage of volume within this airway.

The velocity profiles for this airway (RS6) are shown in Fig. 5.1B – the profile on the left corresponds to the plane of the bifurcation, spanning from the interior to the exterior of the airway's bend, and the profile on the right is the anterior-posterior plane of the airway (normal to the plane of bifurcation) [vaHP04]. At the inner airway wall surface, the flow velocity is zero which is the no-slip boundary condition [VeSt82]. The

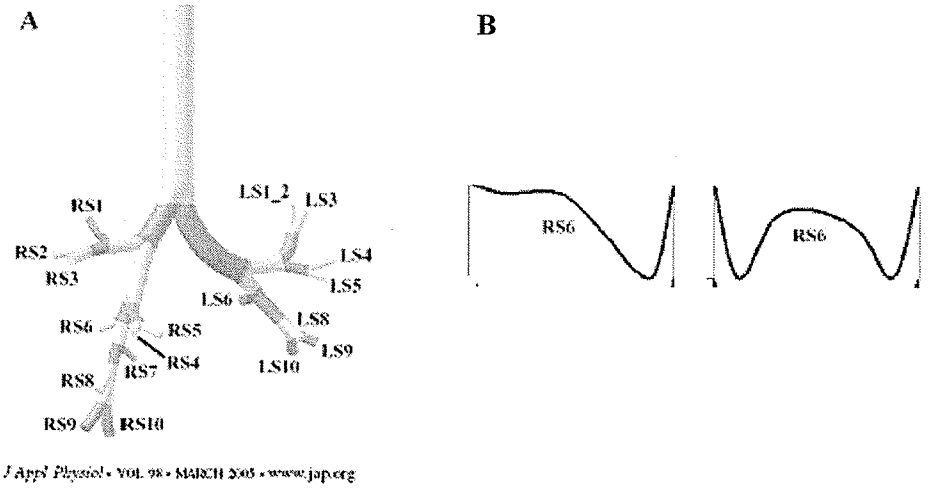

Fig. 5.1: Model of airways, and velocity profiles of airway RS6 [vaHP04]. A (left): Three-dimensional construction of lung airways within right and left lung lobes; RS6 through RS10 correspond to the right lower lung lobe. B: Velocity profiles for the bifurcation plane (left profile) and anterior-posterior plane (right profile) for airway RS6. Vertical axis is normalized velocity and horizontal axis indicates location within airway plane. (*Images used with permission from the American Physiological Society; see Appendix C.*)

experiment upon which the velocity profiles of Fig. 5.1B were based assumed a constant inspiratory air flow in the trachea of 0.5 L/s and smooth inner airway walls that did not expand during breathing. These assumptions were used in the development of the lung sound generation model.

Quantitative approximations to the velocity profiles determined experimentally for airway RS6, as shown in Fig. 5.1B, were found via curve fitting using basic functions (sinusoids and square waves), and smoothing these approximate fits with polynomial functions (Appendix D contains the algorithm used for the approximations). The resulting velocity profiles are shown in Fig. 5.2. (Though theoretically the estimation is accurate, it is not possible to experimentally validate it. Incorporating airways other than RS6 would require quantitative estimation of the velocity profiles of these other airways as well. Given that experimental validation would not be possible, any error in estimation would cumulate across several airways.)

Vortices were found to develop within airway RS6 for the input flow studied [vaHP04]. Theoretically, the reduction of velocity at the airway wall (due to the no-slip condition) along the exterior of the bend in a curved airway reduces pressure at the wall

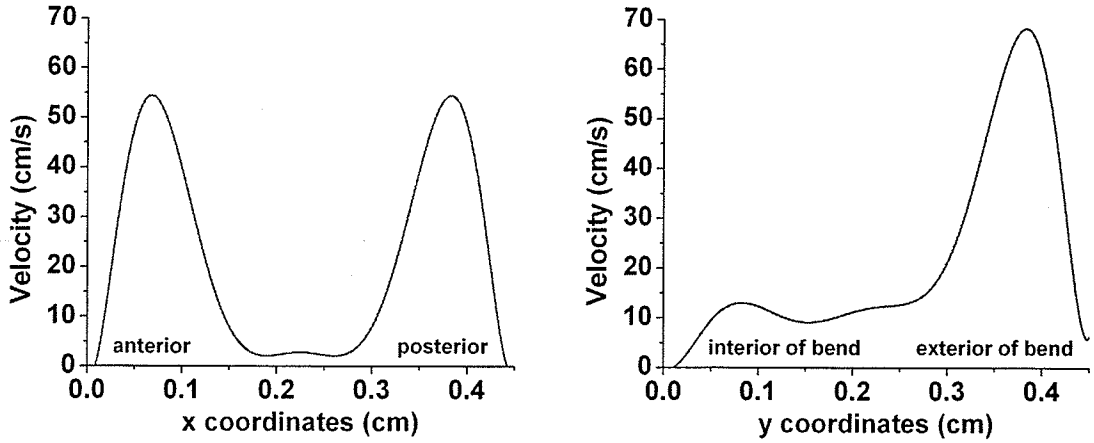

Fig. 5.2: Quantitative velocity profiles found for anterior-posterior (left) and bifurcation planes for airway RS6.

relative to the centre of the airway, and as a result a secondary flow develops in the centre of the airway that moves toward the wall of the exterior of the bend [VeSt82]. This results in a pair of vortices, approximately symmetric about the anterior-posterior plane [VeSt82].

The vorticity of flow depends on the differential circulation per unit of area enclosed in a control surface [Blak86], [VeSt82]. For each element of the closed curve, *dl*, an element of circulation, $d\Gamma$, is determined by the product of the length of *dl* and the tangential component of the velocity of air at element *dl* [VeSt82]. Circulation of a vortex, then, is represented by the integral around a closed curve (the control surface) of an element of circulation, $d\Gamma$ [VeSt82]:

$$\Gamma = \oint_C V \cos(\psi) dl \,. \tag{5.1}$$

The angle ψ is the angle between the tangent to the closed surface at *dl* and the velocity (*V*) stream intersecting the surface at *dl* [VeSt82]. The calculation of sound pressure produced by vortical flow is outlined in the following section.

5.4.3 Sound Generation

Modeling was based on lung sounds resulting from air flow following an airway bifurcation [Blak86]. Calculation of the circulation of vortical flow, Γ (5.1), during inspiration of air in lung airways immediately following a bifurcation may be approximated as $|\Gamma|$ [HaPa79] shown below:

$$|\Gamma| = 2\pi V r \sin(\alpha) \,. \tag{5.2}$$

Here, $|\Gamma|$ depends on *V*; the radius of the airway, *r*; and half of the branching angle, α. For the airway used in this work the radius was 2.25 mm (based on the diameter mentioned in

Section 5.4.1) and the branching angle was 60°. Velocity profiles for the anterior-posterior and bifurcation planes were discussed above and shown in Fig. 4.2

The acoustic fluid equation depends on the velocity potential, Φ, which in turn depends on vortical circulation [AuSr06]:

$$\Phi = \frac{\Gamma}{2\pi}\theta \;\cong\; \Phi = \frac{|\Gamma|}{2\pi}\theta \;. \tag{5.3}$$

The value of θ is the polar coordinate of a nodal location. The acoustic equation may now be defined [Bath96]:

$$\nabla^2\Phi = \frac{1}{c^2}\ddot{\Phi} \;, \tag{5.4}$$

where c is the speed of sound in air, calculated as 35300 cm/s [Nave05]. The boundary conditions for (5.4) are based on the momentum and continuity equations of motion of an ideal gas [Bath96], [Quin87],

$$\rho\dot{V} + \nabla\mathbf{p} = 0 \quad \text{(Momentum)}, \tag{5.5}$$

$$\beta\nabla V + \dot{\mathbf{p}} = 0 \quad \text{(Continuity)}. \tag{5.6}$$

The constant β is the bulk modulus of air and is defined as $c^2\rho$ [Nave05], where $\rho = 1.14 \cdot 10^{-3}$ g/cm^3 (i.e., the density of air) [CiSF02]. There are two boundary conditions associated with these equations, which are found by defining V and sound pressure, $\mathbf{p}$, in terms of Φ [Bath96]:

$$V = \nabla\Phi \quad \text{and} \quad \mathbf{p} = -\rho\dot{\Phi} \;. \tag{5.7}$$

Change in pressure across an airway, Δp, that occurs during breathing can be approximated using the flow equation for non-laminar flow [Fung90],

$$\dot{Q} = \frac{1}{Z(N_R)}\frac{\pi d^4}{128}\frac{\Delta p}{\mu L} \;, \tag{5.8}$$

where $\mu = 186 \cdot 10^{-6}$ dyne s/cm^2 for air (viscosity) [MoIn68], d and L are the airway diameter and length respectively (defined above), and $Z(N_R)$ for inspiratory flow at a bifurcation is [Fung90],

$$Z(N_R) = \gamma\left(\frac{d}{L}N_R\right)^{1/2} . \tag{5.9}$$

The value of γ for airway RS6 was found experimentally as 0.175 [vaHP04]. The Reynolds number N_R may be found using,

$$N_R = \frac{\bar{V}d}{\nu} , \tag{5.10}$$

in which $\bar{V}$ is the mean velocity and ν is the kinematic viscosity of the gas within the airway, which is 0.163 cm^2/s for air [West77]. The Reynolds number is a dimensionless number that is used to provide indication of deviations from laminar flow (discussed in Chapter 3). For instance, the critical Reynold's number, N_{Rcrit}, for transition from laminar to turbulent flow on inspiration in the trachea at resting breathing rate (approximately 15 breaths/minute [West74]) is about 2300 [Fung90]. Above about N_R = 420, infinitesimal disturbances in respiratory flow grow with time [PeSS71].

As mentioned above, a flow of 0.5 L/s was input in the trachea for modeling [vaHP04]; air flow within lung airways beyond the trachea will be a fraction of this value, according to the proportion of lung volume of each airway. Since airway RS6 is an airway leading into the RLL, its flow may be estimated using the percentage of lung volume provided by the RLL, which is approximately 22.5% [HoPH00]. This results in a (mean) velocity within airways of the first bifurcation of the RLL of,

$$\bar{V} = \frac{Flow}{Area} = \frac{1}{2}\frac{(500\text{cm}^3/\text{s})0.225}{2.6\text{cm}^2} = \frac{1}{2}43.27\text{cm/s} = 21.64\text{cm/s} . \tag{5.11}$$

After finding values for N_R and $Z(N_R)$ and rearranging (5.8), Δp may be determined as:

$$\Delta p = \frac{\dot{Q} Z(N_R) 128 \mu L}{\pi d^4} = \frac{(56.25)(0.805)(128)(0.000186)(1.27)}{\pi (0.45)^4} = 10.63 \text{ dyne/cm}^2. \quad (5.12)$$

In Pascals (Pa), Δp = 1.063 Pa. The sound pressure produced in airway RS6 represents a fraction of this theoretical pressure difference. Experimentally, the viscous pressure drop in airways of the fourth generation was found to be approximately 1.1 Pa [vaHP04], which corresponds well with this theoretical value.

5.4.4 Formulation of Finite Element Analysis

Due to the presence of curvature in an airway cross-section, linear triangular elements were the elements of choice. Though it has been found that for sound produced by flow in ducts, quadratic quadrilateral elements produced more accurate results than linear triangular and quadrilateral elements [Quin87], quadrilateral (and higher order) elements are not ideal for time-dependent field problems [Sege84]. Nodal locations were chosen by forming a grid of squares and using corners as nodes, and Delaunay triangulation was used to form the finite elements, shown in Fig. 5.3 and Fig. 5.4.

Galerkin's method to solve the acoustic equation (5.4) begins with defining the residual integral per element, *e*, as [Sege84],

$$\{R^{(e)}\} = -\int_A [N]^T \nabla^2 \Phi dA + \int_A [N]^T [N] \left(\frac{1}{c^2}\right) \{\ddot{\Phi}^{(e)}\} dA. \quad (5.13)$$

The matrix $[N]$ contains the shape functions of the chosen element, which serve as the weighting coefficients [Sege84]. Shape functions for triangular elements mapped to the natural coordinate system (ξ, η) were used. Evaluation of the second term in $\{R^{(e)}\}$ involves the consistent formulation [Sege84] for time-dependent field problems, which requires representing this term as,

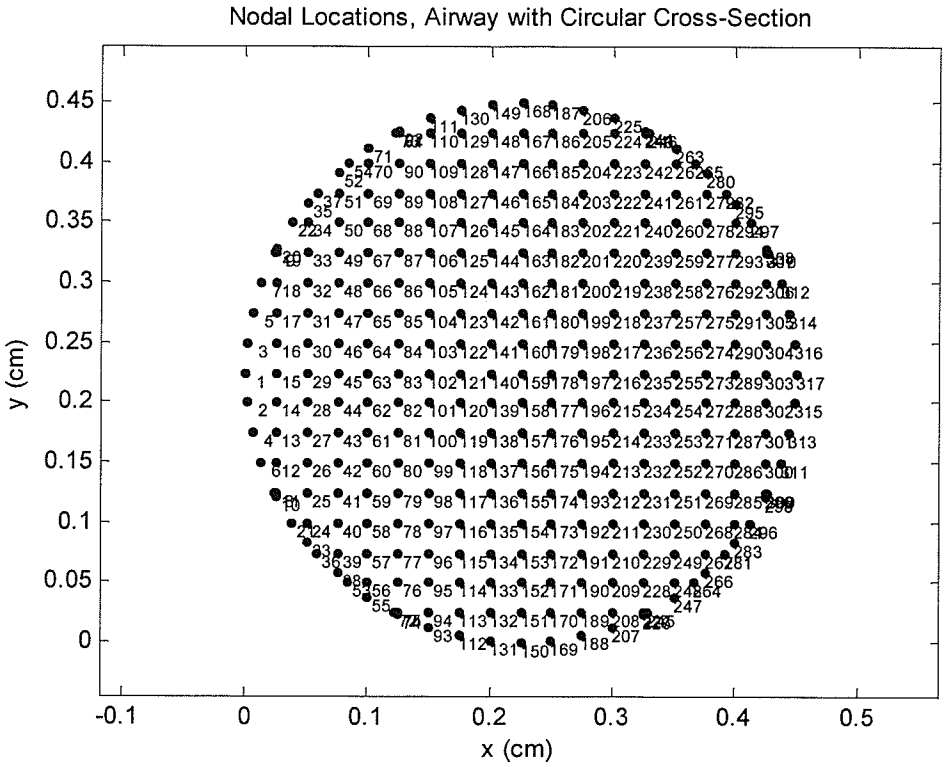

Fig. 5.3: Nodal locations for finite element model of sound generation.

$$\int_A \left(\frac{1}{c^2}\right)[N]^T[N]dA\{\ddot{\Phi}^{(e)}\} = [c^{(e)}]\{\ddot{\Phi}^{(e)}\}, \tag{5.14}$$

in which $[c^{(e)}]$ is defined as [Sege84],

$$[c^{(e)}] = \frac{1}{c^2}\sum_{j=1}^{m}\sum_{k=1}^{n} w_j w_k N^T(\xi_i,\eta_k)N(\xi_i,\eta_k)|J(\xi_i,\eta_k)| \ . \tag{5.15}$$

The weight, w, is defined as per the Gauss-Legendre integration method and J is the Jacobian matrix [Sege84]. The first term of (5.13) may also be re-written, as $[k^{(e)}]\{\Phi^{(e)}\}$. Applying the direct stiffness procedure to both re-defined terms of $\{R^{(e)}\}$ produces the general formula to be solved via time-dependent field analysis [Bath96], [Sege84],

$$[C]\{\ddot{\Phi}\} + [K]\{\Phi\} = 0 \ . \tag{5.16}$$

Prior to proceeding with the expansion of this equation in order to formulate an algorithm that may be used to solve for $\{\Phi\}$, it is important to note that $[k^{(e)}]$ is [Sege84],

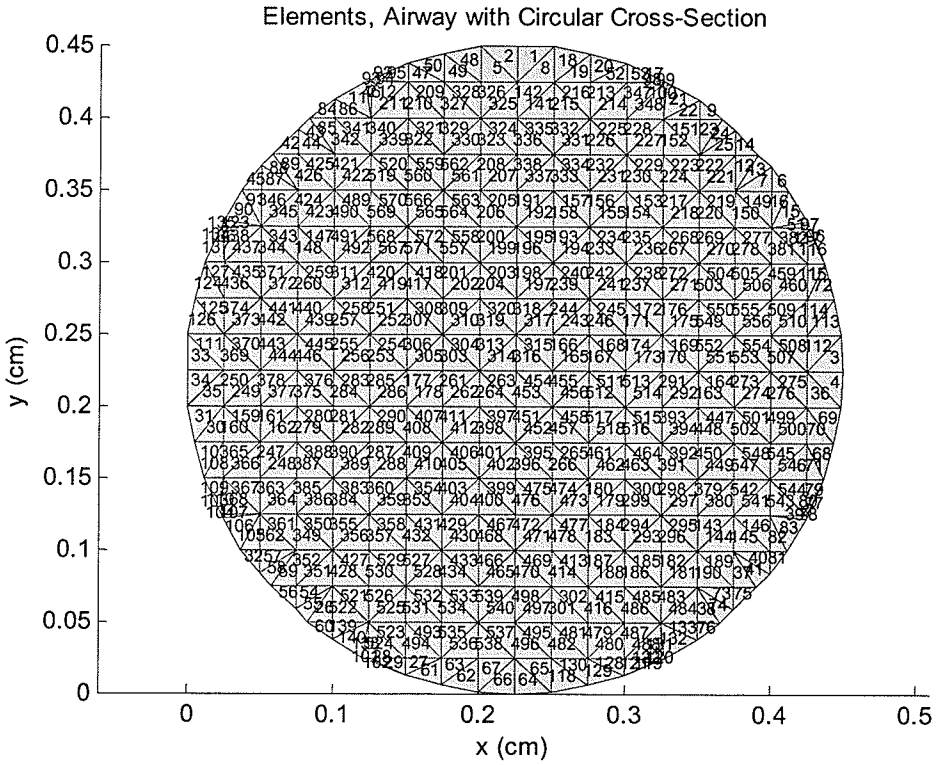

Fig. 5.4: Triangulation of airway cross-section for finite element model of sound generation.

$$\left[k^{(e)}\right] = \int_A [B]^T [D][B] dA \ , \tag{5.17}$$

where the gradient matrix $[B]$ has the general form [Sege84],

$$[B] = [J]^{-1} \begin{bmatrix} \dfrac{\partial [N]}{\partial \xi} \\ \dfrac{\partial [N]}{\partial \eta} \end{bmatrix} , \tag{5.18}$$

and for this study, the matrix $[D]$ is defined as,

$$[D] = \begin{bmatrix} 1 & 0 \\ 0 & 1 \end{bmatrix}, \text{ or } D_x = D_y = 1. \tag{5.19}$$

Now, $[k^{(e)}]$ may be found using,

$$\left[k^{(e)}\right] = \sum_{j=1}^{m} \sum_{k=1}^{n} w_j w_k B^T(\xi_i, \eta_k) DB(\xi_i, \eta_k) \left| J(\xi_i, \eta_k) \right| . \tag{5.20}$$

Using the central difference theorem [Bath96] to determine $\{\ddot{\Phi}\}$ and $\{\dot{\Phi}\}$, (5.16) may be rearranged to provide a value for $\{\Phi\}$ ($\{\Phi\}$ is set to $\{\Phi\}_{2\Delta t}$ in this study):

$$\{\Phi\}_{2\Delta t} = [H]^{-1}[C](2\{\Phi\}_{\Delta t} - \{\Phi\}_0), \text{ where } [H] = [C] + \Delta t^2[K]. \qquad (5.21)$$

The initial values for $\{\Phi\}_0$ were set to zero. This assumption may be justified by considering the flow on which velocity profiles were based (Fig. 5.2), i.e. 0.5 L/s, which is within a low range (tidal flow) for healthy adults [GHPM05] and also school-aged children (see Appendix B for examples). It is reasonable to assume that until flow (at the mouth) reaches approximately 0.5 L/s, there is very little sound, and in this thesis sound pressure and hence Φ (according to (5.7)) may be specified as zero initially. For $\{\Phi\}_{\Delta t}$, (5.3) has been used to calculate the initial value per node.

In order to incorporate time-dependence in the model, the nodal positions varied. An approximation to the displacement has been obtained by adding fractional Brownian motion (fBm) [Duec03], [EmMa02] to the nodal positions using fBm synthesized by the Cholesky technique [Duec03], [EmMa02] (divided by 1000). Chapter 4 provided an outline of fBm and this particular type of fBm. A value of 0.7 was used as the Hurst exponent, H, because this value corresponds well with the average H found for lung sounds within 200 ms [GnMo05], and also because Cholesky fBm is stationary for this H value at the number of samples within this period of time [Duec03], i.e. 2048 samples (corresponding to the recorded lung sounds used in the thesis work).

The length of time series (or number of iterations/changes in nodal location per node) used in this study has been chosen by considering human breathing patterns. During a normal inspiratory breath, flow accelerates, reaches a plateau, and decelerates, over approximately one second [GnKP05]. The plateau is usually quite short, on the

order of a few hundred milliseconds, depending on a subject's individual breathing pattern. To allow enough samples to obtain meaningful results, 10240 iterations were used, which corresponds to one second when the sampling frequency is 10240 Hz; this was the sampling frequency that was used to acquire the data that were used for model validation (which were employed in previous work [GnKP05], [GnMP05b] and presented in Chapter 6). A theoretical time step of $\Delta t = 0.0001$ s was used, which is approximately equivalent to 1/10240. Using (5.7) to calculate sound pressure per node per time step formed a time series representing the model-generated sound pressure.

Validation of the model results was achieved by comparing the model time series and PSD estimates with real lung sound data acquired from healthy children and children with poor lung function and/or asthma at flows including 0.5 L/s (see Chapter 6). Since the lung sounds that are available for use have been recorded on the surface of the chest, while the model provides lung sounds generated within airways, sound transmission from airways to the body surface has also been modeled, as outlined in the next section.

5.5 Lung Sound Transmission Model

5.5.1. Background

Chapter 3 presented general information pertaining to lung sound transmission. Further review regarding respiratory sound transmission reveals that higher frequency sound has been found to transmit at higher speeds than low frequency sound through components of the chest [LeSe96], [WADS92]. It has been suggested that at high frequencies, the inertia of airway walls causes sound to travel further inside the lumen [WSGS90] whereas low frequency sound induces wall motion and is thus coupled more

directly to the parenchyma [WADS92]. These latter postulations were made after experimentation with the acoustic circuit model [WSGC89] mentioned in Section 5.2.

Different respiratory conditions may influence time- and frequency-domain characteristics of lung sounds as they pass through the lung parenchyma, but other thoracic tissues such as muscles, bone, fat and skin likely have little effect on lung sounds, other than overall attenuation [WADS92]. This is due to the speed of sound wave transmission through these latter materials relative to the frequency content of lung sounds near their source, which has been reported as roughly 750 Hz when measured internally near lung airways with an esophageal microphone [MDKP97]. Considering the lowest sound transmission speed of the tissues mentioned above, that of fat at 140000 cm/s [Duck90], [WoWh86], and dividing this by 750 Hz, the resulting minimum wavelength of sound through tissue surrounding the parenchyma is 188 cm. This value is several times larger than the thickness of tissues, and the distance between the lung airways in which sound is produced and the chest wall of a typical human – for instance, the radial distance between the inner trachea and chest wall has been suggested to be 10 cm [GoJC89], [WSGC89].

As shown in Table 5.1, speed of sound through the parenchyma actually changes with inflation – it has been shown that it is maximally 25000 cm/s in the deflated lung and rapidly decreases along a parabolic curve to a minimum of 2500 cm/s at total lung capacity [BSRW05]. The air flow at which lung sound generation was modeled, i.e. 0.5 L/s, is such that the volume of air added during inspiration at this flow will not be much greater than the *FRC*. The speed of sound through the parenchyma at *FRC*, approximately 3500 cm/s [BSRW05], is therefore the speed that will be referred to in

Table 5.1
Physical Properties of Tissues Pertaining to Lung Sounds [Duck90], [WoWh86]

Material	Density, ρ (g/cm^3)	Water (% mass)	Sound, c (cm/s)	Thickness (cm)
Rib bone	1.410	22.4	210000	1.4
Skin	1.110	65.4		0.3
Blood	1.060	79		N/A
Lung-deflated	1.050	79.8	25000	
Skeletal muscle	1.050	74.1	150000	1.4
Airway wall (smooth muscle)	1.040	74.1	150000	0.1
Water	0.99337	100	152400	N/A
Adipose tissue	0.950	21.2	140000	1.0
Lung-TLC	0.260	79.8	2500	
Air	0.00114		35300	N/A

lung sound transmission modeling. The resulting minimum wavelength of lung sound for this speed is 4.7 cm, a reasonable theoretical value. Thus, only the parenchyma's influence on sound will be considered in modeling the transmission of the lung sounds that were generated as described in the preceding section.

Scatter of sound is another consideration in sound transmission – elastic scattering occurs when the acoustic pressure waves generated by air flow are incident upon the elastic airway wall, resulting in vibrations in the wall [Ihle98]. It is known that scatter loss increases with frequency, and is 10-15% for ultrasound frequencies in soft tissue [Duck90]. Thus, at audio frequencies, scattering in the body is likely not of significant concern and was not considered in modeling.

Sound transmission through lung parenchyma has been modeled by a number of researchers using a few different approaches. A frequently cited lung sound transmission model [WSGC89] was developed via an acoustic circuit constructed to simulate transmission of broad band sounds from the mouth to sites over the trachea and posterior chest. This one-dimensional circuit model was outlined in Section 5.2. Using a white noise input, band-limited over 100-600 Hz, the PSD of the model output as well as that of

sound transmitted through the lungs of four healthy male subjects were measured at the trachea and chest-wall sites. The PSD curves roughly matched qualitatively, but no quantitative evaluation was presented. The model results also indicated that the air/water composition of the parenchyma attenuated the transmitted signal increasingly as the proportion of air increased; the authors noted that this phenomenon has been found in past work experimentally. Despite the realistic results the authors also acknowledged the limitations of their model. Note that the use of white noise may lead to erroneous results because the speed of sound from within airways to the chest is frequency-dependent [LeSe96]; this sound transmission decreases with increasing frequency [GoJC89], [WSGS90] as discussed in Section 5.3. Furthermore, the route (a tube) from the acoustic driver to a subject's mouth affects the input sound by introducing resonances.

5.5.2 Model Formulation

A. Framework

Rather than using an aggregate of air and water with one alveolar size, which is another limitation of the aforementioned model [WSGC89], a two-medium representation of lung parenchyma employing air and tissue has been used to study the distortion of pressure wave history by the parenchyma [GrWN02] one-dimensionally, and was used in this present work also. In that model, a mass-spring chain system approximates a biperiodic stack of tissue (t) and air (a), with composite elastic modulus E and density ρ [GrWN02], [WSGC89] acting as equivalent spring constant and mass, respectively:

$$K = \left(\frac{h_t}{E_t} + \frac{h_a}{E_a} \right)^{-1}, \text{ and} \tag{5.22}$$

$$m = \rho_t h_t + \rho_a h_a . \tag{5.23}$$

The proportion of air and tissue in the composite parameters, h_a and h_t, may be chosen to correspond to regions of the parenchyma. The pressure, $p_n(t)$, per mass-spring combination, n, is based on the equations of motion for the mass-spring chain, i.e. [GrWN02],

$$m\ddot{u}_1 + K(u_1 - u_2) = p_1(t) \text{ for the initial pressure, and} \tag{5.24}$$

$$m\ddot{u}_n + K(u_n - u_{n-1}) + K(u_n - u_{n+1}) = 0, \quad \forall n = 2,3,\ldots, \tag{5.25}$$

where u_n is the axial displacement of the n^{th} mass. Pressure in the n^{th} spring may be found using

$$p_n = K(u_n - u_{n-1}). \tag{5.26}$$

Pressure in the n^{th} mass, which was used in the study, is [ElRa97], [GrWN02]

$$p_n(t) = \delta_{n1} p_1(t) + 2n \int_0^t \frac{J_{2n}[2\omega_0(t-\tau)]}{(t-\tau)} p_1(t) d\tau, \tag{5.27}$$

where, J is the Bessel function of the first kind, and δ_{ij} is the Kronecker delta [GrWN02]. In discrete form, the pressure may be calculated as [ElRa97],

$$p_n(t) = p_{n-1}(t) - \frac{\sigma_n(t)}{K}, \text{ with} \tag{5.28}$$

$$\sigma_n(t) = 1 - \sum_{k=0}^{n-1} \frac{2^{n-k} n!}{k!} \frac{J_{n+k}(\beta t)}{(\beta t)^{n-k}}, \ \beta = 2\omega_0, \ \omega_0 = \sqrt{K/m}. \tag{5.29}$$

Based on the n^{th} mass pressure formulation (though the value of n was not indicated), it was shown that with increasing alveolar size (i.e., h_a), the cut-off frequency above which sounds do not propagate in the lung periphery decreased [GrWN02]. This suggests that sound propagating from central airways to the lung periphery will lose most of its high frequency energy through the first few airways, because their size is large with respect to alveoli which increase in presence towards the lung periphery. When lung

volume and hence the sizes of airways decrease, the passage of high frequency lung sounds would theoretically increase, and as mentioned above this has been found experimentally [BSRW05]. These rather meaningful results using one-dimensional n^{th} mass pressure prompted the application of the mass-spring sound pressure propagation model to the study of lung sounds.

B. Statistical Component: Pareto Distribution

In order to suitably incorporate the structure of the parenchyma, it is important to consider the distribution of airways and any pattern that may be deduced from their natural organization. It is known that there are many more airways of small diameter than there are those with large diameter within the lung [Weib84]. Statistically, this phenomenon may be described using the Pareto distribution [BaNe03]. The Pareto distribution was named after Vilfredo Pareto (1848-1943), an Italian-born Swiss professor in economics, who invented it to describe income distribution [JoKo70]. In its original form, it stated the number of people, Y, whose income was at least b, as $Y = Ab^{-k}$ [JoKo70], [RoLo86], in which k is called the shape parameter, and A is a proportionality constant. In this context of the Pareto distribution, increasing k would result in decreasing the number of people with an income greater than b.

The generalized form of the Pareto distribution produces a distribution with a long right tail and it is sometimes referred to as heavy-tailed. In this distribution, the probability that a random variable X is greater than a value x, which has a (necessarily positive) minimum value x_m, is [BaNe03],

$$P(X > x) = \left(\frac{x}{x_m}\right)^{-k}, x \geq x_m, \tag{5.30}$$

and the probability density function (in general form) is,

$$f(x) = \frac{k\varphi^k}{(x-\xi)^{k+1}}, x \geq \xi + \quad , \varphi > 0. \tag{5.31}$$

The parameters ξ and φ in (5.31) are known as the scale and location parameters, respectively, and k is called the shape parameter as indicated above. Changing the scale parameter results in changing $f(x)$ (5.31) such that $f(x)$ increases as ξ decreases. The location parameter allows measurement of X from a non-zero value [RoLo86]. Increasing the value of k causes the values of the random numbers of a (generated) Pareto distribution to increase per (5.31), thus increasing x_m, resulting in a decrease in the probability shown in (5.30). Figure 5.5 shows examples of the generalized Pareto distribution for different values of the parameters, obtained using the "gprnd" and "gppdf" function in Matlab®.

Referring back to (5.23), in this study the Pareto distribution provided values of the proportion of tissue h_t, (and h_a using 1-h_t), by normalizing the random variables. Based on the information presented above with regard to k, increasing k would increase tissue proportion h_t. Since airway wall thickening is a known condition of asthma

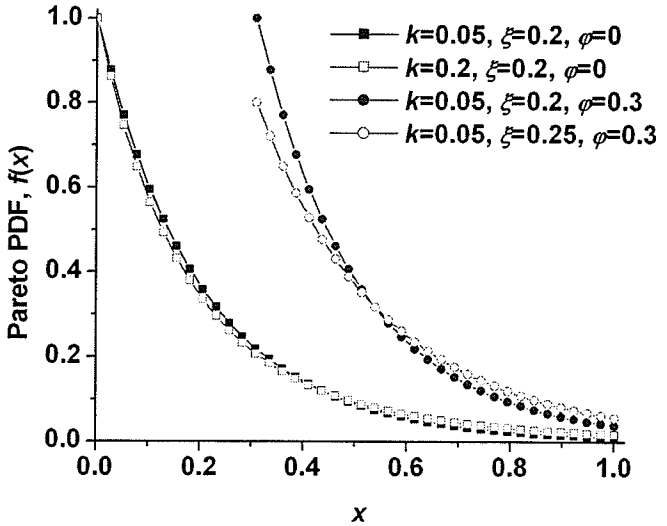

Fig. 5.5: Effects of changing parameters of the Pareto distribution (axes are normalized).

[CPKH00], an increase in tissue proportion could theoretically correspond to an asthmatic state. The other parameters, ξ and φ, should be set such that their sum is less than a minimum value [BaNe03], see (5.31). In terms of lung airways, this minimum may be thought of as minimum airway diameter, i.e., that of alveoli, which has been found to be 0.2 mm on average [ONJK04].

C. Further Details

The model for lung sound transmission has been formulated by incorporating h values obtained from the Pareto distribution in the n^{th} mass pressure formula (5.27). The values of ρ for air and tissue used in the model are presented in Table 5.1, and values of E are E_a = 142.05x10^4 dyne/cm^2 and E_t = 6.5625x10^8 dyne/cm^2 calculated using $E = c^2\rho$ [Fung90]. Due to the presence of the factorial in (5.29), the maximum limit for n is 169; above this value, the first ratio in the summation results in "NaN" because the factorial of any number beyond 170 is considered infinity in Matlab®. Intuitively, because there are roughly 300 million alveoli distributed on approximately 14 million ducts in the average lung [Weib84], the number of layers of mass-spring chain elements representing different airway and alveolar sizes can be quite high. Results presented subsequently are therefore based on the output of the lung sound transmission model at the maximum n = 169.

5.6 Optimization of Model Parameters: The Genetic Algorithm

In system modeling, global optimization of model parameters in an automated manner may be performed using deterministic or stochastic methods [LiRh98]. Each type of method operates based on an objective function of the model output, which minimizes (or maximizes) when optimal model parameters (and hence the model output) have been

reached. Parameters are drawn from a search space that ideally includes the global optimum [Vinc03]. Deterministic optimization methods involve analysis of the deterministic mathematical characteristic of a problem studied [LiRh98]. These techniques are often referred to as gradient-based, because the optimization procedure minimizes an objective function that is continuously differentiable, and requires knowledge of its gradient [Bhat05]. Stochastic, or direct search, methods may be applied to objective functions that are non-differentiable or discontinuous (i.e., functions that do not possess "nice" mathematical properties) [HoJK96]. These methods incorporate a stochastic component in the parameter search by drawing random samples from regions of the search space where parameters that improve optimization values are found (in an iterative process) [Vinc03]. Initialization for both deterministic and stochastic optimization methods requires some knowledge of parameter bounds, at least sufficient to make a reasonable guess [Bhat05].

When a clear advantageous optimization method does not exist, a genetic algorithm is a logical choice [Vinc03]. Genetic algorithms are direct search techniques [DuHS01], [HoJK96], [Vinc03]. Though it is difficult to make general statements with regards to the performance of a genetic algorithm because its operation is highly dependent on the application [DuHS01], it has been shown that in general, a genetic algorithm stores and exploits more information about a search space through its iteration than many other heuristic search techniques [Vinc03]. Several areas of a search space are concurrently investigated by a genetic algorithm, which reduces the probability of becoming trapped in local (rather than global) optima [Vinc03].

The process of natural evolution inspires the operation of a genetic algorithm [Vinc03], and the components of genetic algorithms are duly named [Mich96]. The collection of candidate parameters is generally referred to as a *population*, and members of the population are called *individuals* or *chromosomes* [Mich96]. Each chromosome contains one or more model parameters, known as *genes*, which are usually encoded, most commonly using binary, Gray, or integer coding [Vinc03]. Permissible gene values are contained within *allele* values, which provide bounds for initialization and searching [Vinc03]. The particular combination of genes within a chromosome is termed the *genotype*, and the resulting model output the *phenotype*. Once an encoding scheme has been chosen, an initial population may be formed by randomly sampling from within the allele bounds (a *mating pool* of sorts) [DuHS01], [Vinc03]. Populations typically contain between 30 and 100 members [CFPF94].

Objective function values are calculated for each phenotype, and results are ranked, thereby assigning a level of *fitness* to chromosomes [Vinc03]. Selection of which chromosomes to retain is generally proportional to fitness, with high probability of selection assigned to high-fitness chromosomes, and in most cases there is also some allowance for inclusion of low-fitness chromosomes in order to preserve diversity [DuHS01]. A value known as the *generation gap* dictates the number of chromosomes to retain [CFPF94], leaving at least one *parent* chromosome on which to base a new population [DuHS01]. To replenish a population, the remaining gene(s) may be replicated; inverted; or may undergo crossover. The crossover genetic operator involves mating two parent individuals by choosing a random split point along one of them and interchanging the regions beyond the split point between the two, thus creating two

offspring. If more than one pair of parent individuals exists, crossover is applied to a random selection with a likelihood, P_{co}, of between 0.6 and 1.0 [BeBM93]. To maintain diversity and allow for full exploitation of the search space [Vinc03], mutation may be applied to the offspring [BeBM93]. This genetic operator entails changing values within a chromosome, with each value having a low probability, P_{mut}, of being mutated. (It is important to point out that if P_{co} and P_{mut} values are too low, exploration of the search space becomes computationally costly (and long) [DuHS01], [Vinc03]. On the other hand, values that are too high cause excess exploitation of selected regions of the search space, which may prevent more optimal regions from being discovered.) The ranking procedure is iteratively repeated, with new generations created per iteration, until a desired level of fitness (or objective value) is reached. Alternatively, it is common to pre-define a maximum number of generations [CFPF94].

In this study, in order to determine appropriate parameter bounds (or alleles), a manual exploratory analysis of model parameters was performed, as advocated in [Vinc03]. The objective function was the MSE between features of real and model lung sounds (i.e., PSD as indicated above). Per subject, the 10 lowest MSE values per feature were determined, and parameters corresponding to features having MSE values within the "top 10" were used to provide bounds. Parameter bounds for k, ξ, and φ will be presented in Chapter 6.

The genetic algorithm was implemented using the Genetic Algorithm Toolbox designed for Matlab® [CFPF94]. Binary encoding was used, with 20 bits per gene. The initial population contained 30 individuals, and there were 10 generational loops. Values

of P_{co} and P_{mut} were 0.7 and P_{co}/L_{ind} respectively (where L_{ind} is the number of bits in an individual). These values were chosen as per examples in [CFPF94].

5.7 Summary

This chapter provided the framework for modeling generation and transmission of lung sounds, and optimization of the model. To reiterate, (5.16) was used to evaluate (5.4), with initial values dictated by (5.3), incorporating velocity profiles corresponding to 0.5 L/s found in [vaHP04] (quantified in our work using (5.11)) and an approximation of vortical flow circulation $|\Gamma|$ per [HaPa79]. This evaluation provided the derivative of velocity potential, $\{\dot{\Phi}\}$, which was then used in (5.7) to calculate sound pressure per node. This process was repeated 10240 times, with nodal location changing per iteration by the addition of values from a fBm sequence to account for time variation. Per time step, generated sound pressure was averaged across all of the nodes of the airway cross-section because the airway is relatively small with a radius of 0.225 cm. This resulted in a 10240-sample signal, which was used as input to the transmission portion of the model, described in Section 5.5.

CHAPTER 6

Lung Sound Model Validation and Discussion

"Despite two centuries of experience with pulmonary auscultation, the physical basis of the acoustic phenomena of the human respiratory system has not been precisely elucidated, primarily because the anatomy of the lung is complex, the morphologic features of the respiratory system are variable, and there is little opportunity for analysis in vivo." [KoKT98]

6.1 Introduction

This chapter deals with experimental validation and results of the lung sound model presented in Chapter 5. The output of the lung sound generation model was used as input to the transmission model, and the parameters of the transmission model were then optimized using a genetic algorithm as outlined in Chapter 5. The objective function was the mean square error (MSE) between frequency domain features of the model lung sounds relative to those of lung sounds acquired over the posterior right lower lobe (RLL) of nine healthy children. Time domain features were examined also, but not used in the objective function. Features included fractal dimensions (time domain) and average power spectral density (PSD) over 70-200 and 450-800 Hz. The usefulness of the theoretical model as a diagnostic tool was assessed by tuning the model using RLL lung sounds from nine children with poor lung function and/or asthma (five asthmatics).

6.2 Data Employed in Model Validation

Lung sounds were recorded from two groups of children. Group 1 consisted of nine healthy children (two females) with normal lung function [GnKP05]. Group 2 included children who were referred to the Winnipeg Children's Hospital for pulmonary function testing (PFT) and bronchodilator (BD) challenge [GnMP05b]. Lung sounds

from nine children in Group 2 who had either previously been diagnosed with asthma (five children, one female) or who had lung function parameters (defined below) measured at less than 80% of predicted values at baseline (four children, two females) were used in this study. Table 6.1 shows anthropometric and PFT data. Forced expiratory volume in one second (FEV_1); the ratio between FEV_1 and forced vital capacity (FVC), FEV_1/FVC; and the forced expiratory flow at which 50% of volume has been expired (FEF_{50}) were significantly different ($p < 0.05$, t-test) between Group 1 and Group 2 children (at baseline).

Lung sounds were recorded over the right and left lower lung lobes (RLL, LLL respectively) posteriorly. Each subject wore a nose clip and breathed through a three-inch cardboard mouthpiece connected to a pneumotachograph (Biopac) at flows gradually increasing from 7.5-30 mL/s/kg over 50 s, followed by a 5 s breath hold (to provide noise reference). Four recordings were obtained from each subject. Group 1 subjects provided two successive recordings (trials 1H and 2H), rested for 15 minutes, and provided two more successive lung sound recordings (trials 3H and 4H). Lung sounds were recorded from Group 2 subjects before (trial 1A) and after (trial 2A) spirometry, and 15 minutes following inhalation of BD medication (trial 3A), with another recording obtained after

Table 6.1
Anthropometric and Lung Function Data for Study Subjects in Groups 1 and 2

Group	Weight (kg)	Height (cm)	BMI (kg/m^2)	Age (y)	*FEV_1 ($\%_{pred.}$)	ΔFEV_1 ($\%_{improv.}$)	*FEV_1/FVC ($\%_{pred.}$)	*FEF_{50} ($\%_{pred.}$)	ΔFEF_{50} ($\%_{improv.}$)
1 (H) $n = 9$	50.7 ± 12.9	156.7 ± 8.1	20.4 ± 3.5	11.9 ± 1.4	93.4 ± 13.7	N/A	84.3 ± 5.0	95.7 ± 22.7	N/A
2 (A) $n = 9$	46.5 ± 19.5	151.7 ± 17.9	19.6 ± 4.8	12.3 ± 3.2	77.2 ± 17.9	6.6 ± 7.5	71.6 ±11.3	58.7 ± 35.1	30.4 ± 19.5

* indicates significant difference ($p<0.05$) between the two groups
%pred. – percent of predicted value; %improv. – improvement in %pred. post-bronchodilator treatment (applies to Group 2 subjects only)

subjects performed spirometry post-BD (trial 4A). For Group 2 subjects, lung sounds were recorded in the PFT lab rather than in the Respiratory Acoustics Laboratory at the Manitoba Institute of Child Health, where the lung sounds of Group 1 subjects were recorded.

Only the post-PFT, pre-BD lung sounds from Group 2 were used, which were the second-trial recordings, because Group 1 did not undergo BD treatment. Group 1 provided two successive lung sound recordings post-PFT, and the second trial was used in this work also. As well, the RLL lung sounds were used in model validation from both groups.

As discussed in Chapter 5, model-generated lung sounds were based on one flow, i.e. 0.5 L/s. A weight-standardized flow of 15 mL/s/kg ± 20% was chosen so that flow from all subjects was within a ± 20% range of 0.5 L/s (a trade-off between conforming to the model's flow and allowing comparison between subjects). This resulted in flows with mean ± standard deviation (SD) of 0.76 ± 0.19 L/s for Group 1 and 0.70 ± 0.29 L/s for Group 2. PSD of inspiratory lung sounds corresponding to these flows per 100 ms (Hanning) window (shifted by 50 ms) was obtained per subject (using Matlab®). Frequency and signal-to-noise ratio (SNR) were obtained at every 5 dB step of lung sound PSD beginning with 10 dB and decreasing to -60 dB. Frequency and PSD at which SNR was greater than 3 dB were compared statistically. Characteristics of most interest were frequency and PSD at lower (low) and upper (up) bounds (f_{low}, P_{low}, f_{up}, P_{up}) and also the maximum SNR and corresponding frequency (f_{max}, SNR_{max}).

6.3 Comparison between Model and Real Lung Sounds

Figure 6.1 shows a block diagram of the lung sound model components. Both frequency- and time-domain characteristics provided sources of features for comparison between the output of the lung sound model and recorded lung sounds. In the frequency domain, the PSD, calculated as indicated above, was used. The Katz fractal dimension (KFD), which has been shown to be useful for classification of lung sounds before and after bronchial constriction in children in one of our studies [GnMP04], was the time domain feature. Details of its calculation were outlined in Chapter 4. It was also calculated within 100 ms windows, shifted by 50 ms. In order to compare equal-length vectors, the KFD data were re-sampled such that the number of samples equaled the minimum number per group.

As noted in Chapter 5, the genetic algorithm [CFPF94] was used to optimize model parameters. The objective function was the MSE between the model and real lung

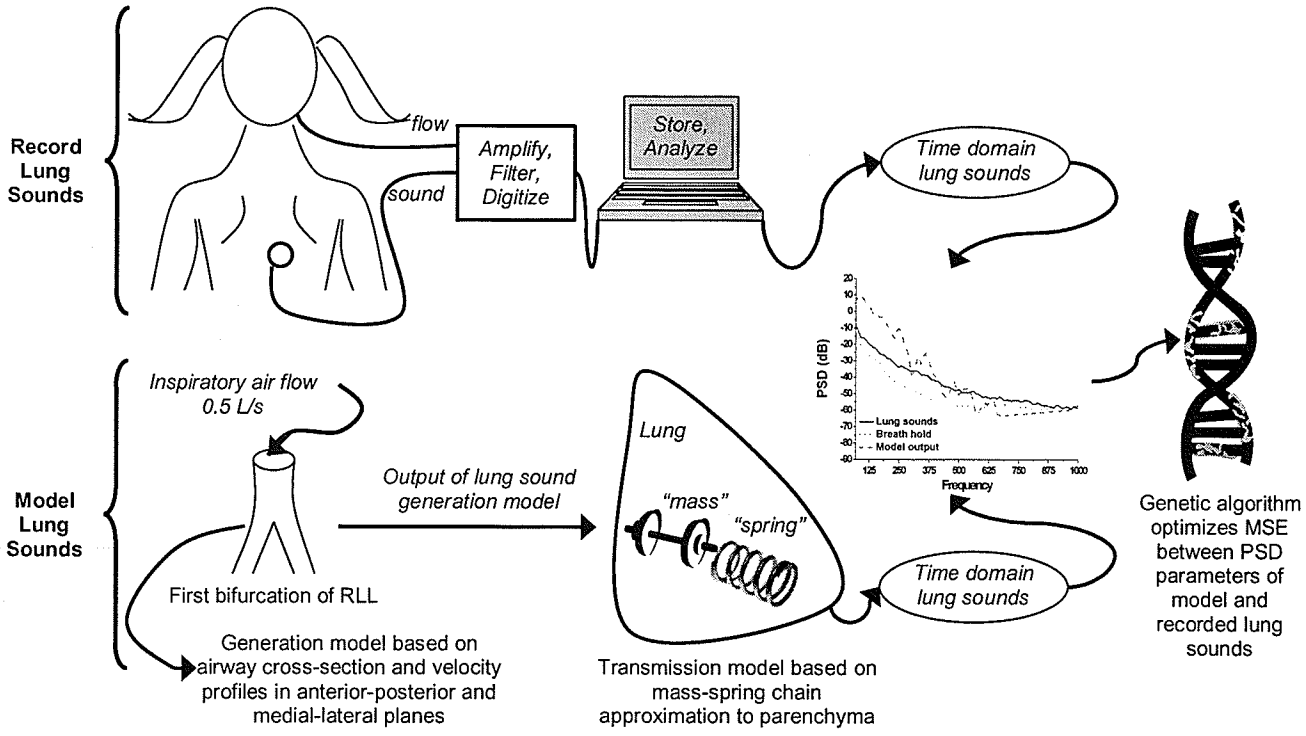

Fig. 6.1: Block diagram of the lung sounds model and validation scheme.

sound PSD features. The initial population size was 30. An elitist strategy was used to rank and remove high-MSE individuals, keeping the six best individuals per each of ten generations. Crossover mutation created new individuals. Binary values with 20-bit precision were used to encode parameters.

To compare the model output, i.e. a pressure signal, with the lung sounds that were recorded via an accelerometer, the former signal should be scaled. Theoretically the mass per unit area of the chest wall (in g/cm^2) is the scaling factor [WSGC89].

6.4 Model Results

6.4.1 Characteristics of Recorded Lung Sounds

The PSD characteristics examined exhibited a few trends (Table 6.2). The lower frequency bound, f_{low}, was higher for Group 1 than for Group 2. The mean upper frequency bounds were different by at least 100 Hz, with Group 2 having higher f_{up}. In terms of f_{max}, that of healthy subjects was higher, but P_{max} and the maximum value of SNR were lower. Again, there was an approximately 100 Hz difference between mean values of Group 1 and Group 2.

6.4.2 Lung Sound Generation and Transmission Model Results and Validation

Generated sound pressure was averaged across all of the nodes of the airway cross-section (shown in Fig. 5.3) because the airway is relatively small, with a radius of 0.225 cm. This generated signal was used as input to the lung sound transmission model, and validation was performed on the output of the transmission model. Values of k, ζ, and φ that produced model features similar (in the MSE sense) to features of real lung sounds are presented later in this section.

Table 6.2
PSD Characteristics of Group 1 and Group 2 Lung Sounds

Group	f_{low} (Hz)	P_{low} (dB)	SNR_{low} (dB)	f_{up} (Hz)	P_{up} (dB)	SNR_{up} (dB)	f_{max} (Hz)	P_{max} (dB)	SNR_{max} (dB)
1	60.0 ± 0	0	7.2 ± 4.9	662.0 ± 81.4	-55	4.1 ± 0.5	355.6 ± 36.4	-40	12.2 ± 3.4
2	45.0 ± 10.0	0	6.0 ± 3.3	777.1 ± 197.6	-55	4.3 ± 0.6	247.8 ± 39.3	-35	14.0 ± 4.7

As mentioned above, theoretically the model lung sounds should be scaled using chest wall mass per unit area, which is roughly BMI. Referring to Table 6.1, the mean BMI value for each group was approximately 20 kg/m^2, or 2 g/cm^2, which translates into a scaling factor of 0.5. However, it was found that 0.8 provided a better match between model and real lung sounds.

Acceptable model parameter bounds for the genetic algorithm were determined via preliminary investigation of effects of parameters on features of model lung sounds. Overall, as the values of k increased, the frequency content of the output signals increased. For example, with ξ = (1:10:2000)/20000, and φ = 2, frequencies at a PSD of -20 dB for k = 0.1, 0.15, and 0.2 were 88, 100.3, and 111.3 Hz respectively. This result is quite encouraging, because it corresponds with experimental findings of increased frequency in sound through a lung with reduced air content [ElRa97], [GrWN02], which could occur due to the thickening of airway walls that is a condition of asthma [CPKH00]. (That is, it is conceivable that the proportion of tissue would exceed that of air.) The result suggests that the theoretical proposition noted in Chapter 5, i.e. that airway constriction would correspond with higher k values, is reasonable. Section 6.5 contains further discussion on this issue.

All of the features of model lung sounds were determined after removing the first 5120 samples of the 10240-sample output, because up to approximately 2048 samples the

mean of the model lung sounds drifted upwards from zero (but returned to zero by 5120 samples). For each set of parameters, an ensemble of five model outputs was obtained, in order to account for the statistical nature of the signals and provide a sufficient number of 100 ms windows within which to calculate features (accounting for overlap, 45 windows were used).

The lung sound model validation was performed in two stages – one based on low frequencies, and one on high frequencies. The low frequencies were defined as 70-200 Hz, which encompasses the frequencies of Group 1 lung sounds that were found to be significantly different from those of Group 2 lung sounds (as presented above). As well, in this region, SNR was greater than 3 dB; above this SNR threshold any background noise may be disregarded. The high frequency range covered 450-800 Hz; this range was chosen so as to include the f_{up} frequencies of Group 1 and Group 2 lung sounds. Also, for Group 1 lung sounds, 450-800 Hz covers roughly the same range of SNR values (averaged across subjects) as 70-200 Hz.

For the 70-200 Hz frequency range and also KFD, bounds for k, ξ, and φ were

Table 6.3:
Model Parameter Values per Group 1 Subject and Corresponding MSE for PSD over 70-200 Hz and KFD

	Per subject					Leave one out				
				MSE (%)					MSE (%)	
	k	**	φ	PSD 70-200 Hz	KFD	k	ξ **	φ	PSD 70-200 Hz	KFD
H1	0.16	16559.49	2.98	0.54	0.84	0.10	18603.63	2.97	2.79	1.44
H2	0.09	19230.80	3.12	0.69	0.47	0.11	18269.72	2.96	0.74	0.47
H3	0.13	18543.39	2.90	1.06	0.74	0.11	18355.65	2.98	1.94	0.78
H4	0.13	18320.39	3.08	1.24	0.45	0.11	18383.52	2.96	2.48	0.68
H5	0.11	18714.39	3.03	1.34	0.48	0.11	18334.27	2.97	3.12	0.34
H6	0.12	18921.70	2.53	1.35	0.68	0.11	18308.36	3.03	1.93	0.31
H7	0.06	17692.26	3.09	0.53	1.02	0.12	18462.04	2.96	2.79	0.76
H8	0.11	19832.91	2.87	0.64	0.98	0.11	18194.46	2.99	2.01	0.47
H9	0.09	17573.24	3.17	0.35	0.80	0.11	18476.92	2.95	0.72	0.94
mean	0.11	18376.51	2.97	0.77	0.73				2.06	0.68
SD	0.03	981.60	0.19	0.37	0.20				0.86	0.36

**the numerator for is (1:10:2000)

[0.05, 0.2], (1:10:2000)/[10000, 20000], and [1.8, 3.2] respectively (determined via trial and error). For 450-800 Hz, k was unchanged, while bounds of ξ and φ were (1:1:200)/[1000, 2000] and (0.002:0.1:20)/[45, 55]. After ten generations of the genetic algorithm, parameter sets corresponding to the three lowest MSE values were examined per subject. If the value of k in the parameter set with the lowest MSE (set 1) matched that of the parameter set with the second lowest MSE (set 2), then set 1 was used (six subjects). Otherwise, if the value of k in set 2 matched that of the parameter set with the third lowest MSE (set 3), then set 2 was used (two subjects, H5 and H9). If there were no matches among the three sets, then set 1 was used (one subject, H6). Table 6.3 presents the resulting parameters per subject along with average MSE per feature for the 70-200 Hz PSD range and KFD. Model parameters per subject were averaged across eight subjects, and the model output based on the parameter average was compared with lung sound features of the left-out subject. This procedure was performed nine times, such that each subject was left out once, and MSE results are also shown in Table 6.3.

Examples of time domain model and recorded lung sounds are shown in Fig. 6.2. The KFD values of the model lung sounds that were tuned using the parameters of the Pareto distribution obtained via the low frequency PSD analysis are compared with those of lung sounds from one healthy subject (H4) and of the average across the other eight subjects in Fig. 6.3.

The MSE for average PSD within 450-800 Hz was quite low, with an average of 0.000764 ± 0.000325%, and hence the leave-one-out assessment was not repeated for these features. The average parameter values were k = 0.087 ± 0.030, ξ = (1:1:200)/(1819.3 ± 162.4), and φ = (0.002:0.1:20)/(49.08 ± 3.23). Figure 6.4 shows a

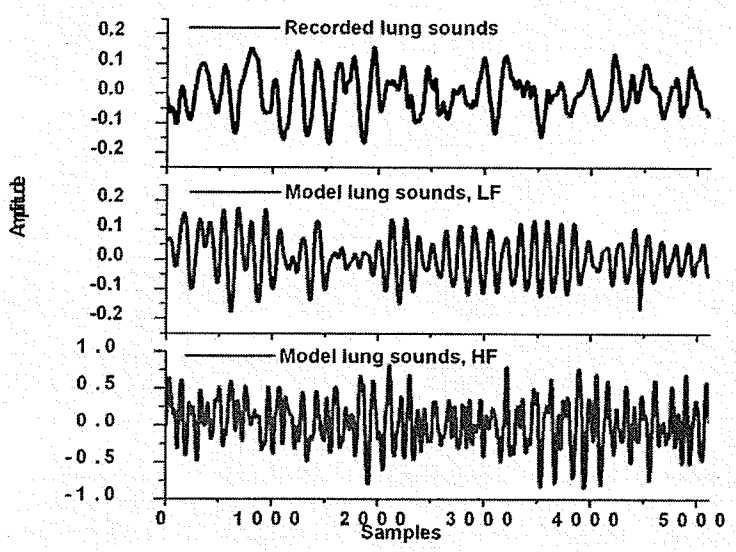

Fig. 6.2: Examples of time-domain model and recorded lung sounds, subject H4.

comparison between the model lung sounds tuned using the high frequency PSD values and the PSD of one healthy subject (H4).

In order to gain insight into the potential for application of the model in diagnosis of AHR or asthma, the model was tuned using Group 2 lung sounds as well. Though the lung sound generation portion of the model, which provided input to the transmission

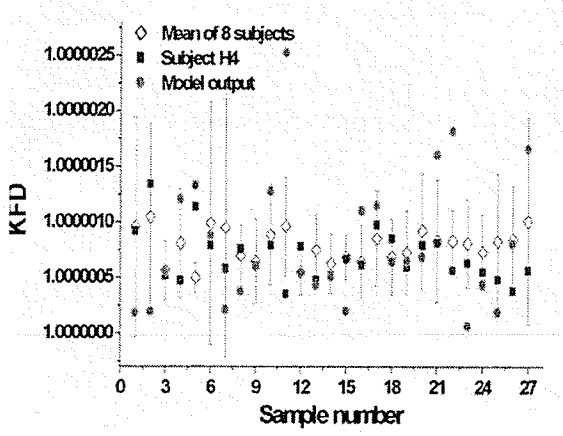

Fig. 6.3: KFD values of lung sounds from subject H4; mean ± SD of KFD across remaining eight healthy subjects, and KFD of model lung sounds (lowest MSE relative to subject H4).

system, was developed based on properties of flow within a healthy airway, this procedure may be justified by considering that it is not definitively known whether it is changes in lung sound generation or in transmission that are responsible for changes in lung sounds with disease. Table 6.4 shows parameter values for Group 2 after 10 generations of the genetic algorithm chosen as described above for healthy subjects (parameter set 1 ended up being used for each subject). Using a Student's *t*-test (two-tailed, heteroscedastic) to compare parameters of Group 1 and Group 2 subjects, it was found that the *k*-values between Group 1 and asthmatic Group 2 subjects were significantly different ($p = 0.014$). The mean value of k across the asthmatic subjects is higher than that of the healthy subjects, at 0.15 ± 0.02 and 0.11 ± 0.03 respectively. Encouragingly, this result complies with the theoretical expectation noted in Chapter 5, that higher values of k could imply airway constriction.

The high frequency features did not offer discriminatory power. A simultaneous match of high and low frequency features of model and real lung sounds was not achieved. Possible contributions to this difference will be elaborated on in the Discussion.

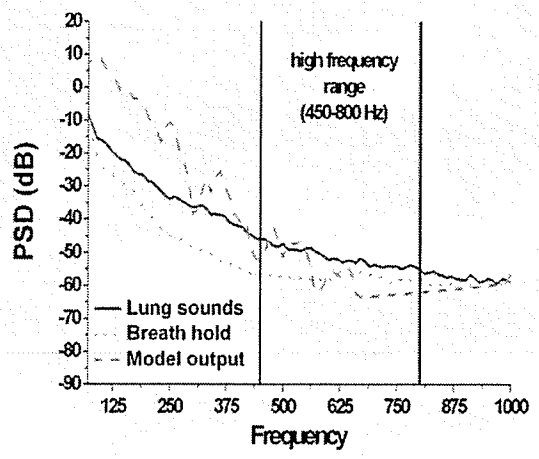

Fig. 6.4: Comparison between the model lung sounds tuned using the high frequency PSD values and the PSD of one healthy subject (H4).

6.5 Discussion

6.5.1 Possible Justifications for Model Results

There are several issues pertaining to modeling lung sounds that need to be considered with respect to the particular protocol used in this work. General categories include the effects of the following on real lung sounds: measurement transducer (sensor); sensor location; and noise, including heart sounds. The accelerometer sensor used in this work may cause frequency-dependent distortion to sounds measured on the chest: near approximately 100 and 900 Hz, the sensitivity of the sensor is higher and attenuation is lower relative to between these frequencies [Veva84]. This phenomenon, and also the finding that the mean frequency of maximum attenuation of sound transmitted to the posterior RLL was found to be 436 Hz [PoSY01] (indicated in Chapter 5), provide some justification (albeit crude) for the deviation between model and real

Table 6.4:
Model Parameter Values per Group 2 Subject and Corresponding MSE for PSD over 70-200 Hz and KFD

	k	ξ (denominator)**	φ	MSE (%) PSD 70-200 Hz	KFD
A1	0.16	15861.61	2.81	1.15	0.84
A2	0.16	19796.02	2.73	0.37	0.47
A3	0.12	17789.50	3.16	1.50	0.74
A4	0.17	16477.14	2.95	0.89	0.45
A5	0.13	18641.66	3.18	0.79	0.48
A6	0.13	11747.26	2.83	0.75	0.68
A7	0.10	18358.37	2.91	0.55	1.02
A8	0.11	18971.57	3.11	0.61	0.98
A9	0.06	19937.30	3.12	0.96	0.80
mean†	0.13	17508.94	2.98	0.84	0.29
SD	0.03	2557.477	0.17	0.34	0.10
mean	0.15	17713.19	2.96	0.94	0.27
SD	0.02	1593.91	0.20	0.42	0.08

**the numerator for ξ is (1:10:2000)
†across all subjects; ᶜacross subjects 1A:5A (asthmatic)

lung sounds outside of the low and high frequency ranges studied.

That a simultaneous match between low and high frequency ranges of model and recorded lung sounds was not achieved could relate to past findings pertaining to behavior of sound transmission relative to sound frequency. Work examining the phase delay of sound transmission through the lungs [PLDW95] found that the delay is higher at frequencies below 300 Hz relative to higher frequencies, and also that gas density affects sound transmission only at frequencies above 300 Hz, with delay increasing as density decreases. It has been suggested that the pathway for sound transmission through the lungs changes with frequency (in healthy adult subjects) [WADS92]. To support this claim it was noted that at lower frequencies, i.e. below a few hundred Hz, sound energy couples into the parenchyma by vibration of airway walls within the first few airway generations (i.e. the largest airways), whereas at higher frequencies, the larger airway walls act as conduits of sound energy which as a result travels into alveoli and smaller airways [WADS92].

The posterior RLL as a sensor location is desirable for a few reasons. It has been found that lung sounds recorded over this site during bronchial constriction, along with sounds obtained from other sites on the chest but not at the trachea, were significantly different from those obtained at baseline [PCOH97]. Another advantage of using the posterior RLL location is that lung sounds recorded here are minimally affected by heart sounds, relative to left-side and anterior chest wall regions. Recall that the frequencies across which PSD values were averaged corresponded to regions where SNR of lung sounds was greater than 3 dB, which indicates that lung sound intensity was at least double that of any background noise (including heart sounds).

The choice to use airway RS6 as the basis for lung sound generation modeling was made mainly because theoretically it was the most proximal airway to the location of the sound sensor used in recording lung sounds. As well, the velocity profiles resulted in vortex motion within this airway [vaHP04]. In addition, as mentioned above, it was necessary to estimate quantitatively the velocity profile within this airway (only qualitative profiles were provided in [vaHP04]); since RS6 is within the first bifurcation of the RLL, the value of flow within this airway could be calculated using half of the percentage of volume within this lung lobe. Though the estimation is accurate in theory, it is not possible to experimentally validate it. Incorporating airways other than RS6 would require quantitative estimation of the velocity profiles of these other airways as well. Given that experimental validation would not be possible, any error in estimation would cumulate across several airways.

The use of one airway as the sound generator is another issue that warrants discussion. Lung sounds are will be produced by several airways during the inspiration and expiration of air, and the sounds produced by each airway will interact. As well, it is not definitively known how much of the sound produced in the trachea and bronchi during inspiration (the breath phase of focus in the thesis) would travel along airways into airway RS6.

Furthermore, there may be heterogeneity between breaths in terms of airways through which air flows, and also in terms of airways that constrict [KCSM05]. It has been shown that in response to certain types of bronchial provocation, some airways constrict while others may dilate [KCSM05]. Variability also exists in terms of airway structure within and between individuals, which will be addressed further in Appendix B.

These issues indicate that more than one sound recording site (as used in the thesis work) may be required in order to adequately capture an airway response, which has been studied, e.g. in [PCOH97].

Other topics, specific to this study, that merit discussion include the method of validation; the use of a generated lung sound signal vs. white noise; and the performance of the developed model relative to that of other models. Regarding validation, though both generation and transmission of lung sounds were modeled in this work, only the output of the transmission system may be validated using real lung sounds, because sound recorded from within the airway upon which the generation model was based is not available. Nonetheless, with the generation model's output as input to the transmission model, the results produce features that match well (with MSE less than 5%) with those of real data within the flow range employed in the generation model (i.e., 0.5 L/s).

An assumption made in past lung sound modeling work [WSGC89] is that the parenchyma may be approximated as an aggregate of air bubbles in water, which is a closed-cell model [PoSY01]. One bubble (or "alveolar") diameter was assumed for the whole parenchyma. The use of the Pareto distribution in the proposed model seems to be a more realistic approach, because there aren't only two main airway sizes (i.e. bronchi and alveoli as suggested in [WSGC89]). Furthermore, the closed-cell framework may not be valid throughout the whole bandwidth used in [WSGC89], i.e. 100-600 Hz; an open-cell model may be valid up to 300 Hz [PoSY01]. Indeed, it was found that two different transmission models were needed, to represent low (70-200 Hz) and high (450-800 Hz) frequency ranges.

Whereas past work [WSGC89] provided only PSD estimates of model output, the proposed model in this thesis is able to provide time-domain signals as well. This expands the number of features that may be used to compare model predictions with experimental lung sound data, and also the manner in which the model may be validated. This model also allows for both qualitative and quantitative comparison with real lung sounds; only a qualitative comparison between PSD of the model and recorded lung sounds from four subjects was provided in [WSGC89].

In terms of the potential diagnostic use of the proposed model, the results suggest that there is promise. The values of k were found to be significantly different between Group 1 and Group 2 subjects (tuning based on PSD within 70-200 Hz). This result suggests that it may be possible to decipher inspiratory lung sounds of healthy subjects from those of asthmatics (without adventitious sounds). To date, one study has shown that band-limited average power of inspiratory lung sounds of children with poor lung function differs significantly from that of healthy children at baseline [TaPa96].

In Chapter 5 it was suggested that the parameters of the Pareto distribution would change for lung sounds of asthmatic subjects as a result of an increase in tissue proportion due to inflammation and thickening of the airway walls that is known to occur in asthma [IYHY06]. It is important to point out that another structural abnormality associated with asthma is air-trapping in the smaller airways, which can be present simultaneously with airway wall thickening [IYHY06]. It is not known which of these two phenomena would occur to a greater extent. It is possible that increased air content may be a more significant presence than airway wall thickening, especially if mucous in airways is minimal. Both air content and airway wall thickening (or composition) may be

detected using imaging of the lung [IYHY06]; however, such images were not available for the subjects in our studies and it is thus only possible to postulate as to the source of changes in model parameters.

The use of the output of the generation model as input to the transmission model, while providing a novel lung sound model incorporating both aspects of production of chest-wall lung sounds, required that the data used to validate the model match with the generation output in terms of flow and approximate recording site, and airway condition (i.e., theoretically corresponding to that of healthy subjects). The significant difference in one of the model parameters suggests that changes in sound transmission characteristics (proportions of air and tissue in this case) may influence changes in lung sounds more than changes in sound generation. A different approach, that of using a white noise input to the model and the mouths of subjects (requiring a breath hold with open glottis), would allow verification of this postulation. This method imposes the assumption that sound is generated mainly in the trachea, but it would offer the ability to tune the model for any subject.

Of course, the generation model could be expanded upon, to incorporate the effects of other airways in which sound may be generated, airway wall elasticity and corrugation, moisture and mucus in airways, and changes in airways that may occur in asthma. This would warrant a new study in and of itself, and is beyond the goals of the present work, considering that the lung sound model is one portion of the thesis work and not the sole focus of the work (Appendix A lists prior publications).

Unlike in past work, in this work automated model parameter optimization was achieved, using the genetic algorithm [CFPF94]. Results of the leave-one-out analysis

performed based on the average parameter values found for Group 1 subjects (Table 6.3) indicated that the optimized model parameters were meaningful. The number of subjects used to tune and validate the model may be increased, though this thesis work did involve more subjects than past work on lung sound modeling, e.g. seven [PoSY01] or five [WSGC89] subjects, with nine healthy subjects and nine with poor lung function or asthma.

6.5.2 On Sound Generation and Vortices as Sound Sources

The generation model was based on velocity profiles developed by authors who had modeled fluid dynamics within several generations of airways [vaHP04]. That particular study was the most thorough study to date at the time of model development, in terms of the number of airways studied and the structural accuracy of the model. The choice to use past findings on fluid flow in lung airways for the thesis, rather than creating a fluid dynamical model from scratch using computational fluid dynamics, was driven by a few factors. Firstly, to simulate airflow dynamics within an airway branching system such as that within the lungs requires a massive and very time consuming computation [SWLL05]. As well, computational fluid dynamic techniques for airflow in ducts with non-rigid (elastic) walls are not mature [SWLL05]. The most that can be achieved at present is to employ extremely simple geometries with low Reynolds number flow [Davi04]. Considering all of these issues, using computational fluid dynamics for the purpose of generating sound would constitute a thesis in and of itself; as mentioned above, the lung sound modeling was only a component of the work done towards this thesis (see list of publications in Appendix A).

The velocity profiles provided by past work and quantified in the thesis were employed in a theoretical model of lung sound generation during inspiration of air by a

pair of vortices [HaPa79]. That model had been validated by the authors in a physical model of an airway bifurcation made of fiberglass, and also by lung sounds recorded from four adult male subjects [HaPa79]. (It has also been experimentally shown that a vortex pair in open air generates sound [STAH05].) Though several studies have examined particle transport by air flow in lung airways, few have tied in sound generation by fluid dynamics. Hardin and Patterson [HaPa79] presented a theoretical model of flow-generated sound in lung airways that was unique and adaptable to airway size, which made it attractive for use in the thesis.

More recent work in modeling sound generation in lung airways was also based on circulation of two vortices on inspiration of air [KWAW01]. That work was mentioned in Chapter 5. The geometry of the model was formed using high resolution x-ray computed tomography images of a porcine right middle lung lobe that were segmented and used to construct a three-dimensional porcine airway with three branches (each branch having its own bifurcations). However, air flow simulation results were presented for a single bifurcation, and were shown via a figure. The authors found that a dipole vortex flow field formed in each daughter airway, just following the bifurcation, using an inspiratory flow with a Reynolds number of 500 [KWAW01]. Details of the sound generated in the porcine model were not presented, even though the authors indicated that the objective of their study of vortex flow in airways was to generate lung sounds. Results of the propagation of an artificial pulse near the center of a lung in the thorax of Visible Human data were briefly outlined.

In order for sound pressure to emerge from the motion of vortices, there needs to be a time-dependency, according to the acoustical fluid equation presented in Chapter 5

[Bath96], [Cole62]. Fluid motion always involves some change in properties of a fluid with time, with the change depending not only on the time interval but also upon the position within the fluid [Cole62]. In an ideal fluid, vorticity and circulation are independent of time [Cole62]. However, in practice, no exactly ideal fluid exists and also, system energy dissipation occurs, which means that a vortex region of fluid can move with time [Cole62]. In fact, fluid motion is almost always inherently unstable, and randomly so [Cole62], [Davi04]. It was not clear how the time-dependence of the sound pressure formulation was obtained from the vortical circulation component of the model of vortical flow in lung airways [HaPa79]. However, this was accounted for in the thesis work by incorporating fractional Brownian motion (fBm) in the movement of nodes per iteration of the finite element model to simulate motion with time.

How well the output of the generation model matches with a sound signal produced in the particular airway studied is impossible to determine in this work, since a recording of sound within this airway in vivo is not available. A physical model of airways would provide a means by which to validate the output of the generation model.

6.5.3 Further Considerations Pertaining to Model Implementation

The lung sound generation and transmission model, in its present state, is not applicable in a clinical setting. Its generation component requires elaboration, in terms of incorporation of the effects of sound generated in airways surrounding the airway that was the focus of the model, and validation as mentioned in the preceding section. Having to tune the transmission portion of the model within two different frequency ranges is also not ideal, since lung sounds recorded on the chest contain both low and high frequency phenomena within one signal, though some justification for this result was provided in Section 6.5.1.

The lung sound recordings acquired for analysis thus far have been acquired under consistent conditions: e.g., breathing at target flows or at tidal volume breathing rates; sitting still in a quiet room; short (one to two minute) lengths of recording. The adaptation necessary for physiological systems to operate in more true-to-life situations [CVFG04] is of minor concern, which reduces the difficulty involved in developing deterministic equations for the respiratory system pertaining to lung sounds. This implies that future implementation of respiratory sounds in a clinical diagnostic setting would require a few restrictions, such as subject posture (also found to influence lung sounds [JJKB99]) and air flow (which would have to be measured). However, these are relatively minor impediments considering the maximal breathing maneuvers required for standard PFT. It would be ideal to develop methods of lung sound analysis by which it would be possible to account for variability in the above-listed aspects of data recording.

Validation of the model was achieved by tuning the model using lung sounds recorded from children under particular protocols. Though as mentioned above, the number of subjects surpassed the numbers used in past work in modeling lung sounds, a wider range of subjects would be necessary in order to determine the usefulness of the model for different subjects, e.g. adults, and different protocols and recording conditions. Lung sounds were recorded while subjects were seated; it is not possible to determine how model results would change for lung sounds recorded from other body postures.

In the generation model, the effects of boundaries on shear stress and velocity, other than the no-slip condition, were not taken into account, because the model was developed based on velocity profiles that were obtained in past work [vaHP04]. Using these profiles also necessitated that the recorded lung sounds used in model validation

were acquired at flows that were comparable to the flow on which velocity profiles were based, and that the generation model be based on one lung airway (RS6). Ideally, as mentioned above, a dynamical model of flow and velocity profiles within several airways should be developed, and this model should incorporate different inner airway wall surfaces that include corrugation and mucus. As discussed in Chapter 2, corrugation of the inner airway is more prominent in asthmatic relative to healthy airways, which are relatively smooth. Such a model would also allow for more flexibility in terms of sensor location, air flow, and airway condition, which in turn would offer more insight into the physiology of lung sound generation in different subjects.

The lung sound generation and transmission model as a whole is novel. In the generation model, incorporating fBm was a new approach to account for the time-dependency of vortices. In the transmission model, the novelty was in the use of the Pareto distribution to vary the proportion constants. Automatic tuning of the parameters of the transmission model via the genetic algorithm has also not been previously applied in modeling lung sounds. The latter two aspects of the model along with its potential to provide time-domain data are its main strengths and overall it comprises a unique approach.

CHAPTER 7

Conclusions and Recommendations

"The viewpoint in attempting to (1) consider a subset of signals and (2) extract the 'information' they convey in order to (3) derive a diagnostic is far from being sufficient. Other observables, primarily clinical data, must be considered, because they support the generation and verification of pathophysiological hypotheses and determine the type and modality of the proposed measures when they do not follow standard or systematic procedures." [Coat02]

7.1 Conclusions

The thesis work was comprised of several studies, with each resulting in new information pertaining to inspiratory lung sounds recorded from healthy subjects and patients undergoing pulmonary function testing (PFT) to determine airway hyper-responsivity. This thesis presented detail on a selection of these studies, dealing with heart sounds in lung sounds (Chapter 3), analyses of lung sounds based on fractal and chaos theories (Chapter 4), and modeling the generation and transmission of lung sounds (Chapters 5 and 6). These studies represent the major contributions of the graduate work. Other work has been published, as listed in Appendix A. For the sake of continuity and flow, work that has been done on lung sound variability in healthy subjects and changes in intensity with induced bronchial provocation in patients is provided in Appendix B.

The work in heart sounds appears in a few publications [GHPM05], [GnMo03], [GnMo07], [GnMP03], and was therefore not covered at length in the thesis. Localization of heart sounds using waveform fractal dimensions was examined in [GnMo03]. A recursive least squares (RLS) adaptive filter was developed for localizing and filtering heart sounds from lung sounds in [GHPM05], [GnMP03]. The use of the RLS filter in both localization and removal of heart sounds from lung sounds is novel. This filter

provided very good results both quantitatively and qualitatively, and it could be of use to future researchers who would like to separate heart and lung sounds. Quantitative and qualitative analyses of the performance of selected adaptive filtering techniques for removing heart sounds from lung sounds, including that of [GnMP03], were presented in [GHPM05]. The use of such analyses could ideally be incorporated as a standard assessment of adaptive filtering applied to lung sounds for heart sound removal. A review of separating heart sounds from lung sounds is provided in [GnMo07].

Analysis of lung sounds using geometrical and dynamical state space parameters is a fairly new area of research, and the thesis work presented in Chapter 4 contributes to this field by its study of the effect of flow and sensor locations on these parameters, as well as differences in parameters before and after induced bronchial constriction. Connections were drawn between state space parameters of recorded lung sounds and what is known about the generation of these sounds. Results indicated diagnostic potential in these parameters, and also determinism in lung sounds, which was useful from the point of view of modeling.

The lung sounds model presented in Chapters 5 and 6 is, as a whole, novel. Many past theories were woven together to create the generation and transmission aspects of the model, and for this reason, it incorporates many assumptions and simplifications (see Chapter 5). However, the particular combination employed in this thesis of theory of sound generation by vortical flow in airways with transmission of this sound through the thorax is a novel approach to modeling lung sounds. The transmission model also incorporates the use of the Pareto distribution to provide proportions of air and tissue in the parenchyma, which has not been used in past work. Though results were promising in

terms of the potential application of the model to decipher lung sounds of healthy subjects from those of asthmatics, the model is in a preliminary stage and has limitations as outlined in Chapter 6.

The work presented in the thesis prompts a renewed focus on both lung sound generation and transmission in order to gain insight into physiological aspects of lung sounds and their diagnostic potential. As indicated in Chapter 2, existing methods for diagnosis of airway hyper-responsiveness (AHR) and asthma have their limitations and a method based on objective characterization of lung sounds could potentially alleviate some of these restrictions. A method incorporating lung sounds that would require only one lung sound recording is tempting. Signal processing via state space analysis and also the work in modeling in this thesis did not conclusively indicate whether this could be possible, but did provide justification in working towards this goal. In the former work, parameters did change with airway and recording conditions, and in the latter, there was a significant difference in a parameter of the tuned model between lung sounds from healthy children and from children with asthma. Expanding on this work and incorporating the recommendations presented in this chapter will hopefully lead to further advances in lung sounds research for diagnosis and/or monitoring of AHR and asthma.

7.2 Recommendations

7.2.1 State Space Analysis

The analysis of lung sounds using geometrical and dynamical state space parameters outlined in Chapter 4 presented some interesting results. However, as

discussed in that chapter, it is not possible to determine with certainty the source(s) of changes in the parameters between lung sounds recorded at different flow rates and from different sensor locations, or between lung sounds recorded at different stages in the methacholine challenge (MCh). Though it is possible that the observed state space features related to the underlying flow dynamics producing lung sounds, to prove this would require detailed information pertaining to air flow patterns and also state space parameters of the flow, which was not available for the data studied. Theoretical and realistic physical models of lung sound generation and transmission are required, to provide further information on the relation of state space parameters to flow and recorded lung sounds.

The effects of noise in recorded data on the state space parameters should also be investigated. Such a study would ideally involve obtaining reference recordings of all possible noise sources in recorded lung sounds, and/or modeling these noises. State space analysis is limited in that filtering of data, both in terms of reduction of the bandwidth of a signal or selective removal of particular frequency ranges (e.g. in order to remove or reduce noise other than broad-band noise), should be avoided as it could alter the dynamics in the time series [ZbDZ02]. Of course, as mentioned in Chapter 4, some filtering is necessary, to satisfy the Nyquist criterion. In addition, a sensor may in itself effectively filter data due to its particular frequency response. The restriction on filtering likewise restricts the ability to assess how sensitive state space parameters are to changes in frequency components of data under analysis.

Noise due to heart sounds was accounted for in the thesis by analyzing lung sounds including heart sounds, and excluding them by avoiding regions where they

occurred. As presented and discussed in Chapter 4, there were differences in parameters between these two analyses, which indicates that the techniques are not robust to heart sound noise.

The techniques applied in the thesis were designed for noisy and short time series, though the noisiness pertains to broad-band noise. Regarding length, theoretically state space analysis requires infinite data length, which in reality does not exist. Analysis of lung sounds was not performed across a whole signal but within regions corresponding to inspiratory flow at plateau (i.e. transition between inspiration acceleration and deceleration), because the data to which state space analysis is applied should be stationary. A higher sampling frequency would provide more samples within the time series, which could allow determining whether the analysis would be useful for other, shorter regions of lung sounds, e.g. sounds corresponding to flow acceleration.

A further consideration pertaining to the lung sounds analyzed via state space measures is that the data sets were acquired under two separate protocols. For instance, the healthy subjects breathed at target flows and sounds were acquired in a noise-controlled environment, whereas the patients breathed tidally in a clinical setting that was more susceptible to interferences. Ideally, data being compared should be obtained under consistent conditions so as to eliminate sources of discrepancies due to factors other than those pertaining to the signal analysis alone.

Can state space analysis of time series "prove" that any given data are chaotic? Based on time series alone, the answer is no. Many factors come into play in state space analysis, and in any signal processing technique for that matter, in terms of the particular methods chosen and the pertinent parameters, which generally require user-specification.

There is no standard technique for state space analysis of lung sounds because the field is relatively young, with only a handful of published studies as indicated in Chapter 4. A single study comparing different techniques using a great number of lung sound signals recorded under several different conditions should be performed.

7.2.2 Modeling Lung Sounds

Several issues pertaining to the lung sound generation and transmission model developed in the thesis were outlined in Chapter 6. This section will reiterate those that are most significant in terms of future work. Firstly, fluid dynamical modeling of air in airways and sound generation by such flow should be incorporated in any lung sound model. This would allow for much more flexibility in terms of the lung sounds that may be used for model validation, e.g., sounds recorded from locations other than the posterior RLL and at other flows – the model is limited to 0.5 L/s. As discussed in Chapter 6, such an undertaking would require considerable advancement in terms of computational fluid dynamics, since at present the most that can be achieved is to employ simple geometries and flow regimes.

Validation of the transmission portion of the model could be attempted using a sinusoidal signal both as input to the model, and to the mouths of human subjects while recording the sound transmitted to their chest. The subjects would be required to cease breathing and maintain an open glottis. The model parameters could be tuned such that the model output matched the recorded transmitted sinusoids, which might allow accounting for attenuation and phase delay in terms of parameter values.

Considering that there is variability in many aspects of lung structure and sound, and also in fluid dynamics, as outlined in Chapters 2 and 3 and Appendix B, one must question whether any one model would be universally applicable. Any lung sound model

should therefore account for such variability via its parameters. The use of the Pareto distribution in the model developed in the thesis does account for variability in that the proportion constants are drawn from the distribution. But other physiological aspects must be considered, such as subject anthropometrics and respiratory status. The range of the types of subjects used in model validation should be widened to account for these considerations.

Another recommendation pertains to heart sounds. One of the findings of the research into filtering heart sounds from recorded lung sounds was that heart sounds minimally affect lung sounds recorded over the posterior right lower lobe (RLL) and lung sounds recorded at high flows. For the former reason, and because the signal to noise ratio of lung sounds used in the model validation was greater than 3 dB within the frequency ranges studied, heart sounds were not accounted for in the model. If the model is to be expanded on and applied to regions other than the posterior RLL, future work should account for the effect of heart sounds on the model. It has been shown, for instance, that heart sounds significantly impact lung sounds recorded over the right upper lobe anteriorly up to 300 Hz [GHPM05].

Indeed, incorporating lung sounds recorded over more than one region would likely be preferable using one recording location if the model were to be developed further for clinical application, in order to adequately capture an airway response or a difference between lung sounds recorded from healthy subjects. This ties in with heterogeneity in breathing and bronchial constriction as presented in Chapter 2, as well as with the variability mentioned above. Other considerations pertaining to model implementation were presented in Chapter 6.

Until a comprehensive and accurate theoretical model of lung sound generation and transmission has been achieved, the results of any lung sound signal processing study can never truly be validated, because without a model it is not possible to decipher exactly what certain features of lung sounds truly represent. A model with parameters indicative of respiratory status would allow for tuning model parameters so as to match its output with recorded lung sounds, with the particular parameter values of diagnostic use. Of course, its utility in a clinical setting would have to be assessed, in part by comparing it with current standards in diagnosis of asthma and AHR. Considering the recommendations presented in this chapter a lung sounds model may be within reach.

REFERENCES

[AbMo04] M. Aboofazeli and Z. Moussavi, "Analysis of normal swallowing sounds using nonlinear dynamic metric tools," in *Proc. 26th Annu. Int. Conf. IEEE Eng. Medicine Biology Soc., EMBC'04,* vol. 2, pp. 3812-3815, Sept. 2004.

[ABST93] H. D. I. Abarbanel, R. Brown, J. J. Sidorowich, and L. Sh. Tsimring, "The analysis of observed chaotic data in physical systems," *Rev. Mod. Phys.*, vol. 65, no. 4, pp. 1331-1392, 1993.

[AJHA06] C. Ahlström, P. Johansson, P. Hult, and P. Ask, "Chaotic dynamics of respiratory sounds," *Chaos Soliton. Fract.*, vol. 29, pp. 1054-1062, 2006.

[ALHA05] C. Ahlström, O. Liljefelt, P. Hult, and P. Ask, "Heart sound cancellation from lung sound recordings using recurrence time statistics and nonlinear prediction," *IEEE Sig. Process. Lett.*, vol. 12, pp. 812-815, 2005.

[AlKa02] S. S. Alsmadi and Y. P. Kahya, "Online classification of lung sounds using DSP," in *Proc. 24th Annu. Int. Conf. IEEE Eng. Medicine Biology Soc., EMBC'02*, vol. 2, pp. 1771-1772, Oct. 2002.

[AuSr06] D. J. Auld and K. Srinivas, "Aerodynamics for Students," Aerospace, Mechanical and Mechatronic Engineering, University of Sydney, 2006. Available: http://www.ae.su.oz.au/aero/fprops/poten/node25.html

[BaLu05] J. H. T. Bates and K. R. Lutchen, "The interface between measurement and modeling of peripheral lung mechanics," *Respir. Physiol. Neurobiol.*, vol. 148, no. 1-2, pp. 153-164, 2005.

[BaMM99] M. Banbrook, S. McLaughlin, and I. Mann, "Speech characterization and synthesis by nonlinear methods," *IEEE Trans. Speech & Audio Process.*, vol. 7, no. 1, pp. 1-17, 1999.

[BaNe03] N. Balakrishnan and V. B. Nevzorov, *A Primer on Statistical Distributions*, 1 ed. Hoboken, NJ: John Wiley & Sons, Inc., 2003.

[Bath96] K.-J. Bathe, *Finite Element Procedures*, 2 ed. Upper Saddle River, NJ: Prentice-Hall, Inc., 1996.

[BaUM97] M. Banbrook, G. Ushaw, and S. McLaughlin, "How to extract Lyapunov exponents from short and noisy time series," *IEEE Trans. Sig. Process.*, vol. 48, pp. 1378-1382, 1997.

[BDMM92] R. Beck, U. Dickson, M. D. Montgomery, and I. Mitchell, "Histamine challenge in young children using computerized lung sounds analysis," *Chest*, vol. 102, no. 3, pp. 759-763, Sept. 1992.

[BeBM93] D. Beasley, D. R. Bull, and R. R. Martin, "An overview of genetic algorithms: Part I, Fundamentals," *University Computing*, vol. 15, no. 2, pp. 58-69, 1993.

[Bhat05] S. Bhatnagar, "Adaptive multivariate three-timescale stochastic approximation algorithms for simulation based optimization," *ACM Trans. Modeling and Comp. Simulation*, vol. 15, no. 1, pp. 74-107, Jan. 2005.

[BHCP04] M. Barzanji, J. Holbrow, D. Castillo, and H. Pasterkamp, "Diagnostic value of auscultation during bronchial provocation in children," *Am. J. Respir. Crit. Care Med.*, vol. 167, Abstracts Suppl., p. A187, 2004.

[Blak86] W. K. Blake, "Theory of sound and its generation by flow," in *Mechanics of flow-induced sound and vibration - Volume 1: General concepts and elementary sources*. F. N. Frenkiel and G. Temple, Eds. London: Academic Press, Inc.; Harcourt Brace Jovanovich, Publishers, 1986, pp. 88-105.

[Boha00] A. B. Bohadana, "Lung sounds in asthma and chronic obstructive pulmonary disease," *Monaldi Arch. Chest Dis.*, vol. 55, no. 6, pp. 484-487, Dec. 2000.

[BPKE00] G. S. Berlyne, K. Parameswaran, D. Kamada, A. Efthimiadis, and F. E. Hargreave, "A comparison of exhaled nitric oxide and induced sputum as markers of airway inflammation," *J. Aller. Clin. Immunol.*, vol. 106, no. 4, pp. 638-644, 2000.

[BPPM05] S. R. Boser, H. Park, S. F. Perry, M. G. Ménache, and F. H. Y. Green, "Fractal geometry of airway remodeling in human asthma," *Am. J. Respir. Crit. Care Med.*, vol. 172, pp. 817-823, 2005.

[BSRW05] P. J. Berger, E. M. Skuza, C. A. Ramsden, and M. H. Wilkinson, "Velocity and attenuation of sound in the isolated fetal lung as it is expanded with air," *J. Appl. Physiol.*, vol. 98, no. 6, pp. 2235-2241, 2005.

[Casd90] M. Casdagli, "Chaos and deterministic versus stochastic nonlinear modeling," *J. R. Stat. Soc. B*, vol. 54, no. 2, pp. 303-328, 1990.

[CFPF94] A. Chipperfield, P. Fleming, H. Pohlheim, and C. Fonseca, *Genetic Algorithm Toolbox for Use with Matlab: User's Guide*, 1.2 ed. University of Sheffield: Department of Automatic Control and Systems Engineering, 1994.

[ChAG97] S. Charleston, M. R. Azimi-Sadjadi, and R. Gonzalez-Camarena, "Interference cancellation in respiratory sounds via a multiresolution joint time-delay and signal-estimation scheme," *IEEE Trans. Biomed. Eng.*, vol. 44, no. 10, pp. 1006-1019, Oct. 1997.

[ChAz96] S. Charleston and M. R. Azimi-Sadjadi, "Reduced order Kalman filtering for the enhancement of respiratory sounds," *IEEE Trans. Biomed. Eng.*, vol. 43, no. 4, pp. 421-424, Apr. 1996.

[ChBe06] M. Chan-Yeung and A. Becker, "Primary prevention of childhood asthma and allergic disorders," *Curr. Opin. Aller. Clin. Immunol.*, vol. 6, no. 3, pp. 146-151, 2006.

[ChCh83] R. M. Cherniack and L. Cherniack, *Respiration in Health and Disease*, 3 ed. Philadelphia, PA: W. B. Saunders Company, 1983.

[ChTo92] B. Cheng and H. Tong, "On consistent nonparametric order determination and chaos," *J. R. Stat. Soc. B*, vol. 54, no. 2, pp. 427-449, 1992.

[CIGP97] G. Chi-Lem, Y. Inaba, M. Greenberg, and H. Pasterkamp, "Critical flow to generate breath sound does change during bronchial constriction," *Am. J. Respir. Crit. Care Med.*, vol. 157, no. 3, Abstracts Suppl., p. A540, 1997.

[CiSF02] B. Cichocki, P. Szymczak, and F. Feuillebois, "Effective boundary conditions for creeping flow along a periodic rough surface," *Fluid Mechanics and its Applications: Tubes, Sheets and Singularities in Fluid Dynamics*, vol. 71, pp. 349-354, 2002.

[CKIC97] K. H. Chon, J. K. Kanters, N. Iyengar, R. J. Cohen, and N. H. Holstein-Rathlou, "Detection of chaotic determinism in stochastic short time series," in *Proc. 19th Annu. Int. Conf. IEEE Eng. Medicine Biology Soc., EMBC'97*, vol. 3, pp. 275-277, 1997.

[Coat02] J.-L. Coatrieux, "Signal processing and physiological modeling - Part I: Surface analysis," *Crit. Rev. Biomed. Eng.*, vol. 30, no. 1-3, pp. 9-35, 2002.

[Cohe86] A. Cohen, *Biomedical Signal Processing, Volume I: Time and Frequency Domain Analysis*. Boca Raton, FL: CRC Press Inc., 1986.

[CoLa84] A. Cohen and D. Landsberg, "Analysis and automatic classification of breath sounds," *IEEE Trans. Biomed. Eng.*, vol. 31, no. 9, pp. 585-590, Sept. 1984.

[Cole62] G. H. A. Cole, *Fluid Dynamics: An Introductory Account of Certain Theoretical Aspects Involving Low Velocities and Small Amplitudes*. London: Methuen & Co., Ltd., 1962.

[Conr77] M. Conrad, "Functional significance of biological variability," *Bull. Math. Biol.*, vol. 39, pp. 139-156, 1977.

[CPKH00] N. G. Carroll, S. Perry, A. Karkhanis, S. Harji, J. Butt, A. L. James, and F. H. Y. Green, "The airway longitudinal elastic fiber network and mucosal folding in patients with asthma," *Am. J. Respir. Crit. Care Med.*, vol. 161, pp. 244-248, 2000.

[CVFG04] E. Conte, A. Vena, A. Federici, R. Giuliani, and J. P. Zbilut, "A brief note on possible detection of physiological singularities in respiratory dynamics by recurrence quantification analysis of lung sounds," *Chaos Soliton. Fract.*, vol. 21, pp. 869-877, 2004.

[Davi04] P. A. Davidson, *Turbulence: An Introduction for Scientists and Engineers*. New York, NY: Oxford University Press, 2004.

[deBF04] L. P. L. de Oliveira, B. E. J. Bodmann, and D. Faistauer, "General fractal-discrete scheme for high-frequency lung sound production," *Phys. Rev. E*, vol. 69, no. 1, pp. 011905-1-011905-5, 2004.

[dMPC05] P. A. de Jong, N. L. Müller, P. D. Paré, and H. O. Coxson, "Computed Tomographic imaging of the airways: Relationship to structure and function," *Eur. Respir. J.*, vol. 26, no. 1, pp. 140-152, 2005.

[DPAD66] P. Dejours, R. Puccinelli, J. Armand, and M. Dicharry, "Breath-to-breath variations of pulmonary gas exchange in resting man," *Respir. Physiol.*, vol. 1, no. 1, pp. 265-280, 1966.

[Duck90] F. A. Duck, *Physical Properties of Tissue: A Comprehensive Reference Book*. San Diego, CA: Academic Press Ltd., 1990.

[Duec03] S. Dueck, "Synthesis of fractional Brownian motion: An evaluation of the simulation techniques of Mandelbrot-van Ness and Cholesky," University of Manitoba, Department of Electrical and Computer Engineering Report, pp. 1-29, 2003.

[DuHS01] R. O. Duda, P. E. Hart, and D. G. Stork, *Pattern Classification*, 2 ed. New York, NY: John Wiley & Sons, Inc., 2001.

[EaCh00a] J. E. Earis and B. M. G. Cheetham, "Current methods used for computerized respiratory sound analysis," *Eur. Respir. J.*, vol. 10, no. 77, pp. 586-590, 2000.

[EaCh00b] J. E. Earis and B. M. G. Cheetham, "Future perspectives for respiratory sound research," *Eur. Respir. J.*, vol. 10, no. 77, pp. 641-646, 2000.

[ElRa97] M. El-Raheb, "Simplified analytical models for transient uniaxial waves in a layered periodic stack," *Int. J. Solids Structures*, vol. 34, no. 23, pp. 2969-2990, 1997.

[EmMa02] P. Embrechts and M. Maejima, *Selfsimilar Processes*. Princeton, NJ: Princeton University Press, 2002.

[FadB05] D. Faistauer, L. P. L. de Oliveira, and B. E. J. Bodmann, "General discrete modeling of lung sound production in normal subjects," *Physiol. Meas.*, vol. 26, pp. 109-122, 2005.

[Fung90] Y. C. Fung, *Biomechanics: Motion, Flow, Stress, and Growth*. New York, NY: Springer-Verlag, Inc., 1990.

[GaCu96] N. Gavriely and D. W. Cugell, "Airflow effects on amplitude and spectral content of normal breath sounds," *J. Appl. Physiol.*, vol. 80, no. 1, pp. 5-13, Jan. 1996.

[GaPA81] N. Gavriely, Y. Palti, and G. Alroy, "Spectral characteristics of normal breath sounds," *J. Appl. Physiol.*, vol. 50, no. 2, pp. 307-314, Feb. 1981.

[Gedd05] L. A. Geddes, "Retrospectroscope: Birth of the stethoscope," *IEEE Eng. Med. Biol. Mag.*, vol. 23, no. 1, pp. 84-86, Jan. 2005.

[GESK92] E. Ç. Güler, T. Engin, B. Sankur, and Y. P. Kahya, "Spectral analysis of respiratory sounds in healthy and pathological subjects," in *Proc. IEEE Int. Biomed. Eng. Days*, pp. 70-74, Aug. 1992.

[GHPM05] J. Gnitecki, I. Hossain, H. Pasterkamp, and Z. Moussavi, "Qualitative and quantitative evaluation of heart sound reduction from lung sound recordings," *IEEE Trans. Biomed. Eng.*, vol. 52, no. 10, pp. 1788-1792, 2005.

[Gilb89] S. G. Gilbert, *Pictorial Human Embryology*. Toronto, ON: University of Toronto Press, 1989.

[GlMa88] L. Glass and M. C. Mackey, *From Clocks to Chaos: The Rhythms of Life*. Princeton, NJ: Princeton University Press, 1988.

[GMBP04] J. Gnitecki, S. Maiti, M. Barzanji, and H. Pasterkamp, "Does flow standardized breath sound intensity indicate changes in airway diameter?," *Can. Respir. J.*, vol. 11, no. 3, p. 237, 2004.

[GnKP05] J. Gnitecki, G. Katz, and H. Pasterkamp, "Effects of time, breathing apparatus and sensor location on flow-specific lung sound intensity in healthy children," *Can. Respir. J.*, vol. 12, no. 3, p. 164, 2005.

[GnMo03] J. Gnitecki and Z. Moussavi, "Variance fractal dimension trajectory as a tool for heart sound localization in lung sound recordings," in *Proc. 25th Annu. Int. Conf. IEEE Eng. Medicine Biology Soc., EMBC'03*, vol. 3, pp. 2420-2423, Sept. 2003.

[GnMo05] J. Gnitecki and Z. Moussavi, "The fractality of lung sounds: A comparison of three waveform fractal dimension algorithms," *Chaos Soliton. Fract.*, vol. 26, pp. 1065-1072, 2005.

[GnMo07] J. Gnitecki and Z. Moussavi, " Separating heart sounds from lung sounds," *IEEE Med. Biol. Mag.*, vol. 27, no. 1, pp. 20-29, Jan. 2007.

[GnMP03] J. Gnitecki, Z. Moussavi, and H. Pasterkamp, "Recursive least squares adaptive noise cancellation filtering for heart sound reduction in lung sound recordings," in *Proc. 25th Annu. Int. Conf. IEEE Eng. Medicine Biology Soc., EMBC'03*, vol. 3, pp. 2420-2423, Sept. 2003.

[GnMP04] J. Gnitecki, Z. Moussavi, and H. Pasterkamp, "Classification of Lung Sounds during Bronchial Provocation Using Waveform Fractal Dimensions," in *Proc. 26th Annu. Int. Conf. IEEE Eng. Medicine Biology Soc., EMBC'04*, vol. 2, pp. 3844-3847, Sept. 2004.

[GnMP05a] J. Gnitecki, Z. Moussavi, and H. Pasterkamp, "Geometrical and dynamical state space parameters of lung sounds," in *Proc. 5th Int. Workshop on Biosignal Interpretation, BSI'05*, vol. 5, pp. 113-116, Sept. 2005.

[GnMP05b] J. Gnitecki, Z. Moussavi, and H. Pasterkamp, "Differences between healthy and asthmatic lung sounds before and after induced bronchodilation," in *Proc. 8th Annu. University of Manitoba Graduate Students Conf., GradCON'05*, Oct. 2005.

[GNRC95] N. Gavriely, M. Nissan, A. H. Rubin, and D. W. Cugell, "Spectral characteristics of chest wall breath sounds in normal subjects," *Thorax*, vol. 50, no. 12, pp. 1292-1300, Dec. 1995.

[GoJC89] V. Goncharoff, J. E. Jacobs, and D. W. Cugell, "Wideband acoustic transmission of human lungs," *Med. Biol. Eng. Comput.*, vol. 27, no. 5, pp. 513-519, Sept. 1989.

[Gray74] H. Gray, *Gray's Anatomy*. Philadelphia, PA: Running Press, 1974.

[GrWN02] Q. Grimal, A. Watzky, and S. Naili, "A one-dimensional model for propagation of transient pressure waves through the lung," *J. Biomech.*, vol. 35, pp. 1081-1089, 2002.

[Gros89] P. G. Gross, *The Use of a Piezoelectric Polymer Transducer to Study the Frequency Partition of Chest Wall Sounds*. PhD Thesis, Northwestern University, 1989.

[GSTP03] J. Gnitecki, K. Shirota, M. Takase, and H. Pasterkamp, "Detection of respiratory airflow by phonospirometry," *Am. J. Respir. Crit. Care Med.*, vol. 167, Abstracts Suppl., p. A544, 2003.

[HaPa79] J. C. Hardin and J. L. Patterson Jr., "Monitoring the state of the human airways by analysis of respiratory sound," *Acta Astronaut.*, vol. 6, no. 9, pp. 1137-1151, Sept. 1979.

[HaPa97] L. J. Hadjileontiadis and S. M. Panas, "Adaptive reduction of heart sounds from lung sounds using fourth-order statistics," *IEEE Trans. Biomed. Eng.*, vol. 44, no. 7, pp. 642-648, July 1997.

[HaPa98] L. J. Hadjileontiadis and S. M. Panas, "A wavelet-based reduction of heart sound noise from lung sounds," *Int. J. Med. Inf.*, vol. 52, no. 1-3, pp. 183-190, Oct. 1998.

[HaRe03] L. J. Hadjileontiadis and I. T. Rekanos, "Detection of explosive lung and bowel sounds by means of fractal dimension," *IEEE Sig. Process. Lett.*, vol. 10, no. 10, pp. 311-314, 2003.

[HeHe06] J. L. Heraghty and A. J. Henderson, "Highlights in asthma 2005," *Arch. Dis. Child.*, vol. 91, no. 5, pp. 422-425, 2006.

[HiWW91] H. A. Hidalgo, M. J. Wegmann, and W. W. Waring, "Frequency spectra of normal breath sounds in childhood," *Chest*, vol. 100, no. 4, pp. 999-1002, Oct. 1991.

[HKPW01] P. Harper, S. S. Kraman, H. Pasterkamp, and G. R. Wodicka, "An acoustic model of the respiratory tract," *IEEE Trans. Biomed. Eng.*, vol. 48, no. 5, pp. 543-550, May 2001.

[HMAA00] L. T. Hall, J. L. Maple, J. Agzarian, and D. Abbott, "Sensor system for heart sound biomonitor," *Microelectronics J.*, vol. 31, no. 7, pp. 583-592, 2000.

[HoCu68] K. Horsfield and G. Cumming, "Morphology of the bronchial tree in man," *J. Appl. Physiol.*, vol. 24, no. 3, pp. 373-383, 1968.

[Hogg78] J. C. Hogg, "Bronchial asthma," in *The Lung: Structure, Function and Disease (International Academy of Pathology Monograph)*. W. M. Thurlbeck, Ed. Baltimore, MD: The Williams & Wilkins Company, 1978.

[HoJK96] C. R. Houck, J. A. Joines, and M. G. Kay, "A genetic algorithm for function optimization: A Matlab implementation," *ACM Trans. Math. Software*, 1996.

[HoMo02] I. Hossain and Z. Moussavi, "Respiratory airflow estimation by acoustical means," in *Proc. 24th Annu. Int. Conf. IEEE Eng. Medicine Biology Soc., EMBC'02*, vol. 2, pp. 1476-1477, 2002.

[HoMo03] I. Hossain and Z. Moussavi, "An overview of heart-noise reduction of lung sounds using wavelet transform based filter," in *Proc. 25th Annu. Int. Conf. IEEE Eng. Medicine Biology Soc., EMBC'03*, vol. 1, pp. 458-461, 2003.

[HoPH00] M. Howatson Tawhai, A. J. Pullan, and P. J. Hunter, "Generation of an anatomically based three-dimensional model of the conducting airways," *Annals of Biomed. Eng.*, vol. 28, pp. 793-802, 2000.

[HSTF01] S. Hirsch, J. L. Shapiro, M. A. Turega, T. L. Frank, R. M. Niven, and P. I. Frank, "Using a neural network to screen a population for asthma," *Ann. Epidemiol.*, vol. 11, no. 6, pp. 369-376, Aug. 2001.

[Ihle98] F. Ihlenburg, "Finite Element Analysis of Acoustic Scattering," in *Applied Mathematical Sciences Series*, vol. 132. J. E. Marsden and L. Sirovich, Eds. 1998, pp. 1-224.

[InPr99] P. W. Ind and N. B. Pride, "Assessment of airway responses and the cough reflex," in *Lung Function Tests: Physiological Principles and Clinical Applications*. J. M. B. Hughes and N. B. Pride, Eds. London, England: W. B. Saunders, 1999, pp. 219-232.

[IRFP86] V. K. Iyer, P. A. Ramamoorthy, H. Fan, and Y. Ploysongsang, "Reduction of heart sounds from lung sounds by adaptive filtering [published erratum appears in *IEEE Trans. Biomed. Eng.* vol. 35, no. 1, pp. 76, Jan.1988]," *IEEE Trans. Biomed. Eng.*, vol. 33, no. 12, pp. 1141-1148, Dec.1986.

[IYHY06] R. Ito, A. Yokoyama, H. Hamada, Y. Yasuhara, N. Kohno, and J. Higaki, "Effect of inhalated bronchodilators on air trapping in patients with stable asthma," *J. Asthma*, vol. 43, pp. 125-129, 2006.

[JJKB99] A. Jones, R .D. Jones, K. Kwong, and Y. Burns, "Effect of positioning on recorded lung sound intensities in subjects without pulmonary dysfunction," *Phys. Ther.*, vol. 79, no. 7, pp. 682-690, July 1999.

[JLBK89] M. Jahed, S. J. Lai-Fook, P. K. Bhagat, and S. S. Kraman, "Propagation of stress waves in inflated sheep lungs," *J. Appl. Physiol.*, vol. 66, no. 6, pp. 2675-2680, 1989.

[JoKo70] N. L. Johnson and S. Kotz, "Pareto Distribution," in *Continuous Univariate Distributions – 1.* Boston, MA: Houghton Mifflin Company, 1970, pp. 233-249.

[Katz88] M. J. Katz, "Fractals and the analysis of waveforms," *Comput. Biol. Med.*, vol. 18, no. 3, pp. 145-156, Mar. 1988.

[KBYC03] Y .P. Kayha, E. Bayatli, M. Yeginer, K. Ciftci, and G. Kilinc, "Comparison of different feature sets for respiratory sound classifiers," in *Proc. 25th Annu. Int. Conf. IEEE Eng. Medicine Biology Soc., EMBC'03*, pp. 2853-2856, 2003.

[KCSM05] C. Kotaru, A. Coreno, M. Skowronski, G. Muswick, R. C. Gilkeson, and E. R. McFadden, Jr., "Morphometric changes after thermal and methacholine bronchoprovocations," *J. Appl. Physiol.*, vol. 98, pp. 1028-1036.

[Kins94] W. Kinsner, "Batch and real-time computation of a fractal dimension based on variance of a time series," Dept. of Electrical and Computer Engineering, University of Manitoba, Winnipeg, MB, Technical Report DEL94-6, 1994.

[KKRJ04] A. Kandaswamy, C .S. Kumar, R. P. Ramanathan, S. Jayaraman, and N. Malmurugan, "Neural classification of lung sounds using wavelet coefficients," *Comput. Biol. Med.*, vol. 34, no. 6, pp. 523-537, Sept. 2004.

[KoKT98] V. I. Korenbaum, Y. V. Kulakov, and A. A. Tagiltsev, "A new approach to acoustical evaluation of human respiratory sounds," *Biomed. Instrumen. Technol.*, vol. 32, no. 2, pp. 147-154, 1998.

[KoRu92] M. Kompis and E. Russi, "Adaptive heart-noise reduction of lung sounds recorded by a single microphone," in *Proc. 14th Annu. Int. Conf. IEEE Eng. Medicine Biology Soc., EMBC'92*, pp. 691-692, 1992.

[KoRu97] M. Kompis and E. W. Russi, "Computer-based lung sound simulation," *Med. Biol. Eng. Comput.*, vol. 35, no. 3, pp. 231-238, 1997.

[KPKT98] S. S. Kraman, H. Pasterkamp, M. Kompis, M. Takase, and G. R. Wodicka, "Effects of breathing pathways on tracheal sound spectral features," *Respir. Physiol.*, vol. 111, no. 3, pp. 295-300, Mar. 1998.

[KPPW06] S. S. Kraman, G. A. Pressler, H. Pasterkamp, and G. R. Wodicka, "Design, construction, and evaluation of a bioacoustic transducer testing (BATT) system for respiratory sounds," *IEEE Trans. Biomed. Eng.*, vol. 53, no. 8, pp. 1711-1715, 2006.

[Kram83] S. S. Kraman, "Does the vesicular lung sound come only from the lungs?," *Am. Rev. Respir. Dis.*, vol. 128, no. 4, pp. 622-626, Oct. 1983.

[Kram84] S. S. Kraman, "The relationship between airflow and lung sound amplitude in normal subjects," *Chest*, vol. 86, no. 2, pp. 225-229, Aug. 1984.

[KrWa90] S. S. Kraman and P. M. Wang, "Airflow-generated sound in a hollow canine airway cast," *Chest*, vol. 97, no. 2, pp. 461-466, Feb. 1990.

[KWAW01] K. L. Kruse, P. T. Williams, G. O. Allgood, R. C. Ward, S. S. Gleason, M. J. Paulus, N. Munro, G. Mahinthakumar, C. Narasimhan, J. R. Hammersley, and D. E. Olson, "Flow simulation in a 3-D model of pig airways and connection to lung sounds," *Proc. SPIE*, vol. 4368, pp. 168-176, 2001.

[KWOP95] S. S. Kraman, G. R. Wodicka, Y. Oh, and H. Pasterkamp, "Measurement of respiratory acoustic signals. Effect of microphone air cavity width, shape, and venting," *Chest*, vol. 108, no. 4, pp. 1004-1008, Oct. 1995.

[KWWC06] R. Kumar, B. Wang, X. Wang, C. Chen, J. Yang, L. Fu, and X. Xu, "Bronchodilatory responses in Chinese children from asthma index families and the general population," *J. Aller. Clin. Immunol.*, vol. 117, no. 6, pp. 1257-1263, 2006.

[LaMo04] L. J. Lazareck and Z. Moussavi, "Classification of normal and dysphagic swallows by acoustical means," *IEEE Trans. Biomed. Eng.*, vol. 51, no. 12, pp. 2103-2112, 2004.

[LBBA06] L. Loland, F. F. Buchvald, L. Brydensholt Halkjær, J. Anhøj, G. L. Hall, T. Persson, T. Grove Krause, and H. Bisgaard, "Sensitivity of bronchial responsiveness measurements in young infants," *Chest*, vol. 129, no. 3, pp. 669-675, 2006.

[LeSe96] A. H. Leung and S. Sehati, "Sound transmission through normal and diseased human lungs," *Eng. Sci. Edu. J.*, pp. 25-31, 1996.

[LiRh98] J. Li and R. R. Rhinehart, "Heuristic random optimization," *Computers Chem. Eng.*, vol. 22, no. 3, pp. 427-444, 1998.

[LiSZ03] Y. Liu, R. M. C. So, and C. H. Zhang, "Modeling the bifurcating flow in an asymmetric human lung airway," *J. Biomech.*, vol. 36, pp. 951-959, 2003.

[LLZW03] A. M. Li, C. Lex, A. Zacharasiewicz, E. Wong, E. Erin, T. Hansel, N. M. Wilson, and A. Bush, "Cough frequency in children with stable asthma:

Correlation with lung function, exhaled nitric oxide, and sputum eosinophil count," *Thorax*, vol. 58, no. 11, pp. 974-978, 2003.

[LoMu84] R. Loudon and R. L. Murphy Jr., "Lung sounds," *Am. Rev. Respir. Dis.*, vol. 130, no. 4, pp. 663-673, Oct. 1984.

[LuDW95] S. Lu, P. C. Doerschuk, and G. R. Wodicka, "Parametric phase-delay estimation of sound transmitted through intact human lung," *Med. Biol. Eng. Comput.*, vol. 33, no. 3, pp. 293-298, May 1995.

[LuGi97] K. R. Lutchen and H. Gillis, "Relationship between heterogeneous changes in airway morphometry and lung resistance and elastance," *J. Appl. Physiol.*, vol. 83, no. 4, pp. 1192-1201, 1997.

[Luis64] A. A. Luisada, "The areas of auscultation and the two main heart sounds," *Med. Times.*, vol. 92, pp. 8-11, Jan. 1964.

[LuLQ88] Y.-S. Lu, W.-H. Liu, and G.-X. Qin, "Removal of the heart sound noise from the breath sound," in *Proc. 10th Annu. Int. Conf. IEEE Eng. Medicine Biology Soc., EMBC'88*, pp. 175-176, 1988.

[McKu58] V. A. McKusick, *Cardiovascular Sound in Health and Disease.* Baltimore, MD: The Williams & Wilkins Company, 1958.

[Mack99] P. T. Macklem, "Foreword to Lung Function Tests: Physiological Principles and Clinical Applications," in *Lung Function Tests: Physiological Principles and Clinical Applications*. J. M. B. Hughes and N. B. Pride, Eds. London, England: W. B. Saunders, 1999, p. ix.

[MaGa94] M. Mahagnah and N. Gavriely, "Repeatability of measurements of normal lung sounds," *Am. J. Respir. Crit. Care Med.*, vol. 149, no. 2 pt. 1, pp. 477-481, Feb. 1994.

[Marm04] V. Z. Marmarelis, *Nonlinear dynamic modeling of physiological systems.* Hoboken, NJ: John Wiley & Sons, Inc., 2004.

[MaSS94] L. P. Malmberg, R. Sorva, and A. R. Sovijärvi, "Frequency distribution of breath sounds as an indicator of bronchoconstriction during histamine challenge test in asthmatic children," *Pediatr. Pulmonol.*, vol. 18, no. 3, pp. 170-177, Sept. 1994.

[MDKP97] G. R. Manecke Jr, J. P. Dilger, L. J. Kutner, and P. J. Poppers, "Auscultation revisited: The waveform and spectral characteristics of breath sounds during general anesthesia.," *Int. J. Clin. Monit. Comput.*, vol. 14, no. 4, pp. 231-240, Nov. 1997.

[Melb01] H. Melbye, "Auscultation of the lungs, still a useful examination?," *Tidsskr Nor Laegeforen*, vol. 121, pp. 451-454, 2001.

[MHMO99] T. D. Mast, L. M. Hinkelman, L. A. Metlay, M. J. Orr, and R. C. Waag, "Simulation of ultrasonic pulse propagation, distortion, and attenuation in the human chest wall," *J. Acoust. Soc. Am.*, vol. 106, no. 6, pp. 3665-3677, Dec. 1999.

[Mich96] Z. Michalewicz, *Genetic Algorithms + Data Structures = Evolution Programs*, 3 ed. New York, NY: Springer-Verlag, 1996.

[MJJH96] R. Maciejewski, M. Jarosz, B. Jarosz, and T. Hermanowicz, "Variability of modes of division of the superior lobar bronchi in the right and left lungs," *Folia Morphol. (Warsz.)*, vol. 55, no. 3, pp. 167-174, 1996.

[MNMO90] M. J. Mussell, Y. Nakazono, Y. Miyamoto, S. Okabe, and T. Takishima, "Distinguishing normal and abnormal tracheal breathing sounds by principal component analysis," *Japan. J. Physiol.*, vol. 40, pp. 713-721, 1990.

[MoFT04] Z. Moussavi, D. Flores, and G. Thomas, "Heart sound cancellation based on multiscale products and linear prediction," in *Proc. 26th Annu. Int. Conf. IEEE Eng. Medicine Biology Soc., EMBC'04*, pp. 3840-3843, 2004.

[MoIn68] P. M. Morse and K. U. Ingard, *Theoretical Acoustics*. Princeton, NJ: Princeton University Press, 1968.

[Murr26] C. D. Murray, "The physiological principle of minimum work. I. The vascular system and the cost of blood volume," *Proc. National Acad. Science*, vol. 12, pp. 207-214, 1926.

[Muss92] M. J. Mussell, "The need for standards in recording and analyzing respiratory sounds," *Med. Biol. Eng. Comput.* , vol. 30, pp. 129-139, 1992.

[MuVe05] G. Musch and J. G. Venegas, "Positron Emission Tomography imaging of regional pulmonary perfusion and ventilation," *Proc. Am. Thorac. Soc.*, vol. 2, no. 6, pp. 522-527, 2005.

[Nave05] C. R. Nave, "Sound Speed in Gases," Department of Physics and Astronomy, Georgia State University, 2005. Available: http://hyperphysics.phy-astr.gsu.edu/hbase/sound/souspe3.html

[NCSB91] N. Noviski, L. Cohen, C. Springer, E. Bar-Yishay, A. Avital, and S. Godfrey, "Bronchial provocation determined by breath sounds compared with lung function," *Arch. Dis. Child.*, vol. 66, no. 8, pp. 952-955, Aug. 1991.

[NeMa88] T. R. Nelson and D. K. Manchester, "Modeling of lung morphogenesis using fractal geometries," *IEEE. Trans. Med. Imag.*, vol. 7, no. 4, pp. 321-327, 1988.

[NeWG90] T. R. Nelson, B. J. West, and A. L. Goldberger, "The fractal lung: Universal and species-related scaling patterns," *Experentia*, vol. 46, no. 3, pp. 251-254, 1990.

[NiSc85] A. I. Nikiforov and R. B. Schlesinger, "Morphometric variability of the human upper bronchial tree," *Respir. Physiol.*, vol. 59, pp. 289-299, 1985.

[NWKG04] C. Narasimhan, R. Ward, K. L. Kruse, M. Guddati, and G. Mahinthakumar, "A high resolution computer model for sound propagation in the human thorax based on the Visible Human data set," *Comp. Biol. Med.*, vol. 34, pp. 177-192, 2004.

[OhPa93] Y. Oh and H. Pasterkamp, "Interbreath variance of lung sound spectra and effects of data windows and flow gate tolerances," in *Proc. 18th Annu. Int. Lung Sounds Assoc. Conf., ILSA'93*, Lake Louise, Canada, 1993.

[ONJK04] M. Ochs, J. R. Nyengaard, A. Jung, L. Knudson, M. Voigt, T. Wahlers, J. Richter, and H. J. G. Gundersen, "The number of alveoli in the human lung," *Am. J. Respir. Crit. Care Med.*, vol. 169, pp. 120-124, 2004.

[Onys03] S. Onyshko, "Nonlinear Systems Analysis," Course notes, 24.770, University of Manitoba, Dept. of Electrical and Computer Engineering, 2003.

[OudM02] M. Oud, "Internal-state analysis in a layered artificial neural network trained to categorize lung sounds," *IEEE Trans. Syst. Man and Cybernet. - Part A: Syst. and Humans*, vol. 32, no. 6, pp. 757-760, 2002.

[OuDv00] M. Oud, E. H. Dooijes, and J. S. van der Zee, "Asthmatic airways obstruction assessment based on detailed analysis of respiratory sound spectra," *IEEE Trans. Biomed. Eng.*, vol. 47, no. 11, pp. 1450-1455, 2000.

[PaCh87] T. S. Parker and L. O. Chua, "Chaos: A tutorial for engineers," *Proc. of the IEEE*, vol. 75, no. 8, pp. 982-1008, 1987.

[PaGM03] H. Pasterkamp, J. Gnitecki, and S. Maiti, "Characteristics of respiratory sounds standardized to flow from pneumotachograph vs. Respitrace®," in *Proc. 28th Annu. Int. Lung Sounds Assoc. Conf., ILSA'03*, p. 21, Cancun, Mexico, Sept. 2003.

[PaHa00] K. Parameswaran and F. E. Hargreave, "Assessment of airway inflammation in asthma using non-invasive methods," in *Asthma: Epidemiology, Anti-Inflammatory Therapy and Future Trends*. M. A. Giembycz and B. J. O'Connor, Eds. Basel, Switzerland: Birkhäuser Verlag, 2000.

[PaHC71] H. Parker, K. Horsfield, and G. Cumming, "Morphology of distal airways in the human lung," *J. Appl. Physiol.*, vol. 31, no. 3, pp. 386-391, 1971.

[PaKW97] H. Pasterkamp, S. S. Kraman, and G. R. Wodicka, "Respiratory sounds. Advances beyond the stethoscope," *Am. J. Respir. Crit. Care Med.*, vol. 156, no. 3 pt. 1, pp. 974-987, Sept. 1997.

[PaPS96] H. Pasterkamp, R. E. Powell, and I. Sanchez, "Lung sound spectra at standardized air flow in normal infants, children, and adults," *Am. J. Respir. Crit Care Med.*, vol. 154, no. 2 Pt 1, pp. 424-430, Aug. 1996.

[PBKM97] A. Purohit, A. Bohadana, M. C. Kopferschmitt-Kubler, L. Mahr, J. Linder, and G. Pauli, "Lung auscultation in airway challenge testing," *Respir. Med.*, vol. 91, no. 3, pp. 151-157, Mar. 1997.

[PCOH97] H. Pasterkamp, R. Consunji-Araneta, Y. Oh, and J. Holbrow, "Chest surface mapping of lung sounds during methacholine challenge," *Pediatr. Pulmonol.*, vol. 23, no. 1, pp. 21-30, Jan. 1997.

[PeJS92] H. O. Peitgen, H. Jürgens, and D. Saupe, *Chaos and Fractals: New Frontiers of Science*. New York, NY: Springer-Verlag, 1992.

[PeSS71] T. J. Pedley, R. C. Schroter, and M. F. Sudlow, "Flow and pressure drop in systems of repeatedly branching tubes," *J. Fluid. Mech.*, vol. 46, no. part 2, pp. 365-383, 1971.

[PFDR06] S. P. Peters, G. Ferguson, Y. Deniz, and C. Reisner, "Uncontrolled asthma: A review of the prevalence, disease burden and options for treatment," *Respir. Med.*, vol. 100, pp. 1139-1151, 2006.

[PKDW93] H. Pasterkamp, S. S. Kraman, P. D. DeFrain, and G. R. Wodicka, "Measurement of respiratory acoustical signals. Comparison of sensors," *Chest*, vol. 104, no. 5, pp. 1518-1525, Nov. 1993.

[PKMR02] S. Paparis, A. Kotanidou, K. Malagari, and C. Roussos, "Clinical review: Severe asthma," *Crit. Care*, vol. 6, no. 1, pp. 30-44, 2002.

[PLDW95] S. Patel, S. Lu, P. C. Doerschuk, and G. R. Wodicka, "Sonic phase delay from trachea to chest wall: Spatial and inhaled gas dependency," *Med. Biol. Eng. Comput.*, vol. 33, pp. 571-574, 1995.

[PoMi99] D. Popivanov and A. Mineva, "Testing procedures for non-stationarity and non-linearity in physiological signals," *Mathematical Biosciences*, vol. 157, pp. 303-320, 1999.

[PoMT03] M. T. Pourazad, Z. Moussavi, and G. Thomas, "Heart sound cancellation from lung sound recordings using adaptive thresholding and 2D interpolation in time-frequency domain," in *Proc. 25th Annu. Int. Conf. IEEE Eng. Medicine Biology Soc., EMBC'03*, pp. 2586-2589, 2003.

[PoSY01] A. Pohlman, S. Sehati, and D. Young, "Effect of changes in lung volume on acoustic transmission through the human respiratory system," *Physiol. Meas.*, vol. 22, no. 1, pp. 233-243, 2001.

[Pran52] L. Prandtl, *Essentials of Fluid Dynamics with Applications to Hydraulics, Aeronautics, Meteorology, and Other Subjects*. London: Blackie & Son Limited, 1952.

[Prid99] N. B. Pride, "Tests of forced expiration and inspiration: Airflow resistance," in *Lung Function Tests: Physiological Principles and Clinical*

Applications. J. M. B. Hughes and N. B. Pride, Eds. London, England: W. B. Saunders, 1999, pp. 3-25.

[PVSM03] R. Paciej, A. Vyshedskiy, J. Shane, and R. Murphy, "Transpulmonary speed of sound input into the supraclavicular space," *J Appl. Physiol.*, vol. 94, no. 2, pp. 604-611, Feb. 2003.

[QKDK02] C. L .Que, C. Kolmaga, L. G. Durand, S. M. Kelly, and P. T. Macklem, "Phonospirometry for noninvasive measurement of ventilation: Methodology and preliminary results," *J. Appl. Physiol.*, vol. 93, no. 4, pp. 1515-1526, Oct. 2002.

[QKOM01] C. L. Que, C. M. Kenyon, R. Olivenstein, P. T. Macklem, and G. N. Maksym, "Homeokinesis and short-term variability of human airway caliber," *J. App. Physiol.*, vol. 91, no. 3, pp. 1131-1141, Sept. 2001.

[Quin87] D. W. Quinn, "A finite element method for computing sound propagation in ducts," *Mathematics and Computers in Simulation*, vol. 29, no. 1, pp. 51-64, 1987.

[QWLA04] Y. Qiu, A. R. Whittaker, M. Lucas, and K. Anderson, "A preliminary study of contact effects of air coupled stethoscopes," in *Proc. 29th Annu. Int. Lung Sounds Assoc. Conf., ILSA '04,* p. 15, Glasgow, Scotland, Sept. 2004.

[Rice83] D. A. Rice, "Sound speed in pulmonary parenchyma," *J. Appl. Physiol.*, vol. 54, no. 1, pp. 304-308, Jan. 1983.

[Rice85] D. A. Rice, "Transmission of Lung Sounds," *Semin. Respir. Med.*, vol. 6, no. 3, pp. 166-170, Jan. 1985.

[RiOD99] S. Rietveld, M. Oud, and E. H. Dooijes, "Classification of asthmatic breath sounds: Preliminary results of the classifying capacity of human examiners versus artificial neural networks," *Comput. Biomed. Res.*, vol. 32, no. 5, pp. 440-448, Oct. 1999.

[RiRP99] S. Rietveld, L. H. Rijssenbeek-Nouwens, and P. J. Prins, "Cough as the ambiguous indicator of airway obstruction in asthma," *J. Asthma*, vol. 36, no. 2, pp. 177-186, 1999.

[RoCD93] M. T. Rosenstein, J. J. Collins, and C. J. De Luca, "A practical method for calculating largest Lyapunov exponents from small data sets," *Physica D*, vol. 65, pp. 117-134, 1993.

[RoCD94] M. T. Rosenstein, J. J. Collins, and C. J. De Luca, "Reconstruction expansion as a geometry-based framework for choosing proper delay times," *Physica D*, vol. 73, pp. 82-98, 1994.

[RoLo86] V. Rothschild and N. Logothetis, *Probability Distributions*. New York, NY: John Wiley & Sons, Inc, 1986.

[RuTa71] F. Ruelle and F. Takens, "On the nature of turbulence," *Comm. Math. Phys.*, vol. 20, pp. 167-192, 1971.

[SASL98] B. Suki, A. M. Alencar, M. K. Sujeer, K. R. Lutchen, J. J. Collins, J. S. Andrade, E. P. Ingenito, S. Zapperi, and H. E. Stanley, "Life-support system benefits from noise," *Nature*, vol. 393, pp. 127-128, May 1998.

[SaVi03] I. Sanchez and C. Vizcaya, "Tracheal and lung sounds repeatability in normal adults," *Respir. Med.*, vol. 97, no. 12, pp. 1257-1260, Dec.2003.

[SAWT93] I. Sanchez, A. Avital, I. Wong, A. Tal, and H. Pasterkamp, "Acoustic vs. spirometric assessment of bronchial responsiveness to methacholine in children," *Pediatr. Pulmonol.*, vol. 15, no. 1, pp. 28-35, Jan. 1993.

[SBHP94] B. Suki, A.-L. Barabásl, Z. Hantos, F. Peták, and H. E. Stanley, "Avalanches and power-law behavior in lung inflation," *Nature*, vol. 368, pp. 615-618, 1994.

[Scad83] F. G. Scadding, "Definition and clinical categories of asthma," in *Asthma,* 2 ed. T. J. H. Clark and S. Godfrey, Eds. London, England: Chapman and Hall, 1983.

[Sege84] L. J. Segerlind, *Applied Finite Element Analysis*, 2 ed. New York, NY: John Wiley and Sons, 1984.

[SeMa04] A. J. E. Seely and P. T. Macklem, "Complex systems and the technology of variability analysis," *Crit. Care*, vol. 8, no. 6, p. R367-R384, 2004.

[Sevc98] C. Sevcik, "A procedure to estimate the fractal dimension of waveforms," *Complexity International*, vol. 5 1998. Available: http://journal-ci.csse.monash.edu.au/ci/vol05/sevcik/sevcik.html.

[SeWP00] C. Y. Seow, L. Wang, and P. D. Paré, "Airway narrowing and internal structural constraints," *J. Appl. Physiol.*, vol. 88, pp. 527-533, 2000.

[SGLG96] A. B. Sprikkelman, M. H. Grol, M. S. Lourens, J. Gerritsen, H. S. Heymans, and W. M. van Aalderen, "Use of tracheal auscultation for the assessment of bronchial responsiveness in asthmatic children," *Thorax*, vol. 51, no. 3, pp. 317-319, Mar. 1996.

[SGPU00] C. Springer, S. Godfrey, E. Picard, K. Uwyyed, M. Rotschild, S. Hananya, N. Noviski, and A. Avital, "Efficacy and safety of methacholine bronchial challenge performed by auscultation in young asthmatic children," *Am. J. Respir. Crit Care Med.*, vol. 162, no. 3 pt. 1, pp. 857-860, Sept. 2000.

[Sher01] L. Sherwood, *Human Physiology: From Cells to Systems*, 4 ed. Pacific Cove, CA: Brooks/Cole, 2001.

[SKGE94] B. Sankur, Y. P. Kahya, E. Ç. Güler, and T. Engin, "Comparison of AR-based algorithms for respiratory sounds classification," *Comput. Biol. Med.*, vol. 24, no. 1, pp. 67-76, 1994.

[SMPP96] A. R. Sovijarvi, L. P. Malmberg, E. Paajanen, P. Piirila, K. Kallio, and T. Katila, "Averaged and time-gated spectral analysis of respiratory sounds. Repeatability of spectral parameters in healthy men and in patients with fibrosing alveolitis," *Chest*, vol. 109, no. 5, pp. 1283-1290, May 1996.

[STAH05] C. Schram, S. Taubitz, J. Anthoine, and A. Hirschberg, "Theoretical/empirical prediction and measurement of the sound produced by vortex pairing in a low Mach number jet," *J. Sound and Vibration*, vol. 281, pp. 171-187, 2005.

[STPD04] G. Sierra, V. Telfort, B. Popov, L. G. Durand, A. Agarwal, and V. Lanzo, "Monitoring respiratory rate based on tracheal sounds: First experiences," in *Proc. 26th Annu. Int. Conf. IEEE Eng. Medicine Biology Soc., EMBC'04,* pp. 317-320, 2004.

[SWAD06] D. Sistek, K. Wickens, R. Amstrong, W. D'Sousa, I. Town, and J. Crane, "Predictive value of respiratory symptoms and bronchial hyperresponsiveness to diagnose asthma in New Zealand," *Respir. Med.*, vol. 100, no. 12, pp. 2107-2111, 2006.

[SWLL05] K. Sohn, W. J. Warwick, Y. W. Lee, J. Lee, and J. E. Holte, "Investigation of non-uniform airflow signal oscillation during high frequency chest compression," *Biomed. Eng. OnLine*, vol. 4, no. 34, pp. 1-14, 2005.

[TaPa96] M. Takase and H. Pasterkamp, "Detection of Mild Airway Narrowing in Children Based on Spectral Characteristics of Normal Lung Sounds," in *Proc. 21st Annu. Int. Lung Sounds Assoc. Conf., ILSA'96*, Chester, England, 1996.

[vaHP04] C. van Ertbruggen, C. Hirsch, and M. Paiva, "Anatomically based three-dimensional model of airways to simulate flow and particle transport using computational fluid dynamics," *J. Appl. Physiol.*, vol. 98, pp. 970-980, 2004.

[VeSt82] J. K. Vennard and R. L. Street, *Elementary Fluid Dynamics*, 6 ed. New York, NY: John Wiley & Sons, 1982.

[Veva84] H. Vermarien and E. van Vollenhoven, "The recording of heart vibrations: A problem of vibration measurement on soft tissue," *Med. Biol. Eng. Comput.*, vol. 22, pp. 168-178, 1984.

[Vinc03] J. Vincent, "Numerical optimization using genetic algorithms," Technical Report School of Design, Engineering, and Computing, Bournemouth University, 2003, pp. 1-44. Available: http://dec.bournemouth.ac.uk/staff/jvincent/index.html.

[VoGO95] I. V. Vovk, V. T. Grinchenko, and V. N. Oleinik, "Modeling the acoustic properties of the chest and measuring breath sounds," *Acoust. Phys.*, vol. 41, no. 5, pp. 667-676, 1995.

[voHa05] L. von Hertzen and T. Haahtela, "Signs of reversing trends in prevalence of asthma," *Allergy*, vol. 60, no. 3, pp. 283-292, 2005.

[VoZK94] I. V. Vovk, K. E. Zalutskii, and L. G. Krasnyi, "Acoustic model of the human respiratory system," *Acoust. Phys.*, vol. 40, pp. 676-680, 1994.

[WADS92] G. R. Wodicka, A. Aguirre, P. D. DeFrain, and D. C. Shannon, "Phase delay of pulmonary acoustic transmission from trachea to chest wall," *IEEE Trans. Biomed. Eng.*, vol. 39, no. 10, pp. 1053-1059, Oct. 1992.

[WBPS95] N. M. Wilson, P. Bridge, S. B. Phagoo, and M. Silverman, "The measurement of methacholine responsiveness in 5 year old children: Three methods compared," *Eur. Respir. J.*, vol. 8, no. 3, pp. 364-370, Mar. 1995.

[WCBK00] L. R. Waitman, K. P. Clarkson, J. A. Barwise, and P. H. King, "Representation and classification of breath sounds recorded in an intensive care setting using neural networks," *J. Clin. Monit. Comput.*, vol. 16, no. 2, pp. 95-105, 2000.

[WeGo62] E. R. Weibel and D. M. Gomez, "Architecture of the human lung," *Science*, vol. 137, no. 3530, pp. 577-585, 1962.

[Weib63] E. R. Weibel, *Morphometry of the Human Lung*. Berlin, Germany: Springer-Verlag, 1963.

[Weib84] E. R. Weibel, *The Pathway for Oxygen: Structure and Function in the Mammalian Respiratory System*. Cambridge, MA: Harvard University Press, 1984.

[Weib91] E. R. Weibel, "Fractal geometry: A design principle for living organisms," *J. Appl. Physiol.*, vol. 261, p. L361-L369, 1991.

[West74] J. B. West, *Respiratory Physiology: The Essentials*. Baltimore, MD: The Williams & Wilkins Company, 1974.

[West77] J. B. West, *Bioengineering Aspects of the Lung*. New York, NY: Marcel Dekker, Inc., 1977.

[WHDK97] B. R. Wiggs, C. A. Hrousis, J. M. Drazen, and R. D. Kamm, "On the mechanism of mucosal folding in normal and asthmatic airways," *J. Appl. Physiol.*, vol. 83, no. 6, pp. 1814-1821, 1997.

[WiDe97] F. Wilquem and G. Degrez, "Numerical modeling of steady inspiratory airflow through a three-generation model of the human central airways," *J. Biomech. Eng.*, vol. 119, pp. 59-65, 1997.

[WKZP94] G. R. Wodicka, S. S. Kraman, G. M. Zenk, and H. Pasterkamp, "Measurement of respiratory acoustic signals. Effect of microphone air cavity depth," *Chest*, vol. 106, no. 4, pp. 1140-1144, Oct. 1994.

[WoWh86] H. Q. Woodard and D. R. White, "The composition of body tissues," *Br. J. Radiol.*, vol. 59, no. 708, pp. 1209-1218, 1986.

[WSGC89] G. R. Wodicka, K. N. Stevens, H. L. Golub, E. G. Cravalho, and D. C. Shannon, "A model of acoustic transmission in the respiratory system," *IEEE Trans. Biomed. Eng.*, vol. 36, no. 9, pp. 925-934, Sept. 1989.

[WSGS90] G. R. Wodicka, K. N. Stevens, H. L. Golub, and D. C. Shannon, "Spectral characteristics of sound transmission in the human respiratory system," *IEEE Trans. Biomed. Eng.*, vol. 37, no. 12, pp. 1130-1135, Dec. 1990.

[YaMo05] A. Yadollahi and Z. Moussavi, "Measuring minimum critical flow for normal breath sounds," in *Proc. 27th Annu. Int. Conf. IEEE Eng. Medicine Biology Soc., EMBC'05*, pp. 2726-2729, 2005.

[YaMo06] A. Yadollahi and Z. M. K. Moussavi, "A robust method for estimating respiratory flow using tracheal sounds entropy," *IEEE Trans. Biomed. Eng.*, vol. 53, no. 4, pp. 662-668, 2006.

[Yate82] F. E. Yates, "The 10th J. A. F. Stevenson Memorial Lecture: Outline of a physical theory of physiological systems," *Can. J. Physiol. Pharmacol.*, vol. 60, pp. 217-248, 1982.

[YiZh01] L. Yip and Y. T. Zhang, "Reduction of heart sounds from lung sound recordings by automated gain control and adaptive filtering techniques," in *Proc. 23rd Annu. Int. Conf. IEEE Eng. Medicine Biology Soc., EMBC'01*, pp. 2154-2156, 2001.

[ZbDZ02] J. P. Zbilut, D. D. Dixon, and M. Zak, "Detecting singularities of piecewise deterministic (terminal) dynamics in experimental data," *Phys. Lett. A,* vol. 304, pp. 95-101, 2002.

[ZbZS02] J. P. Zbilut, J.-M. Zaldivar-Comenges, and F. Strozzi, "Recurrence quantification based on Liapunov exponents for monitoring divergence in experimental data," *Phys. Lett. A*, vol. 297, pp. 173-181, 2002.

[ZoLy95] V. V. Zosimov and L. M. Lyamshev, "Fractals in wave processes," *Physics-Uspekhi*, vol. 38, no. 4, pp. 347-384, 1995.

APPENDIX A

List of Publications

A.1 Refereed Journal, Magazine, and Conference Proceeding Papers

[1] **J. Gnitecki** and Z. Moussavi, "Separating heart sounds from lung sounds," *IEEE Eng. Med. Biol. Mag.*, vol. 26, no.1, pp. 20-29, 2007.

[2] **J. Gnitecki,** I. Hossain, H. Pasterkamp, and Z. Moussavi, "Qualitative and quantitative evaluation of heart sound reduction from lung sound recordings," *IEEE Trans. Biomed. Eng.*, vol. 52, no. 10, pp. 1788-1792, 2005.

[3] **J. Gnitecki** and Z. Moussavi, "The fractality of lung sounds: A comparison of three waveform fractal dimension algorithms," *Chaos Soliton. Fract.*, vol. 26, no. 4, pp. 1065-1072, 2005.

[4] **J. Gnitecki,** Z. Moussavi, and H. Pasterkamp, "Geometrical and dynamical state space parameters of lung sounds," in *Proc. 5th Int. Workshop on Biosignal Interpretation, BSI'05*, vol. 5, pp. 113-116, 2005.

[5] **J. Gnitecki,** Z. Moussavi, and H. Pasterkamp, "Classification of lung sounds during bronchial provocation using waveform fractal dimensions," in *Proc. 26th Annu. Int. Conf. IEEE Eng. Medicine Biology Soc., EMBC'04*, vol. 2, pp. 3844-3847, 2004.

[6] **J. Gnitecki** and Z. Moussavi, "Variance fractal dimension trajectory as a tool for heart sound localization in lung sound recordings," in *Proc. 25th Annu. Int. Conf. IEEE Eng. Medicine Biology Soc., EMBC'03*, vol. 3, pp. 2420-2423, 2003.

[7] **J. Gnitecki,** Z. Moussavi, and H. Pasterkamp, "Recursive least squares adaptive noise cancellation filtering for heart sound reduction in lung sound recordings," in *Proc. 25th Annu. Int. Conf. IEEE Eng. Medicine Biology Soc., EMBC'03*, vol. 3, pp. 2416-2419, 2003.

[8] **J. Gnitecki,** G. Kler, and Z. Moussavi, "EMG sings of fatigue in anterior and posterior deltoid muscles: Questioning the role of RMS during fatigue," in *Proc. 27th Canadian Medical Biological Eng. Soc. Conf., CMBEC27*, 2002.

A.2 Conference Proceeding Abstracts

[9] J. A. Fiz, J. L. Pang, **J. Gnitecki,** and H. Pasterkamp, "Bronchodilation increases flow-specific inspiratory lung sound intensity," in *Proc. Am. Thorac. Soc.*, vol. 3, Abstracts Issue, p. A455, 2006.

[10] **J. Gnitecki,** Z. Moussavi, and H. Pasterkamp, "Differences between healthy and asthmatic lung sounds before and after induced bronchodilation," in *Proc. 8th Annu. University of Manitoba Graduate Students Conf., GradCON'05*, 2005

[11] **J. Gnitecki,** G. Katz, and H. Pasterkamp, "Effects of time, breathing apparatus and sensor location on flow-specific lung sound intensity in healthy children," *Can. Respir. J.*, vol. 12, no. 3, p. 164, 2005.

[12] **J. Gnitecki** and H. Pasterkamp, "Reproducibility of flow-specific lung sound intensity in healthy children," In *Proc. Am. Thorac. Soc.*, vol. 2, Abstracts Issue, p. A776, 2005.

[13] **J. Gnitecki,** S. Maiti, M. Barzanji, and H. Pasterkamp, "Monitoring airway status by flow standardized breath sound intensity," *Eur. Respir. J.*, vol. 24,

Suppl. 48, p. 225s, 2004.

[14] **J. Gnitecki,** S. Maiti, M. Barzanji, and H. Pasterkamp, "Does flow-standardized breath sound intensity indicate changes in airway diameter?," *Can. Respir. J.*, vol. 11, no. 3, p. 237, 2004.

[15] **J. Gnitecki,** K. Shirota, M. Takase, and H. Pasterkamp, "Detection of respiratory airflow by phonospirometry," *Am. J. Respir. Crit. Care Med.*, vol. 167, Abstracts Suppl., p. A544, 2003.

[16] H. Kiyokawa, **J. Gnitecki,** and H. Pasterkamp, "Effect of deep inspiration on flow standardized inspiratory lung sounds," *Am. J. Respir. Crit. Care Med.*, vol. 167, Abstracts Suppl., p. A544, 2003.

[17] H. Pasterkamp, **J. Gnitecki,** and S. Maiti, "Characteristics of respiratory sound standardized to flow from pneumotachograph vs. Respitrace®," in *Proc. 28th Annu. Int. Lung Sounds Assoc. Conf., ILSA'03*, vol. 28, p. 21, 2003.

[18] S. Kraman, G. Wodicka, **J. Gnitecki,** and H. Pasterkamp, "Promise and problems in the design of an artificial crackle generator for testing lung sound transducers," in *Proc. 28th Annu. Int. Lung Sounds Assoc. Conf., ILSA'03*, vol. 28, p. 35, 2003.

APPENDIX B

Variation and Variability in Lung Structure and Sounds

B.1 Introduction

Many forms of variability may affect the analysis of biological waveforms and systems, including natural variation in structure within and between subjects as outlined in Chapter 2 [SeMa04], and variability in observation or methods of measurement between investigators [EaCh00a]. Regarding the latter point, as articulated by F. E. Yates [Yate82], "... in science, we often would rather use a colleague's toothbrush than his terminology."

Variability may be analyzed using statistical measures; fractal analysis; measurement of entropy; and (considering waveforms) other time- and also frequency-domain techniques [SeMa04]. For biological waveforms, most of these types of analyses are confounded by the need for stationarity in the data. The requirement for stationarity is often addressed by evaluating signals within relatively short windows of time in which stationarity is assumed to be present [SeMa04] (mentioned in Chapter 3 as relevant to lung sounds).

This appendix presents an overview of variation and variability in lung structure and in lung sounds of healthy subjects, which is of importance in the objective assessment of changes in lung sounds with change in respiratory condition. This appendix also outlines thesis work examining such changes, based on lung sounds

acquired from subjects who have undergone pulmonary function testing (PFT) and bronchial provocation due to symptoms or prior diagnosis of asthma.

B.2 Overview of Natural Variation in Lung Structure

The lungs are complex structures and thus by nature lend themselves to many opportunities for variation to occur. Natural variation in lung structure has been assessed using statistical calculations and frequency distributions of measurements of lung airways such as length and diameter [MJJH96], [NiSc85], and also fractal dimensions [HoCu68] (discussed in Chapter 4). Studies have shown intersubject variation in terms of overall structure [MJJH96], [NiSc85], and also variability in measurements within one branching generation on an intrasubject basis [NiSc85]. In terms of intersubject variation, Maciejewski *et al.* [MJJH96] showed that the first division of left and right (upper lobe) bronchi varies greatly between normal individuals, and also between the left and right lung lobes. They studied 100 right lungs and 100 left lungs taken from the cadavers of males and females aged between 18-80 years. In the right lung lobe there were three types of divisions found, with nine variants across these three types. Divisions in the left lung were categorized into two main types, with five variants.

In another study, intersubject variation was shown to be higher at smaller lung airway measurements (diameter and length), whereas intrasubject variability decreased for smaller dimension values relative to its value at larger measurements [NiSc85]. That study also illustrated some methods and trends in studying variability, such as the desire to fit curves and probability density functions. However, it may be unrealistic in some cases to force data into strict quantitative correlations, especially if exclusion or

absorption of data results. Even with normalization using anthropometric parameters such as height and weight, a natural fit to natural variability may not exist.

Nonetheless, relationships between airway dimensions (length and diameter) and airway generations have been developed in past work [HoCu68], [PaHC71], [WeGo62], [Weib91], some of which accounted for variation in measurements and branching style per generation [HoCu68]. Table B.1 outlines a few such relationships.

B.3 A Study on Variability of Lung Sounds in Healthy Children

B.3.1 Introduction

In order to reliably use changes in lung sounds as indicators of bronchial

Table B.1:
Lung Structure Scaling Relationships

Relationship	Variables	Validity per Lung Region	Notes	Authors
Airway branch diameter, d_z: $d_z = d_0 2^{-z/3}$ Total branches $\approx 2^z$	d_0 = tracheal diameter z = generation number	$0 \leq z \leq 9$ Trachea is $z = 0$	Branching considered symmetrically dichotomous	[WeGo62]
Airway branch diameter, d_z: $d_z = a_n b_n^z$ Total branches per generation $\approx 1.38^{T-z}$	a_n, b_n = constants a_1, b_1 = 0.676, 1.175; a_2, b_2 = 1.340, 1.062 a_3, b_3 = 0.330, 1.161 T = 25 (total generations)	a_n, b_n change per generation grouping: z_1 = 1-6, z_2 = 7-16, z_3 = 17-25 Trachea is $z = 25$ d = 0.7 mm in $z = 1$	Alveoli present if $0.4 \leq d \leq 0.6$ mm Accounted for asymmetry, monopody and trichotomy in branching Based on cast of inflated adult lung	[HoCu68]
$L/d \approx 1$ to 1.5	L = length, d = diameter	All generations		[PaHC71]
$L = 1.10 + 2.57d$	L and d as above	$0.7 \leq d \leq 4$ mm		[HoCu68]
Slope of $\log_{10}(L)$ vs. $\log_{10}(z) = 1.37$	L and z as above	All generations	Length fractal dimension	[NeWG90]
Slope of $\log_{10}(d)$ vs. $\log_{10}(z) = 1.26$	d and z as above	All generations	Diameter fractal dimension	[NeWG90]
Two-dimensional Cayley tree fractal model	Hausdorff and similarity fractal dimensions	All generations	Branching considered symmetrically dichotomous	[NeMa88]

response, it is important to develop thresholds for detection of significant change in lung sounds. Past studies of lung sound variability in adults have used analysis of variance (ANOVA) [SaVi03] and coefficient of variation (CoV) to assess sound intensity [MaGa94], [SMPP96] and spectral characteristics such as frequencies below which 50% (F_{50}) and 99% (F_{99}) of lung sound power is contained [SaVi03], [SMPP96]. Those studies compared lung sounds between recordings taken over a matter of: between 10 and 30 minutes (short-term) [MaGa94], [SaVi03], [SMPP96]; days (intermediate term) [MaGa94], [SaVi03], [SMPP96]; weeks [SaVi03]; and months (long term) [SaVi03]. All of those studies employed target flow breathing and involved healthy adult subjects.

The objectives of the work presented in this section were to assess immediate variability (IMV), short-term variability (STV), and the effects of breathing apparatus, sensor location, and flow on lung sound intensity on an intra-subject basis for lung sounds of healthy children. The main hypothesis was that lung sound intensity will not differ between any set of two recordings by greater than 3 dB, thus marking the threshold for change in flow-specific lung sound intensity.

B.3.2 Methods

Nine healthy children ages 10-14 years (two females) with normal lung function participated in the study (Table B.2). Children underwent PFT guided by a respiratory therapist at the Winnipeg Children's Hospital, and afterwards proceeded to the Respiratory Acoustics Lab in the Manitoba Institute of Child Health for recording of lung sounds. Subjects were seated in an anechoic chamber for all lung sounds recordings. Lung sounds were recorded over the right and left lower lung lobes (RLL, LLL respectively) posteriorly while subjects breathed at flows increasing from shallow to deep for 50 s followed by a 10 s breath hold. Flow was recorded simultaneously with lung

sounds using a Biopac pneumotachograph. Subjects breathed through two types of apparatus: a three-inch cardboard mouthpiece wearing a nose clip, and a facemask. The recording sequence was as follows:

1. Two successive trials with the mouthpiece (to test IMV);

2. Two successive trials with the facemask;

3.15-minute break (sensors removed, then reapplied after the break; sensor locations were marked);

4. Steps 1 and 2 (above) repeated (to test STV).

Before taking part in the study, both the subjects and their guardians signed a consent form. Guardians later filled out a respiratory health questionnaire. One subject (1, Table B.2) had hayfever and cough with cold, and another (5, Table B.2) had wheezing that had been treated with inhaled Salbutamol as an infant.

Data were analyzed using spectrograms obtained via fast Fourier transformation (FFT) in Matlab® software. FFT was calculated within a 200 ms Hanning window shifted by 100 ms across lung sounds and breath hold waveforms, providing a frequency

Table B.2
Subject Anthropometric and PFT Data

Subjects	Gender	Height (cm)	Weight (kg)	Age (y)	*FVC* (%)	FEV_1 (%)	FEV_1/ *FVC* (%)	*TLC* (%)
1	female	158	49.0	11	103	93	86	99
2	male	155	51.7	12	108	94	80	106
3	male	162	48.5	13	92	83	83	86
4	male	171	78.2	12	109	96	81	100
5	male	152	57.2	13	108	92	78	104
6	male	151	44.5	12	102	95	86	95
7	male	150	37.0	10	87	82	87	96
8	male	165	56.2	14	123	126	95	126
9	female	146	34.2	10	92	80	83	99

FVC = forced vital capacity; FEV_1 = forced expiratory volume in one second; *TLC* = total lung capacity.

resolution of 5 Hz. Lung sound and breath hold intensity were averaged across 150-300 Hz and 300-600 Hz, and lung sound intensity was sequestered into regions corresponding to 85-100% of maximum flow per inspiratory breath. These regions were further sectioned per 100 mL/s of flow. Bins with less than five lung sound intensity values were excluded from further analysis. Means and standard deviations of differences between recordings of breath hold and lung sounds per octave band and flow bin (lung sounds only) for IMV and STV were determined using Student *t*-tests (Matlab®). Figure B.1 presents an example of a lung sounds spectrogram with corresponding flow signal, with frequency ranges and inspiratory flow regions indicated.

STV was determined for corresponding trials: e.g., trial 1 before the 15-minute break was compared with trial 1 after the break. Only flow bins with lung sounds having signal-to-noise ratio (SNR) surpassing 3 dB were used in the IMV and STV comparisons.

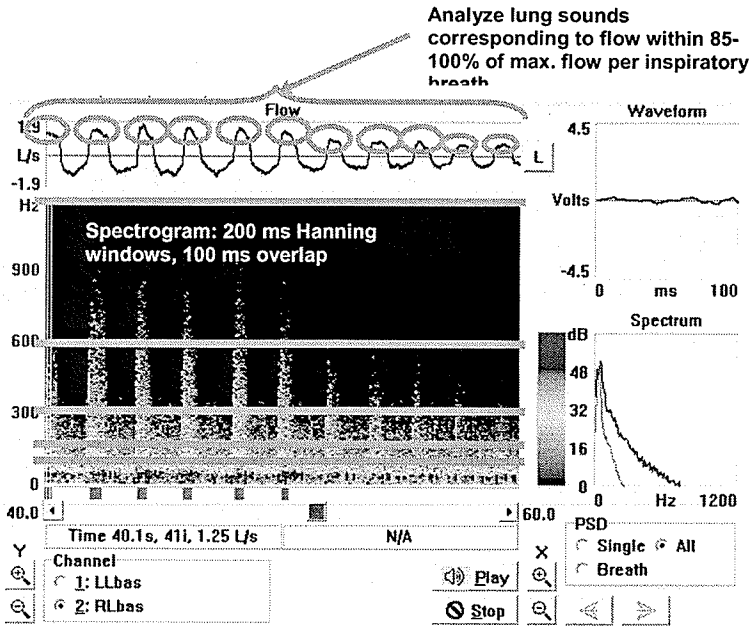

Fig. B.1: Snapshot view of R.A.L.E.® software with inspiratory flow and frequency regions indicated. Also shown is power spectral density (PSD) averaged across inspiratory breaths marked with green tags (shown below spectrogram), and the time-domain waveform within a 100 ms section of the first breath.

This condition was to ensure all subjects surpassed their critical minimum flow [CIGP97]. Maxima of all maxima and minima of all minima, for IMV and STV, were determined for lung sound and breath hold intensity for each breathing apparatus, sensor location, and frequency band.

B.3.3 Results

Tables B.3 and B.4 present results for IMV and STV of lung sound and breath hold intensity in decibels (dB) (mean ± standard deviation, SD). In the tables, results were combined for STV across trial 1's and trial 2's, and for IMV across the sessions before and after the break. For the case with a maximum difference that is greater than 3

Table B.3
Minima and Maxima (dB) for IMV of Lung Sound Intensity (LSI) and Breath Hold Intensity (BHI)

IMV of LSI and BHI	frequency range (Hz)	minima of minima, LSI	maxima of maxima, LSI	maxima of maxima, BHI
LLL, mouthpiece	150-300	0.01 ± 0.64	1.31 ± 0.59	2.07 ± 1.74
	300-600	0.00 ± 0.43	2.31 ± 1.23	0.86 ± 0.65
RLL, mouthpiece	150-300	0.01 ± 0.72	1.75 ± 1.22	2.28 ± 1.02
	300-600	0.00 ± 0.78	1.54 ± 1.46	0.85 ± 0.53
LLL, facemask	150-300	0.00 ± 0.75	2.80 ± 0.86	2.31 ± 2.00
	300-600	0.02 ± 0.68	3.59 ± 0.50	1.05 ± 1.24
RLL, facemask	150-300	0.01 ± 1.01	2.37 ± 0.82	1.62 ± 1.05
	300-600	0.03 ± 1.06	2.60 ± 0.78	0.55 ± 0.63

Table B.4
Minima and Maxima (dB) for STV of Lung Sound Intensity (LSI) and Breath Hold Intensity (BHI)

STV of LSI and BHI	frequency range (Hz)	minima of minima, LSI	maxima of maxima, LSI	maxima of maxima, BHI
LLL, mouthpiece	150-300	0.02 ± 1.38	1.69 ± 0.78	2.44 ± 1.72
	300-600	0.03 ± 0.64	1.64 ± 0.57	0.75 ± 0.43
RLL, mouthpiece	150-300	0.04 ± 0.89	1.86 ± 1.11	2.47 ± 2.37
	300-600	0.02 ± 1.54	1.91 ± 0.93	0.72 ± 0.45
LLL, facemask	150-300	0.03 ± 0.86	2.73 ± 0.96	1.71 ± 1.96
	300-600	0.03 ± 2.00	2.65 ± 0.84	1.16 ± 1.19
RLL, facemask	150-300	0.01 ± 1.29	1.99 ± 0.76	2.34 ± 2.01
	300-600	0.00 ± 0.93	2.95 ± 1.52	1.11 ± 1.41

dB (IMV, LLL, facemask, 300-600 Hz), the breath hold intensity was not significant in terms of either the 3 dB threshold or statistics ($p > 0.05$). In all cases for breath hold sounds, differences decreased with increase in frequency range. This is likely due in part to the presence of heart and muscle sounds increasing variability in lower frequency ranges; these sounds have been discussed in Chapter 3.

Maximum IMV was higher than STV within 300-600 Hz for mouthpiece recordings, both locations; within 150-300 Hz for facemask recordings, both locations; and within 300-600 Hz for facemask, LLL. STV within 150-300 Hz was higher than STV within 300-600 Hz for both locations with the mouthpiece, and for LLL with the facemask, whereas IMV within 150-300 Hz was higher than the 300-600 Hz IMV for both locations with the facemask, and for RLL with the mouthpiece. Subjects with high IMV did not necessarily have high STV and vice-versa. The most fidgety subjects were responsible for the highest IMV of breath hold sound intensity in six of the nine cases presented in Table B.3, and for highest STV of breath hold sound intensity in seven of the nine cases presented in Table B.4. Movements may result in increased muscle noise and hence increased variability.

In terms of breathing apparatus, for both sensor locations and both frequency ranges, maxima of maxima for STV and IMV were higher for facemask recordings than for mouthpiece recordings. In the case with maximum IMV greater than 3 dB (Table B.3), the facemask had been used.

Sensor locations presented the following trends for the facemask recordings: IMV for LLL was higher than for RLL in both frequency ranges, and STV for LLL was higher

than for RLL within 150-300 Hz. For the mouthpiece recordings, IMV and STV for LLL were higher than for RLL within 300-600 Hz.

It is challenging to compare the results in terms of flow between the subjects because subjects breathed within different flow ranges with respect to one another, and also because of the exclusion of flow bins due to an insufficient number of data values per bin (five was the minimum as mentioned earlier). Figures B.2 and B.3 illustrate another dilemma: different subjects have different lung sound intensity at comparable flows. These figures show results based on subjects 9 and 2 (Table B.2) respectively. It seems that larger-sized subjects need to breath at higher flows in order to reach the same sound intensities that smaller subjects reach at lower flows. This observation illustrates the value of using weight-standardized flows, which has been employed in past studies [PaPS96].

B.3.4 Discussion

The use of the facemask for flow recording presents higher IMV and STV than the use of the mouthpiece. This may be due to air leakage between a subject's face and the mask and therefore errors in recording accurate air flow; strapping the facemask to a child's face may be a solution. It would be ideal to use the facemask as opposed to the mouthpiece for recording sounds from very young children; though subjects may switch between oral and nasal breathing, it has been shown that the route of air flow does not have an effect on lung sound intensity [PaGM03]. Lung sounds recorded over the RLL have lower IMV and STV than those from the LLL in over half of the cases presented in Tables B.3 and B.4, which is likely because RLL lung sounds were lower in intensity than lung sounds from the LLL.

STV and IMV were higher within 150-300 Hz in six of the nine cases presented in Tables B.3 and B.4, which may be justified by the presence of heart and muscle sounds within this low frequency range. These sounds may also provide an explanation for the decrease in IMV and STV for breath hold intensity in 300-600 Hz vs. 150-300 Hz.

Overall the healthy subjects exhibited maximal changes in lung sound and breath hold intensity that were less than 3 dB except for one case, for IMV of lung sounds recorded over the LLL with the facemask within 300-600 Hz. The p-values from student t-tests performed for breath hold sounds and within all flow bins for lung sounds did not necessarily correlate with differences defined as significant based on 3 dB. For example, for breath hold sounds, a difference as small as 0.26 ± 0.52 dB was found significant by t-test ($p < 0.05$), whereas 1.16 ± 1.94 dB was found to be non-significant by t-test. This

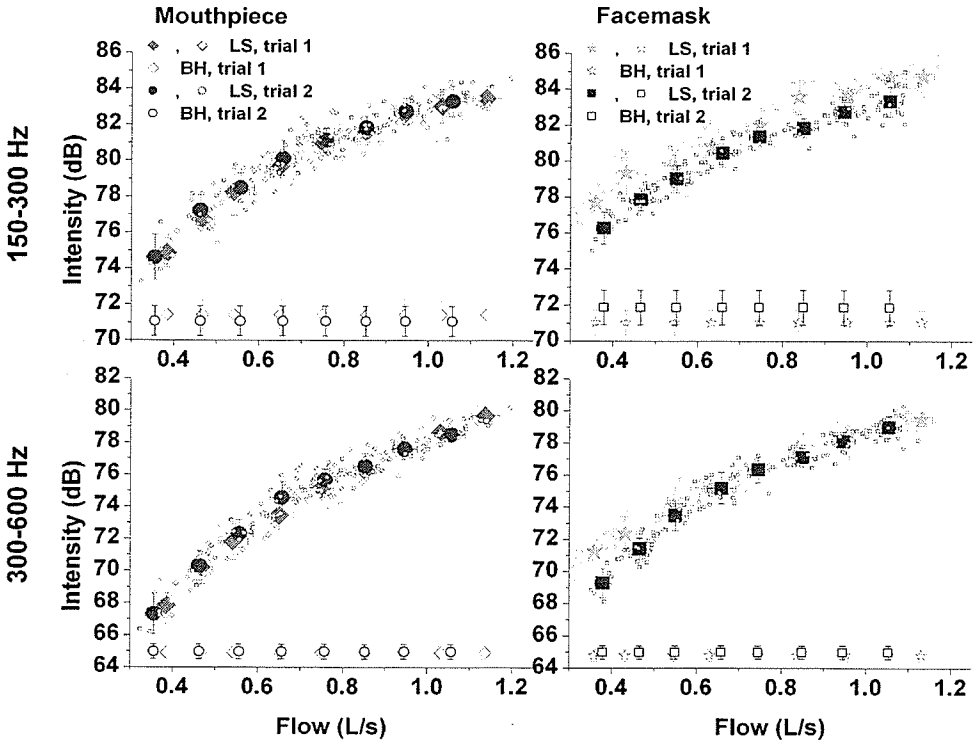

Fig. B.2: IMV example, subject 9, for lung sounds (LS) and breath hold (BH) sounds within 150-300 Hz (top row) and 300-600 Hz (bottom row), recorded with mouthpiece (left column) and facemask (right column).

emphasizes the importance of developing a threshold in dB for quantitative change in lung sound or breath hold intensity as the use of statistical parameters for quantification of lung sounds variability may be misleading. In other studies examining intra-subject variability of lung sounds acquired from healthy individuals [MaGa94], [SaVi03], [SMPP96], statistical measures were solely relied upon as measures of variability. These studies are summarized in Table B.5.

As discussed by Sovijarvi *et al.* [SMPP96], several factors may be responsible for lung sound variability. These include coherence of sensor location between recordings; cardiovascular noise such as heart sounds; external noise; breathing pattern; air flow; and factors of signal conditioning such as thermal noise and clock errors, though these are generally impossible to control. Whereas sensors in the study presented in this section

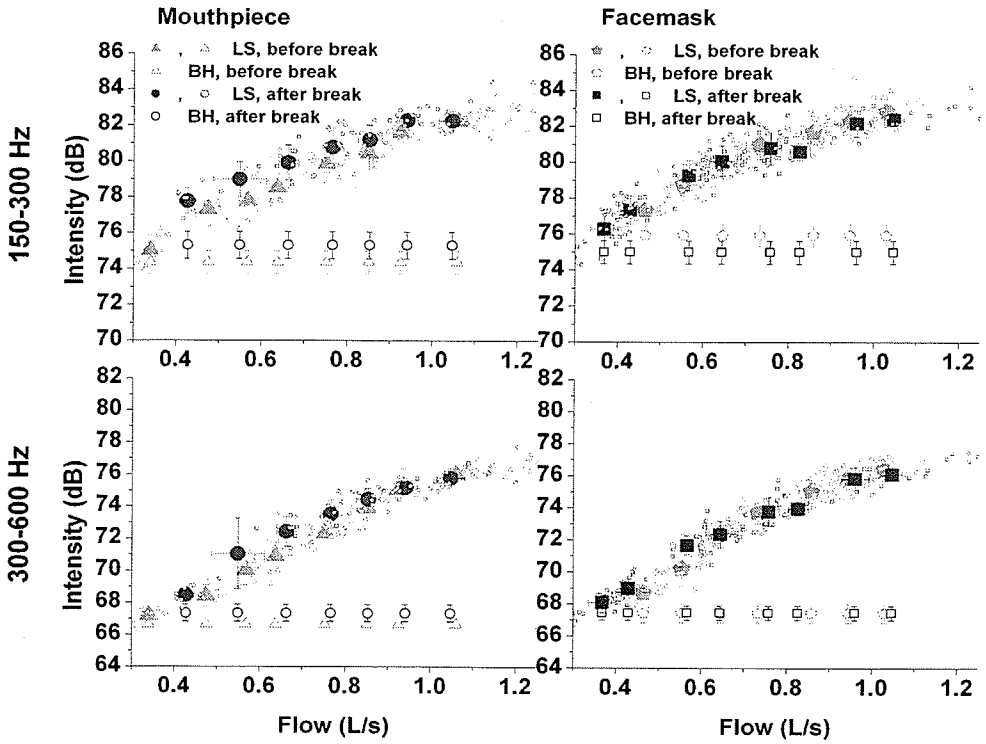

Fig. B.3: STV example, subject 2, for lung sounds (LS) and breath hold (BH) sounds within 150-300 Hz (top row) and 300-600 Hz (bottom row), recorded with mouthpiece (left column) and facemask (right column).

had been removed for the 15-minute break, the sensor location had been marked on each subject, to allow for re-application of sensors without any misplacement. Breath hold was acquired to account for heart sounds and ambient noise, and there were minimal changes between recordings. As well, sounds were recorded in an acoustical chamber. Comparisons were made between lung sounds within 85-100% of maximum flow per breath sectioned into to 100 mL/s flow bins for air flow consistency.

Mahagnah and Gavriely [MaGa94] point out that small variations in sensor positions may account for some variability in recorded sounds, and they found that lung sounds recorded over the right upper and lower lobes were not affected. Given their findings, and because sensor locations were marked, healthy variability findings in the thesis work cannot be explained by possible sensor displacement.

Table B.5
Summary of Past Work in Lung Sound Variability

Authors	[SaVi03]	[SMPP96]	[MaGa94]
Subjects	10, healthy, adult, 6 male	10, healthy, adult, male	
Recording site(s) and sensor	Posterior RLL; accelerometer	Posterior RLL; electret microphone with conical coupler held to skin via rubber belt	Right anterior chest; posterior RLL and LLL; interscapular region, right paravertebral line
Time duration between recordings	10 minutes (STV); 1 day; 1 week; 1 month; 6 months; 1 year	15 minutes (STV); 2 days	30 minutes (STV); 1 week
Variables studied	F_{99} and F_{75} (breath hold intensity subtracted from lung sound intensity)	Lung sound intensity using RMS; F_{50}; frequency of maximum intensity (F_{max})	Amplitude spectra of lung sounds after subtracting breath hold intensity; spectra of one recording was divided by another on a frequency-by-frequency basis
Method	ANOVA	CoV	CoV
Variability	Inspiratory lung sounds, intrasubject averages: 6 ± 1 % for F_{99}; 19 ± 2 % for F_{75}	Inspiratory lung sounds: STV: 18% for RMS; 4.9% for F_{max}; 2.6% for F_{50} 2-day: 41% for RMS; 5.7% for F_{max}; 5% for F_{50}	Inspiratory lung sounds: STV: 32.8 ± 12 % 1-week: 36.9 ± 11.3 %
Note		RMS averaged over whole breath phases	Results presented in terms of average CoV across all recording sites

B.4 Change in Lung Sound Intensity with Bronchial Constriction

As mentioned in Chapters 1 and 2, a decrease in flow-specific lung sound intensity after induced bronchial constriction via methacholine challenge (MCh) relative to lung sound intensity pre-MCh has been shown to be a useful marker of bronchial constriction in children in past work [BHCP04], [PBKM97], [PCOH97] and in the thesis work also [GMBP04], [GnMP04]. The latter two studies [GMBP04], [GnMP04] will be outlined in this section.

B.4.1 Methods

Data were recorded from children presenting for PFT and MCh at the Winnipeg Children's Hospital over the course of the summer of 2003. Lung sounds over the posterior RLL were acquired while subjects breathed through a pneumotachograph and facemask at their own resting (tidal) breathing rate. Flows targeted for analysis that adequately captured breaths during tidal breathing were 15 mL/s/kg for the four responders to MCh and two of the non-responders to MCh, and 7.5 mL/s/kg for the other two non-responders. Lung sounds corresponding to inspiratory flow within 85-100% of these values were analyzed. Lung sounds were recorded for 50 s, followed by a 5 s breath hold. As outlined in Chapter 2 (in general), responders to MCh exhibit bronchial constriction that is measured via spirometry by the forced expiratory volume in one second (FEV_1), which must be at least 20% below its baseline value to indicate constriction. Table B.6 shows anthropometric and lung function data for responders and

Table B.6
Subject Anthropometric Data (Mean ± SD) and ΔFEV_1 Ranges (%)

Subject Group	Age (y)	Height (cm)	Weight (kg)	Gender	ΔFEV_1 range (%)
Responders	11 ± 3	144 ± 13	40 ± 13	3M, 1F	-37 to -29
Non-responders	12 ± 2	155 ± 11	55 ± 19	2M, 2F	-15 to -4

non-responders, as presented in [GnMP04].

Lung sounds from both responders and non-responders to MCh were compared between pre- and post-MCh recordings within frequency bands 75-150, 150-300 and 300-600 Hz. Signals were digitally filtered into these frequency ranges using a fifth order Butterworth filter in Matlab®, and root mean square (RMS) voltage was calculated within 50 ms windows across breath hold and lung sounds within flow plateau regions. Signal-to-noise ratio (SNR) in dB was calculated per window by subtracting breath hold sound from lung sounds in dB using RMS of lung sounds and average breath hold RMS.

B.4.2 Results and Discussion

Figure B.4 shows SNR for lung sounds during inspiratory breaths within 85-100% of maximum flow, averaged across each recording per subject. Each subject is represented by their fall in FEV_1 post-MCh, or ΔFEV_1. Within the 150-300 and 300-600 Hz frequency ranges, all responders to MCh exhibited a greater than 3 dB decrease in lung sound intensity post-MCh (indicated by the asterisks), though non-responders with mild bronchial constriction also show such decrease in lung sounds. This suggests that lung sounds are quite sensitive to changes in airway caliber, at least within the above-noted frequency ranges. Past work [PCOH97] has also shown this sensitivity.

The responder subject who exhibited the most extreme fall in FEV_1 at -37% (Fig. B.4) also exhibited the greatest drop in lung sound intensity in the 75-150 and 150-300 Hz ranges. However, overall there was no correlation between fall in FEV_1 and change in sound intensity, within any frequency range.

The results of this study suggest that automated classification of (band-limited) lung sound SNR may be worthwhile. Classification techniques studied in past work have focused on separating healthy lung sounds from those of patients (i.e., two classes)

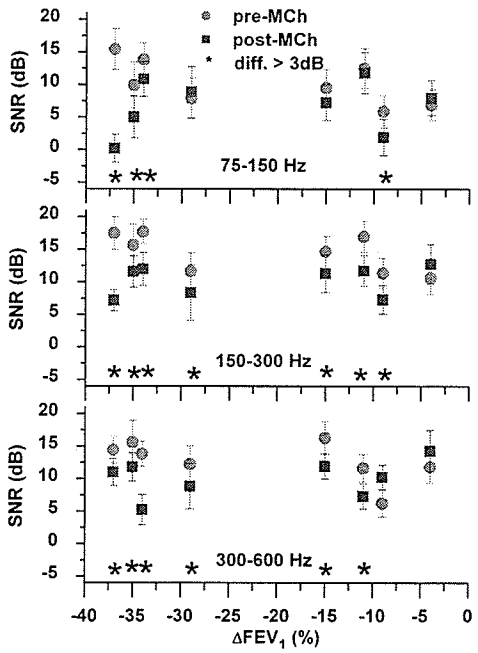

Fig. B.4: Pre- and post-MCh lung sound SNR within three frequency ranges for responders and non-responders to MCh.

[AlKa02], [GESK92], [KBYC03], [MNMO90], [SKGE94], or performing classification on a per-subject basis before and after bronchial provocation for lung [GnMP04] or tracheal [OudM02], [OuDv00] sounds. One-nearest neighbor (NN) [GnMP04], [OudM02], [OuDv00] and *k*-NN [AlKa02], [KBYC03], [SKGE94] classification, a minimum distance classifier [AlKa02], quadratic classification [SKGE94], Parzen PDF estimation [GESK92], [SKGE94], and neural networks [KKRJ04], [OudM02], [RiOD99], [WCBK00] are among a few of the techniques that have been implemented for respiratory sound classification in health and disease. It is obvious that classification between healthy lung sounds and lung sounds containing adventitious sounds recorded from patients would not present much of a challenge for any classifier; however, most past work in classification has involved such a situation.

A one-NN classifier has been presented in a publication [GnMP04] for classification of the lung sounds that were used in the study outlined in this section. It is important to note that in general, according to the *No Free Lunch Theorem* [DuHS01], no

one algorithm for classification is overall superior to (or inferior to) random guessing. The performance of any algorithm will be dependent on prior information, data distribution, amount of training data, and cost or reward functions of a particular problem. Thus, a learning or recognition algorithm claimed to be ideal in one situation will not necessarily perform to the same standard in another.

B.5 Summary

Variability is an important consideration when dealing with biological systems and waveforms. Considering mean values across variables of interest on intra- and intersubject bases provides one way of accounting for variability. Indeed, in lung sounds research, features are averaged across windows of data over several breaths, as discussed in Chapter 3. The finding of the study on healthy variability in lung sounds pertaining to the threshold for change in lung sounds was employed in work presented on change in lung sound intensity with bronchial constriction [GnMP05b].

APPENDIX C

Copyright Permission Forms

The following list contains the title of each copyrighted item, its source, and the page on which the copyright permission form appears in this appendix.

January Gnitecki

From: "Essenpreis, Alice, Springer DE" <Alice.Essenpreis@springer.com>
To: <umgnitec@cc.umanitoba.ca>
Sent: Friday, December 22, 2006 3:18 AM
Subject: WG: Customer question from springer.com

Dear Dr. Gnitecki,

Thank you for your e-mail.
With reference to your request (copy herewith) to re-use material on which Springer controls the copyright, our permission is granted free of charge, on the following conditions:

* it concerns original material which does not carry references to other sources,
* if material in question appears with credit to another source, authorization from and reference to that source is required as well, and permission is also obtained from the author (address is given on the imprint page or with the article);
* allows you non-exclusive reproduction rights throughout the world,
* full credit (book/journal title, volume, year of publication, page, chapter/article title, name(s) of author(s), figure number(s), original copyright notice) is given to the publication in which the material was originally published by adding: With kind permission of Springer Science and Business Media.

Permission free of charge does not prejudice any rights we might have to charge for reproduction of our copyrighted material in the future.

With best regards,

–

Alice Essenpreis
Springer
Rights and Permissions

–

Tiergartenstrasse 17 | 69121 Heidelberg GERMANY
FAX: +49 6221 487 8223
permissions.Heidelberg@springer.com
www.springer.com/rights

–

-----Original Message-----
From: SpringerAlerts@springeronline.com
[mailto:SpringerAlerts@springeronline.com]

Sent: Thursday, December 07, 2006 7:08 PM
To: Permissions Heidelberg
Subject: Customer question from springer.com

I, January Gnitecki, a graduate student at The University of Manitoba, request permission to quote/reproduce the material listed below in preparation of my thesis/practicum for the degree of Doctor of Philosophy in Electrical Engineering.

My thesis/practicum will be microfiched by Library and Archives Canada (LAC). A microfiche copy of the theses/practicum will be available for loan from LAC, and will be reproduced and sold in various formats through LAC's agent, University Microfilms International (UMI). My thesis/practicum may also be submitted in an electronic format to The University of Manitoba, and be accessible to a worldwide audience from both the University of Manitoba's and LAC's Theses Canada (www.collectionscanada.ca/thesescanada) websites. I would be very grateful for your favourable consideration of this request.

Title of article / book: Morphometry of the human lung
Author: E. R. Weibel
Title and number of image: Figure, "Organization of the airway tree by functional zones in relation to generations (z) of dichotomous branching"
Publisher and year: Springer-Verlag, 1963, Berlin

Access to the thesis in digital format is free of charge and therefore, no profit will be realized from the work. Please respond in writing to confirm whether or not you will grant permission for the above-mentioned work to be included in my thesis, as well as any stipulations or royalties that you request.

Thank you very much for your consideration of this request.

Sincerely,

January Gnitecki
PhD Candidate, Department of Electrical and Computer Engineering
University of Manitoba Winnipeg, MB Canada Tel. 204-478-5223 Fax. 204-261-4639

[
sender name: January Gnitecki
sender email: umgnitec@ee.umanitoba.ca
INTERNAL NAME: Rights and Permissions Department - Springer Verlag Heidelberg ORIGINAL URL:
http://www.springer.com/uk/home/rights?SGWID=1-122-[illegible]
]

79 Garden Street
Cambridge, Massachusetts
02138-1499
Phone: 617-495-2600
Fax: 617-495-5898

HARVARD UNIVERSITY PRESS

5 December 2006

January Gnitecki
103-565 Corydon Avenue
Winnipeg, MB
CANADA R3L 0P4
Fax: (204) 261-4639

RE: Reprint Permission Request

Dear Ms. Gnitecki: **HUP Ref. #: 062710**

Thank you for your request for permission to reprint material the following figure* from THE PATHWAY FOR OXYGEN by Ewald R. Weibel:

Figure 10.1, p. 273: Resin cast of a human lung showing the branching pattern of the bronchial tree © which originates from the trachea (T).

Harvard University Press is pleased to authorize permission to reprint this selection in your dissertation entitled MODELING LUNG SOUNDS FRO NON-INVASIVE DETECTION OF AIRWAY STATUS, for submission at University of Manitoba. This permission is nonexclusive, nontransferable, and authorizes distribution in the English language throughout the world. This permission extends to electronic and microfilm versions of your dissertation, which will be produced by University Microfilms International (UMI), and posted in the University of Manitoba digital repository. *Permission granted herein covers use of the material as part of your dissertation in its entirety only.* Please re-apply with full details for any additional publication.

The following credit line must appear adjacent to figure:

Credit Line: Reprinted by permission of the publisher from THE PATHWAY FOR OXYGEN: STRUCTURE AND FUNCTION IN THE MAMMALIAN RESPIRATORY SYSTEM by Ewald R. Weibel, p. 273, Cambridge, Mass.: Harvard University Press, Copyright © 1984 by the President and Fellows of Harvard College.

* For figure 10.3, while Harvard University Press has no objection to your proposed use, the figure is credited to a 1963 Springer publication (see adjacent credit and note on page 301), and is not covered by our copyright. Permission may be required from the original source.

Best wishes on your dissertation.

Sincerely,

Scarlett R. Huffman
Copyright and Permissions

University of Manitoba Dissertation
THE PATHWAY FOR OXYGEN by Ewald R. Weibel

January Gnitecki

From: "Permissions" <Permissions@perseusbooks.com>
To: "January Elizabeth Gnitecki" <umgnitec@cc.umanitoba.ca>
Sent: Wednesday, December 20, 2006 4:26 PM
Subject: RE: permission to reproduce figure

Dear January,

Provided the material is original to our book (as per the caption credit) and this is for limited dissertation distribution only (i.e., 20 copies maximum), you have our permission to use the material.

Should you wish to publish your dissertation in the future, you would need to again contact this office at that time for further permission.

Regards,

Mellisa Brandt
Permissions and Contracts Coordinator
Perseus Books Group
11 Cambridge Center
Cambridge, MA 02142

-----Original Message-----
From: January Elizabeth Gnitecki [mailto:umgnitec@cc.umanitoba.ca]
Sent: Friday, December 15, 2006 4:56 PM
To: Permissions
Subject: RE: permission to reproduce figure

Dear Mellisa,

I have been told by the University of Manitoba libraries that the print run is one. I also want to stress that I will not profit financially from
the thesis being available in print or online.
I hope that this helps.

Best regards,
January Gnitecki

On Fri, 8 Dec 2006, Permissions wrote:

> Date: Fri, 8 Dec 2006 12:18:55 -0500
> From: Permissions <Permissions@perseusbooks.com>
> To: January Elizabeth Gnitecki <umgnitec@cc.umanitoba.ca>
> Subject: RE: permission to reproduce figure

>
> Dear January,
>
> Ordinarily, we grant material for use in graduate theses free of
charge
> provided that the papers will not be sold for money. Since your thesis
> is going to be sold and put online, however,I might have to charge a
> small fee. Could you please let me know the approximate print run
> anticipated for your paper?
>
> Sincerely,
>
> Mellisa Brandt
> Permissions and Contracts Coordinator
> Perseus Books Group
> 11 Cambridge Center
> Cambridge, MA 02142
>
> -----Original Message-----
> From: January Elizabeth Gnitecki [mailto:umgnitec@cc.umanitoba.ca]
> Sent: Thursday, December 07, 2006 1:14 PM
> To: Permissions
> Subject: permission to reproduce figure
>
>
>
> ATTN: Contracts Department, Running Press Book Publishers
>
> Dear Ms. Mellisa Brandt,
>
> I am writing to request permission to include the following material
> from
> "Gray's Anatomy (The Unabridged Running Press Edition of the American
> Classic)," in a graduate thesis. The thesis, entitled "Modeling Lung
> Sounds for Non-Invasive Detection of Airway Status," is part of my
> requirements as a PhD student at the University of Manitoba.
>
> My thesis will be microfiched by Library and Archives Canada (LAC). A
> microfiche copy of the thesis will be available for loan from LAC, and
> will be reproduced and sold in various formats through LAC's agent,
> University Microfilms International (UMI). My thesis may also be
posted
> electronically in the University of Manitoba digital repository
> (https://mspace.lib.umanitoba.ca/dspace/index.jsp), and be accessible
to
> a
> worldwide audience from LAC's Theses Canada
> (www.collectionscanada.ca/thesescanada).
>
> Material requested:
> "Gray's Anatomy (The Unabridged Running Press Edition of the American

> Classic)" 1974, ISBN 0-914294-08-3
> Figure 535, page 970, "A transverse section of the thorax, showing the
> relative position of the viscera and the reflections of the pleurae."
>
> Access to the thesis in digital format is free of charge and
therefore,
> no
> profit will be realized from the work. Please respond in writing to
> confirm whether or not you will grant permission for the
above-mentioned
> work to be included in my thesis, as well as any stipulations or
> royalties
> that you request.
>
> Thank you very much for your consideration of this request.
>
> Sincerely,
> January Gnitecki
>
> *~~*~~*~~*~~*~~*~~*~~*~~*~~*~~*~~*~~*~~*~~*~~*
> January Gnitecki, BScEE, EIT
> PhD Candidate, Electrical Engineering
> University of Manitoba
> Winnipeg, MB, CANADA
> Tel.: +1.204.474.7038
> *~~*~~*~~*~~*~~*~~*~~*~~*~~*~~*~~*~~*~~*~~*~~*
>

~~~~*~~*~~*~~*~~*~~*~~*~~*~~*~~*~~*~~*~~*~~*
January Gnitecki, BScEE, EIT
PhD Candidate, Electrical Engineering
University of Manitoba
Winnipeg, MB, CANADA
Tel.: +1.204.474.7038
~~~~*~~*~~*~~*~~*~~*~~*~~*~~*~~*~~*~~*~~*~~*

Penny Ripka

From:	January Elizabeth Gnitecki [umgnitec@cc.umanitoba.ca]
Sent:	Friday, September 15, 2006 11:12 AM
To:	Penny Ripka
Subject:	permission to reproduce figures

Dear Ms. Ripka,

I am writing to request permission to include the following material from the Journal of Applied Physiology, in a graduate thesis. The thesis, entitled "Modeling Lung Sounds for Non-Invasive Detection of Airway Status," is part of my requirements as a PhD student at the University of Manitoba.
My thesis will be microfiched by Library and Archives Canada (LAC). A microfiche copy of the thesis will be available for loan from LAC, and will be reproduced and sold in various formats through LAC's agent, University Microfilms International (UMI). My thesis may also be posted electronically in the University of Manitoba digital repository (https://mspace.lib.umanitoba.ca/dspace/index.jsp), and be accessible to a worldwide audience from LAC's Theses Canada (www.collectionscanada.ca/thesescanada).

Material requested:
Anatomically based three-dimensional model of airways to simulate flow and particle transport using computational fluid dynamics
Authors: Caroline van Ertbruggen, Charles Hirsch, and Manuel Paiva Journal of Applied Physiology, vol. 98, no. 3, pp. 970-980, 2005 pp. 972, Figure 2 pp. 973, Figure 3 pp. 975, Figure 5

Access to the thesis in digital format is free of charge and therefore, no profit will be realized from the work. Please respond in writing to confirm whether or not you will grant permission for the above-mentioned work to be included in my thesis, as well as any stipulations or royalties that you request.

Thank you very much for your consideration of this request.

Sincerely,
January Gnitecki

~~~~*~~*~~*~~*~~*~~*~~*~~*~~*~~*~~*~~*~~*~~*
January Gnitecki, BScEE, EIT
PhD Candidate, Electrical Engineering
University of Manitoba
Winnipeg, MB, CANADA
Tel.: +1.204.474.7038
~~~~*~~*~~*~~*~~*~~*~~*~~*~~*~~*~~*~~*~~*~~*

APPROVED
By PRipka at 9:16 am, Sep 20, 2006

THE AMERICAN PHYSIOLOGICAL SOCIETY
9650 Rockville Pike, Bethesda, MD 20814-3991

Permission is granted for use of the material specified above provided the publication is credited as the source, including the words "used with permission."

Margaret Reich
Publications Manager & Executive Editor

APPENDIX D

Algorithms

The following list contains the title of each algorithm and the page on which it appears in this appendix.

```
%%%%%%%%%%%%%%%%%%%%%%%%%%%%%%%%%%%%%%%%%%%%%%%%
%%%%%%%%%%%%%%%%%%%%%%%%%%%%%%%%%%%%%%%%%%%%
%%Chua Circuit Algorithm
%%%%%%%%%%%%%%%%%%%%%%%%%%%%%%%%%%%%%%%%%%%%%%%%
%%%%%%%%%%%%%%%%%%%%%%%%%%%%%%%%%%%%%%%%%%%%
%%This program was developed using the simplified form for analysis of the
%%Chua circuit Double scroll equation, as per equations 38.1 and 38.2 in
%%the course notes.  To solve the differential equations dx/dt, dy/dt,
%%and dz/dt, the multi-variable Runge-Kutta fourth order method was
%%used, as per website: http://www.myphysicslab.com/runge_kutta.html.
%%The formula for the nonlinear conductance employed in this program was
%%chosen based on the paper, "Real Time Implementation of Continuous (Chua and
%%Lorenz) Chaotic Generator Models Using Digital Hardware", by Mohamed I. Sobhy,
%%Mohammed A. Aseeri, and Alaa E. R. Shehata.  The formula is:
%%g(vc1) = m0*Vc1+0.5*(m0+m1)*(|Vc1+Bp|-|Vc1-Bp|)
%%%%%%%%%%%%%%%%%%%%%%%%%%%%%%%%%%%%%%%%%%%%%%%%
%%%%%%%%%%%%%%%%%%%%%%%%%%%%%%%%%%%%%%%%%%%%
%%Variables:
%%x0, y0, z0:        initial conditions for simplified analysis
%%s:  multiplier for the step size in the Rung-Kutta algorithm
%%G:  conductance of the linear component of the Chua circuit
%%C1, C2:    capacitance value of the linear component of the Chua circuit
%%L:  inductance of the linear component of the Chua circuit
%%m1, m0:    parameters for the nonlinear negative conductance of the
%%           Chua circuit (the Chua diode component)
%%           (slopes of the three piecewise symmetrical linear approximation
%%           of the nonlinear conductance)
%%alpha, beta:       parameters of the simplified form O.D.E.'s
%%Bp:        breakpoint of the piecewise symmetrical linear approximation of the
%%           nonlinear conductance
%%h:  Runge-Kutta step size variable, also equivalent to tau
%%numsteps: number of iterations
%%Vc1, Vc2: voltages across the capacitances C1 and C2
%%iL: current through inductor L
%%X, Y, Z:   components of the Chua circuit chaotic behavior, as per notes
%%k1, j1, n1, 2, 3, 4: Runge-Kutta algorithm parameters
%%newx:      variable used to simplify Runge-Kutta equations
%%%%%%%%%%%%%%%%%%%%%%%%%%%%%%%%%%%%%%%%%%%%%%%%
%%%%%%%%%%%%%%%%%%%%%%%%%%%%%%%%%%%%%%%%%%%%
x0=0.1; %%chosen by trial and error
y0=0.1; %%chosen by trial and error
z0=0.2; %%chosen by trial and error
s=0.1; %%chosen by trial and error

%%Values for the linear component of the Chua circuit
%%Values are chosen such that alpha = C2/C1 = 9, and beta = C2/LG^2 = 100/7
```

```
C1=1/9;
C2=1; %%C2/C1 = 9 = alpha
G=0.7; %%chosen through trial and error
L=C2/((G^2)*(100/7)); %%C2/LG^2 = 100/7 = beta

%%Chua Diode
m1=2/7; %%as suggested in notes
m0=-1/7; %%as suggested in notes
alpha=9; %%as suggested in notes
%%alpha = C2/C1 = 1/(1/9) = 9
beta=100/7; %%as suggested in notes
Bp=1; %%as suggested in notes

%%Fourth order multi-variable Runge-Kutta ODE algorithm:
h = s*G/C2 %%step size for the Runge-Kutta method
numsteps=4000; %%number of iterations, chosen to be large so that a patterm may be
defined
%%initialize the Vc1, Vc2, and iL values:
Vc1(1)=x0;
Vc2(1)=y0;
iL(1)=z0;
%%Simplified form for analysis
X = Vc1(1)/Bp;
Y = Vc2(1)/Bp;
Z = iL(1)/(Bp*G);

for r=1:numsteps
   k1 = alpha*(Y - (m1*X + 0.5*(m0 - m1)*(abs(X+1) - abs(X-1)))); %%dx/dt
   j1 = X - Y + Z; %%dy/dt
   n1 = -beta*Y; %%dz/dt
   newx = X + (h/2)*k1;
   k2 = alpha*(Y + (h/2)*j1 - (m1*newx + 0.5*(m0 - m1)*(abs(newx+1) - abs(newx-
1))));
   j2 = j1 + (h/2)*(k1 - j1 + n1);
   n2 = n1 - beta*(h/2)*j1;
   newx = X + (h/2)*k2;
   k3 = alpha*(Y + (h/2)*j2 - (m1*newx + 0.5*(m0 - m1)*(abs(newx+1) - abs(newx-
1))));
   j3 = j1 + (h/2)*(k2 - j2 + n2);
   n3 = n1 - beta*(h/2)*j2;
   newx = X + h*k3;
   k4 = alpha*(Y + h*j3 - (m1*newx + 0.5*(m0 - m1)*(abs(newx+1) - abs(newx-1))));
   j4 = j1 + h*(k3 - j3 + n3);
   n4 = n1 - beta*h*j3;
   %%Runge-Kutta formulas for estimating the next steps:
   X = X + (k1 + 2*k2 + 2*k3 + k4)*(h/6);
```

```
  Y = Y + (j1 + 2*j2 + 2*j3 + j4)*(h/6);
  Z = Z + (n1 + 2*n2 + 2*n3 + n4)*(h/6);
  %%Store the new values for Vc1, Vc2, and iL:
  Vc1(r+1) = Bp*X;
  Vc2(r+1) = Bp*Y;
  iL(r+1) = (Bp*G)*Z;
end

figure
plot3(Vc1,Vc2,iL)
title('3D signal trajectory from Chua circuit');
xlabel('Vc1')
ylabel('Vc2')
zlabel('iL')
grid
figure
plot(Vc1,Vc2);
title('2D signal trajectory from Chua circuit');
xlabel('Vc1');
ylabel('Vc2');
grid
figure
plot((0:length(Vc1)-1)*h,Vc1)
title('x - component of trajectory behavior vs. time');
xlabel('t [s]')
ylabel('Vc1(t) [v]');
grid
figure
plot(Vc2)
title('Vc2 (y) component vs. time');
figure
plot(iL)
title('IL (z) component vs. time');
```

```
%%%%%%%%%%%%%%%%%%%%%%%%%%%%%%%%%%%%%%%%
%%%%%%%%%%%%%%%%%%%%%%%%%%%%%%%%%%%%%
%%Geometrical and Dynamical State Space Parameters
%%%%%%%%%%%%%%%%%%%%%%%%%%%%%%%%%%%%%%%%
%%%%%%%%%%%%%%%%%%%%%%%%%%%%%%%%%%%%%
%%This program was developed using methods outlined in Chapter 4 of the thesis
%%%%%%%%%%%%%%%%%%%%%%%%%%%%%%%%%%%%%%%%
%%%%%%%%%%%%%%%%%%%%%%%%%%%%%%%%%%%%%
%%Part I: Opening a Rale *.bin file
%%%%%%%%%%%%%%%%%%%%%%%%%%%%%%%%%%%%%%%%
%%%%%%%%%%%%%%%%%%%%%%%%%%%%%%%%%%%%%
clear
fid=fopen('EW_2_RA_forRL_15mlsk.bin','r'); y=fread(fid,inf,'int16');
if y(1) == 2,
  s1=y(4:y(2)*1024+3)*5/32768; %sound channel 1
  ch2start=y(2)*1024+4;
  s2=y(ch2start+1:ch2start+1024*y(2))*5/32768; %sound channel 2
  flowstart=ch2start+y(2)*1024+1;
  flow=y(flowstart+1:flowstart+y(2)*32); %flow channel
  tagstart=flowstart+y(2)*32+1;
  tags=y(tagstart+1:tagstart+y(2)); %tags defined in RALE software
else,
  s1=y(4:y(2)*1024+3)*5/32768;
  flowstart=y(2)*1024+4;
  flow=y(flowstart+1:flowstart+y(2)*32)*5/32768;
  tagstart=flowstart+y(2)*32+1;
  tags=y(tagstart+1:tagstart+y(2));
end;
num_segments=y(2);
duration=y(2)/10
bad=find(tags==2 | tags==258 | tags==514 | tags==770);
bad=bad(:);
flow_samp_rate=320; %flow sampling rate in Hz
sound_samp_rate=10240; % sound sampling rate in Hz
mass=50;
seg_size=.1;
clear ch
clear chf
clear seg_flow
%%%%%%%%%%%%%%%%%%%%%%%%%%%%%%%%%%%%%%%%
%%%%%%%%%%%%%%%%%%%%%%%%%%%%%%%%%%%%%
%%Part II: Determining tau from autocorrelation
%%%%%%%%%%%%%%%%%%%%%%%%%%%%%%%%%%%%%%%%
%%%%%%%%%%%%%%%%%%%%%%%%%%%%%%%%%%%%%
kpfl1=load('kpfl1_EW_2'); %file marks the onset of breath phases, found earlier
insp_tags=find(tags==256);  %tags marking 100 ms regions of inspiratory flow
```

```
insp_strt=(insp_tags-1); insp_end=(insp_tags);
tag_blocks=[];
dr=1; df=1;
%the following while loop determines blocks of inspiratory tags – i.e. regions of greater
than or equal to two successive 100ms tagged segments
while dr<=length(insp_tags)-1;
   ss=1;
   if dr==1;
      tag_blocks(df,1)=insp_strt(dr);
      dr=dr+1;
      ss=2;
   elseif (insp_strt(dr+1)==insp_strt(dr)+1)&(ss~=2);
      ss=2;
      dr=dr+1;
   elseif (insp_strt(dr+1)>insp_strt(dr)+1)&(ss~=2);
      tag_blocks(df,2)=insp_end(dr);
      df=df+1;
      tag_blocks(df,1)=insp_strt(dr+1);
      dr=dr+1;
      ss=1;
   end
end
tag_blocks(end,2)=insp_end(dr); %this matrix contains start/end points of the inspirations
tagged in RALE
size_blocks=size(tag_blocks); num_blocks=size_blocks(1);
dj=1;
%total number of rows should be: N-(m-1)*tau
%total number of columns should be: m
clear X_base
clear X_pm
%%Find tau from autocorrelation:
pm=1;
max_autocorr=[];
max_autocorr_tau=[];
max_tau=[];
max_autocorr_e=[];
tau_autocorr=[];
tau=[];
while pm<=num_blocks;
   new_seg=[];
   autocorr=[];
   new_seg=s2((tag_blocks(pm,1)/10)*10240:(tag_blocks(pm,2)/10)*10240);
   autocorr=xcorr(new_seg);
   max_autocorr(pm)=max(autocorr);
   max_autocorr_tau(pm)=find(autocorr==max_autocorr(pm));
   max_tau=max_autocorr_tau(pm);
```

```
    new_autocorr=[];
    new_autocorr=autocorr(max_tau:end);
    max_autocorr_e(pm)=(1-(1/2.71828))*max_autocorr(pm);
    fnd_autocorr_e=find(new_autocorr<=max_autocorr_e(pm));
    tau_autocorr(pm)=fnd_autocorr_e(1);
    tau=tau_autocorr(pm);
    pm=pm+1;
end
tau_autocorr=tau_autocorr';
save EW_RL_2_tau_autoc_15 tau_autocorr -ascii
max_autocorr=max_autocorr';
save EW_RL_2_max_autoc_15 max_autocorr -ascii
max_autocorr_e=max_autocorr_e';
save EW_RL_2_e_autoc_15 max_autocorr_e -ascii
%%%%%%%%%%%%%%%%%%%%%%%%%%%%%%%%%%%%%%%%%%%%
%%%%%%%%%%%%%%%%%%%%%%%%%%%%%%%%%%%%%%%%
%%Part III: Find the number of false nearest neighbors
%%%%%%%%%%%%%%%%%%%%%%%%%%%%%%%%%%%%%%%%%%%%
%%%%%%%%%%%%%%%%%%%%%%%%%%%%%%%%%%%%%%%%
numbr_brth=num_blocks; %number of breaths from which plateau values were taken
for kkm=1:num_blocks;
len_blocks(kkm)=length((tag_blocks(kkm,1)/10)*10240:(tag_blocks(kkm,2)/10)*10240)
-1;
end
len_blocks=len_blocks'; %length of each block of inspiratory tags
save EW_RL_2_lenbreaths_15 len_blocks -ascii
pp=1; tt=1;
load EW_RL_2_tau_autoc_15 -ascii
tau_filt=EW_RL_2_tau_autoc_15;
clear X_base
%%Form the Xo matrix:
m=1;
ddr=1;
dmd=1;
pm=1;
tau=1;
Rnew=[];
R=[];
thresh=[];
fndthresh=[];
falseNNperc=[];
numfalseNN=[];
Rnew1=[];
p=0;
maxm=15;
while pm<=num_blocks;
```

```
tau = tau_filt(pm);
m=1;
if len_blocks(pm)>(maxm-1)*tau;
while m<=maxm;
   numrows_base=[];
   numrows_base=len_blocks(pm)-(maxm-1)*tau;
   ddr=1;
   X_base=[];
   new_seg1=[]; new_seg=[];
   new_seg=s2((tag_blocks(pm,1)/10)*10240:(tag_blocks(pm,2)/10)*10240);
   numrows_base=length(new_seg)-(maxm-1)*tau;
   while ddr<=numrows_base;
      dmd=1;
      while dmd<=m;
         X_base(ddr,dmd)=[new_seg(ddr+(dmd-1)*tau)];
         dmd=dmd+1;
      end
      ddr=ddr+1;
   end
   ada=1;
   kp=1;
   szX=size(X_base);
   rr=1;
   if m==1;
      CompDist=[];
      while rr<=szX(1);
         i=1;
         while i<=szX(1);
            if rr==i;
               CompDist(i,rr)=10000;
            else
               CompDist(i,rr)=[sum((X_base(rr,:)-X_base(i,:)).^2)];
            end
            i=i+1;
         end
         fndmindst(rr)=min(CompDist(:,rr));
         R(rr,m-p)=fndmindst(rr);
         findCompmin=find(CompDist(:,rr)==fndmindst(rr));
         save_i(rr)=findCompmin(1); %%the row that is NN to row rr
         lastcol(rr,m-p)=abs((X_base(rr,m)-X_base(save_i(rr),m)));
         Rnew(rr)=R(rr,m-p);
         Rnew1(rr)=Rnew(rr);
         thresh(rr,m-p)=lastcol(rr,m-p)/sqrt(Rnew1(rr));
         rr=rr+1;
      end
   else
```

```
        while rr<=szX(1);
          lastcol(rr,m-p)=abs((X_base(rr,m)-X_base(save_i(rr),m)));
          Rnew(rr)=Rnew1(rr)+lastcol(rr,m-p).^2;
          thresh(rr,m-p)=lastcol(rr,m-p)/sqrt(Rnew1(rr));
          rr=rr+1;
        end
      end

      Rnew1=Rnew;
      fndthresh=find(thresh(:,m-p)>=2);
      numfalseNN(m-p,pm)=length(fndthresh);
      falseNNperc(m-p,pm)=numfalseNN(m-p,pm)/length(Rnew1);
      m=m+1;
    end
    pm=pm+1;
else
    pm=pm+1;
end
end
save numfalseNN_EW_RL_2_15 numfalseNN -ascii
save falseNNperc_EW_RL_2_15 falseNNperc -ascii
%%%%%%%%%%%%%%%%%%%%%%%%%%%%%%%%%%%%%%%%%%%%%%%%%%%%%%%%%%%%%%%%%%%%%%%%
%%Part IV: Find the embedding dimensions
%%%%%%%%%%%%%%%%%%%%%%%%%%%%%%%%%%%%%%%%%%%%%%%%%%%%%%%%%%%%%%%%%%%%%%%%
load numfalseNN_EW_RL_2_15 -ascii
numfalseNN1=numfalseNN_EW_RL_2_15;
sznum=size(numfalseNN1);
m1=1;
while m1<=sznum(2);
  mn=1;
  while mn<=sznum(1);
    if numfalseNN1((15-(mn-1)),m1)~=0;
      indexval(m1)=15-(mn-1);
      mn=sznum(1)+1;
    else
      mn=mn+1;
    end
  end
  m1=m1+1;
end
indexval=indexval'
save EW_RL_2_m_15 indexval -ascii
%%%%%%%%%%%%%%%%%%%%%%%%%%%%%%%%%%%%%%%%%%%%%%%%%%%%%%%%%%%%%%%%%%%%%%%%
```

```
%%Part V: Find tau from Sm
%%%%%%%%%%%%%%%%%%%%%%%%%%%%%%%%%%%%%%%%%%%%%%%%%%%%%%%%%%%%%%%%%%%%%%%%%%%%%%%%%%%%%%%%%%%%%%%%%%%%%%%%%%%%%%%%%%%%%%%%%%%%%%%%%%%%%%%
load('EW_RL_2_m_15');
newm=EW_RL_2_m_15;
clear X_base
clear X_pm
%%Form the Xo matrix:
ada=1;
afa=1;
ddr=1;
dmd=1;
tau=1;
Sm=[];
Sm_new=[];
maxm=max(newm);
pm=1;
while pm<=num_blocks;
  m=newm(pm);
  tau=1;
  while tau<=110;
    if len_blocks(pm)>(maxm-1)*tau;
    numrows_base=[];
    numrows_base=len_blocks(pm)-(m-1)*tau;
    ddr=1;
    X_base=[];
    new_seg=[];
    new_seg=s2((tag_blocks(pm,1)/10)*10240:(tag_blocks(pm,2)/10)*10240);
    while ddr<=numrows_base;
      dmd=1;
      while dmd<=m;
        X_base(ddr,dmd)=[new_seg(ddr+(dmd-1)*tau)];
        dmd=dmd+1;
      end
      ddr=ddr+1;
    end
    ada=1;
    Xo_base=[];
    while ada<=numrows_base;
      afa=1;
      while afa<=m;
        Xo_base(ada,afa)=[new_seg(ada+(afa-1)*0)];
        afa=afa+1;
      end
      ada=ada+1;
    end
```

```
      Xt_base=[];
      Xo_base_new=[];
      Xt_base=X_base;
      Xo_base_new=Xo_base;
      %find distances;
      kp=1;
      distS=[];
      while kp<=ddr-1;
        distS(kp)=[sum((Xt_base(kp,:)-Xo_base_new(kp,:)).^2).^0.5];
        kp=kp+1;
      end
      Sm(tau,pm)=[sum(distS)*(1/(ddr-1))];
      size_save(tau,pm)=[length(Xo_base_new)];
      tau=tau+1;
    else
      pm=pm+1;
    end
    end
    pm=pm+1;
end
save EW_RL_2_Sm_n2_15 Sm -ascii
szSm_base=size(Sm);
for hh=1:szSm_base(2);
    maxSm_base_tau(hh)=find(Sm(:,hh)==max(Sm(:,hh))); %%tells you the value of tau
at which Sm is max
    maxSm_base(hh)=max(Sm(:,hh));
end
maxSm_base=maxSm_base';
maxSm_base_tau=maxSm_base_tau';
save EW_RL_2_maxSm_tau_n_15 maxSm_base_tau -ascii
save EW_RL_2_maxSm_n2_15 maxSm_base -ascii
load EW_RL_2_Sm_n2_15 -ascii
Sm=EW_RL_2_Sm_n2_15;
sizeSm=size(Sm);
numSm=sizeSm(2); %number of Sm curves
for n=1:numSm;
    nSm=Sm(:,n);
    dr=(1:3)';
    slopen=polyfit(dr,nSm(1:3),1);
    dd=4;
    p=[];
    newp=[];
    while dd<=length(nSm);
      t=1:dd;
      p=nSm(1:dd);
      mm=(1:dd)';
```

```
      p=polyfit(mm,nSm(1:dd),1);
      newp(dd-3)=p(1);
      dd=dd+1;
   end
   fndtauSm=find(newp<slopen(1)*0.4);
   tauSm(n)=fndtauSm(1);
end
tauSm=tauSm';
save EW_RL_2_new_tauSm3_n2_15 tauSm -ascii
%%%%%%%%%%%%%%%%%%%%%%%%%%%%%%%%%%%%%%%%%%%%%%%%%%%%
%%%%%%%%%%%%%%%%%%%%%%%%%%%%%%%%%%%%%%%%%%%%%%%%
%%Part V: Find Lyapunov exponents
%%%%%%%%%%%%%%%%%%%%%%%%%%%%%%%%%%%%%%%%%%%%%%%%%%%%
%%%%%%%%%%%%%%%%%%%%%%%%%%%%%%%%%%%%%%%%%%%%%%%%
load('EW_RL_2_m_15');
newm=EW_RL_2_m_15;
load('EW_RL_2_new_tauSm3_n2_15');
Smtau=EW_RL_2_new_tauSm3_n2_15;
pp=1; tt=1;
clear X_base
%%Form the Xo matrix:
ddr=1;
dmd=1;
pm=1;
tau=[];
Sm=[];
Sm_new=[];
R=[];
lamb2=zeros(15,num_blocks);
p=2;
while pm<=num_blocks;
   Rnew1=[];
   Rnew2=[];
   Rnew=[];
   tau=Smtau(pm);
   m=newm(pm);
   if len_blocks(pm)>(maxm-1)*tau;
      numrows_base=[];
      numrows_base=len_blocks(pm)-(m-1)*tau;
      ddr=1;
      X_base=[];
      new_seg=[];
      new_seg=s2((tag_blocks(pm,1)/10)*10240:(tag_blocks(pm,2)/10)*10240);
      while ddr<=numrows_base;
         dmd=1;
         while dmd<=m;
```

```
            X_base(ddr,dmd)=[new_seg(ddr+(dmd-1)*tau)];
            dmd=dmd+1;
        end
        ddr=ddr+1;
    end
    ada=1;
    kp=1;
    szX=size(X_base);
    rr=1;
    CompDist=[];
    while rr<=szX(1)-1;
        i=1;
        while i<=szX(1)-1;
            if rr==i;
                CompDist(i,rr)=10000;
            else
                CompDist(i,rr)=[sum((X_base(rr,:)-X_base(i,:)).^2)];
            end
            i=i+1;
        end

        [sds ind]=sort(CompDist(:,rr));

        Bi=[(X_base(ind(1),:)-X_base(ind(6),:))+(X_base(ind(11),:)-
X_base(ind(16),:))+(X_base(ind(21),:)-X_base(ind(26),:))+(X_base(ind(31),:)-
X_base(ind(36),:))
            (X_base(ind(2),:)-X_base(ind(7),:))+(X_base(ind(12),:)-
X_base(ind(17),:))+(X_base(ind(22),:)-X_base(ind(27),:))+(X_base(ind(32),:)-
X_base(ind(37),:))
            (X_base(ind(3),:)-X_base(ind(8),:))+(X_base(ind(13),:)-
X_base(ind(18),:))+(X_base(ind(23),:)-X_base(ind(28),:))+(X_base(ind(33),:)-
X_base(ind(38),:))
            (X_base(ind(4),:)-X_base(ind(9),:))+(X_base(ind(14),:)-
X_base(ind(19),:))+(X_base(ind(24),:)-X_base(ind(29),:))+(X_base(ind(34),:)-
X_base(ind(39),:))
            (X_base(ind(5),:)-X_base(ind(10),:))+(X_base(ind(15),:)-
X_base(ind(20),:))+(X_base(ind(25),:)-X_base(ind(30),:))+(X_base(ind(35),:)-
X_base(ind(40),:))];
        Bi1=[(X_base(ind(1)+1,:)-X_base(ind(6)+1,:))+(X_base(ind(11)+1,:)-
X_base(ind(16)+1,:))+(X_base(ind(21)+1,:)-X_base(ind(26)+1,:))+(X_base(ind(31)+1,:)-
X_base(ind(36)+1,:))
            (X_base(ind(2)+1,:)-X_base(ind(7)+1,:))+(X_base(ind(12)+1,:)-
X_base(ind(17)+1,:))+(X_base(ind(22)+1,:)-X_base(ind(27)+1,:))+(X_base(ind(32)+1,:)-
X_base(ind(37)+1,:))
```

```
            (X_base(ind(3)+1,:)-X_base(ind(8)+1,:))+(X_base(ind(13)+1,:)-
X_base(ind(18)+1,:))+(X_base(ind(23)+1,:)-X_base(ind(28)+1,:))+(X_base(ind(33)+1,:)-
X_base(ind(38)+1,:))
            (X_base(ind(4)+1,:)-X_base(ind(9)+1,:))+(X_base(ind(14)+1,:)-
X_base(ind(19)+1,:))+(X_base(ind(24)+1,:)-X_base(ind(29)+1,:))+(X_base(ind(34)+1,:)-
X_base(ind(39)+1,:))
            (X_base(ind(5)+1,:)-X_base(ind(10)+1,:))+(X_base(ind(15)+1,:)-
X_base(ind(20)+1,:))+(X_base(ind(25)+1,:)-X_base(ind(30)+1,:))+(X_base(ind(35)+1,:)-
X_base(ind(40)+1,:))];
          Tmat=Bi'*Bi1;
          [Q R]=qr(Tmat');
          if rr==1;
            Q1=Q;
            Rn=R;
            Rnew2=[Rnew2
              Rn];
          elseif rr>1;
            [Qn Rn]=qr(Tmat'*Q1);
            Rnew2=[Rnew2
              Rn];
            Q1=Qn;
          end
          Rnew1=[Rnew1
            R];
          rr=rr+1;
        end
        pkr=1; pdr=1;
        szRnew1=size(Rnew1); limRnew1=szRnew1(1)/szRnew1(2);
        szRnew2=size(Rnew2); limRnew2=szRnew2(1)/szRnew2(2);
        lambpre1=[]; lambpre2=[];
        while pdr<=limRnew2;
          lambpre2(:,pdr)=sum(logm(abs(Rnew2(((pdr-
1)*szRnew2(2)+1:pdr*szRnew2(2)),:))))';
          pdr=pdr+1;
        end
        xxm=1;
        while xxm<=m;
          lamb2(xxm,pm)=(1/limRnew2)*sum(real(lambpre2(xxm,:)));
          xxm=xxm+1;
        end
        pm=pm+1;
      else
        pm=pm+1;
      end
      end
save EW_RL_2_lamb2_15 lamb2 -ascii
```

```
%%%%%%%%%%%%%%%%%%%%%%%%%%%%%%%%%%%%%%%%%%%%%%%%%%%%%%%%%%%%%%%%%%%%%%%%%%%%%%%%%%%%%%%%%%%%%
%%Quantification of Velocity Profiles
%%%%%%%%%%%%%%%%%%%%%%%%%%%%%%%%%%%%%%%%%%%%%%%%%%%%%%%%%%%%%%%%%%%%%%%%%%%%%%%%%%%%%%%%%%%%%
x_coords=0:0.00001:0.45;
y_coords=0:0.00001:0.45;
fcn=sin((20/3)*pi*x_coords);
fcn1=abs((square((6.4)*pi*x_coords,44)+1)-2)/2;
fcn2=1.2*cos(6*pi*(x_coords+0.275));
Vfcn_AP=(880.24/1.425)*((fcn)+abs(fcn1.*fcn2));
x2=new_coords_cm(:,1);
p_AP=polyfit(x_coords,Vfcn_AP,9);
p_AP=[p_AP(1:end-1),0]; %forces zero at boundaries to follow non-slip condition
Vfcn_AP_model=polyval(p_AP, x_coords);
Vfcn_AP_new=polyval(p_AP, x2); %"smoothed" velocity model for A-P plane
figure
plot(x_coords,Vfcn_AP,'m');
hold
plot(x_coords,Vfcn_AP_model,'g')
plot(x2,Vfcn_AP_new,'p');
grid
fcn3=-(4/5)*sin((21/3)*pi*y_coords);
fcn4=square(4*pi*y_coords,30);
fcn5=(square(6.4*pi*y_coords,48)+1)/2;
fcn6=(exp(y_coords).^5)/15;
Vfcn_RL=(129.2/1.854)*(((-(fcn5-1)).*fcn6)+(fcn5.*abs(fcn+(fcn3.*((fcn4+1)/2)))));
y2=new_coords_cm(:,2);
p_RL=polyfit(y_coords,Vfcn_RL,9);
p_RL=[p_RL(1:end-1),0];
Vfcn_RL_model=polyval(p_RL,y_coords);
Vfcn_RL_new=polyval(p_RL,y2);
figure
plot(y_coords,Vfcn_RL,'m');
hold
plot(y_coords,Vfcn_RL_model,'g');
plot(y2,Vfcn_RL_new,'p');
grid
clear fcn fcn1 fcn2 fcn3 fcn4 fcn5 fcn6
```

```
%%%%%%%%%%%%%%%%%%%%%%%%%%%%%%%%%%%%%%%%%%%%
%%%%%%%%%%%%%%%%%%%%%%%%%%%%%%%%%%%%%%%%%
%%Finite Element Grid Formation
%%%%%%%%%%%%%%%%%%%%%%%%%%%%%%%%%%%%%%%%%%%%
%%%%%%%%%%%%%%%%%%%%%%%%%%%%%%%%%%%%%%%%%
%%The following code reads a scanned image of a circle and creates the
%%  boundaries around the circle
I=imread('circle.png'); %reads the *.png image of the circle
I=~I; %set background values = 0, line values = 1;
BW = im2bw(I); %converts image to black and white
imshow(BW)
dim=size(BW);
[r1,c1]=find(I==1);
row_p=r1(1); col_p=c1(1); %indices of the circle boundary
boundary_crcl = bwtraceboundary(BW,[row_p, col_p],'N'); %circle boundary

imshow(I)
hold on;
%%Plot the boundary of the circle:
plot(boundary_crcl(:,2),boundary_crcl(:,1),'g','LineWidth',3);

%%Finding four coordinates on the circle:
start_crcl_horiz=min(boundary_crcl(:,2)); %value of left-most circle position
end_crcl_horiz=max(boundary_crcl(:,2)); %value of right-most circle position
min_crcl_vert=min(boundary_crcl(:,1)); %bottom-most circle position
max_crcl_vert=max(boundary_crcl(:,1)); %top-most circle position

%%Starting and ending points for the grid:
pix_per_vel=25; %number of pixels per finite element
x_start=start_crcl_horiz;
x_end=end_crcl_horiz;
y_start=min_crcl_vert;
y_end=max_crcl_vert;
x_vals=x_start:pix_per_vel:x_end;
y_vals=y_start:pix_per_vel:y_end;
figure
plot(boundary_crcl(:,2),boundary_crcl(:,1))
hold on
pm=1; mr=0; dr=1;
while pm<=length(x_vals);
   fnd_x_ind=find(boundary_crcl(:,2)==x_vals(pm));
   endind=length(fnd_x_ind)+mr;
   strtind=dr;
   x_ind(strtind:endind)=fnd_x_ind;
   y_val_ind(strtind:endind)=boundary_crcl(x_ind(strtind:endind),1);
   x_val_ind(strtind:endind)=boundary_crcl(x_ind(strtind:endind),2);
```

```
   plot(x_val_ind(strtind:endind),y_val_ind(strtind:endind),'r') %plot x-grid lines
   pm=pm+1;
   dr=endind+1;
   mr=endind;
end

fnd_y_226=find(y_val_ind==226);
fnd_x_1=find(x_val_ind==1); fnd_x_451=find(x_val_ind==451);
x_val_ind_new=[x_val_ind(fnd_y_226(1)) x_val_ind((fnd_x_1(end)+1):(fnd_x_451(1)-
1)) x_val_ind(fnd_y_226(end))];
y_val_ind_new=[y_val_ind(fnd_y_226(1)) y_val_ind((fnd_x_1(end)+1):(fnd_x_451(1)-
1)) y_val_ind(fnd_y_226(end))];

pr=1; mp=0; dp=1;
while pr<=length(y_vals);
   fnd_y_ind=find(boundary_crcl(:,1)==y_vals(pr));
   endind_y=length(fnd_y_ind)+mp;
   strtind_y=dp;
   y_ind(strtind_y:endind_y)=fnd_y_ind;
   x_val_ind_y(strtind_y:endind_y)=boundary_crcl(y_ind(strtind_y:endind_y),2);
   y_val_ind_y(strtind_y:endind_y)=boundary_crcl(y_ind(strtind_y:endind_y),1);
   plot(x_val_ind_y(strtind_y:endind_y),y_val_ind_y(strtind_y:endind_y),'g');
   pr=pr+1;
   dp=endind_y+1;
   mp=endind_y;
end

fnd_x_226=find(x_val_ind_y==226);
fnd_y_1=find(y_val_ind_y==1); fnd_y_451=find(y_val_ind_y==451);
x_val_ind_y_new=[x_val_ind_y(fnd_x_226(1))
x_val_ind_y((fnd_y_1(end)+1):(fnd_y_451(1)-1)) x_val_ind_y(fnd_x_226(end))];
y_val_ind_y_new=[y_val_ind_y(fnd_x_226(1))
y_val_ind_y((fnd_y_1(end)+1):(fnd_y_451(1)-1)) y_val_ind_y(fnd_x_226(end))];

coord_val_ind_new=[x_val_ind_new' y_val_ind_new'];
coord_val_ind_y_new=[x_val_ind_y_new' y_val_ind_y_new'];
coord_circum=union(coord_val_ind_new,coord_val_ind_y_new,'rows');
coord_circum=sortrows(coord_circum,1);
assort_vals=union(coord_circum(:,1),coord_circum(:,2));

kp=1;
while kp<=length(assort_vals);
   fnd_crd_val=[];
   fnd_crd_val=find(coord_circum(:,1)==assort_vals(kp));
   len_fnd_crd_val=length(fnd_crd_val);
   if len_fnd_crd_val>2;
```

```
      coord_circum=[coord_circum(1:fnd_crd_val-1,:)
        coord_circum(fnd_crd_val(1),:)
        coord_circum(fnd_crd_val(end),:)
        coord_circum(fnd_crd_val(end)+1:end,:)];
   else
   end
   kp=kp+1;
end

coord_circum=sortrows(coord_circum,2);
kp=1;
while kp<=length(assort_vals);
   fnd_crd_val=[];
   fnd_crd_val=find(coord_circum(:,2)==assort_vals(kp));
   len_fnd_crd_val=length(fnd_crd_val);
   if len_fnd_crd_val>2;
      coord_circum=[coord_circum(1:fnd_crd_val-1,:)
        coord_circum(fnd_crd_val(1),:)
        coord_circum(fnd_crd_val(end),:)
        coord_circum(fnd_crd_val(end)+1:end,:)];
   else
   end
   kp=kp+1;
end
coord_circum=sortrows(coord_circum,1);
plot(coord_circum(:,1),coord_circum(:,2),'m.')

mid_x_val_ind=ceil(length(x_vals)/2);
mid_y_val_ind=ceil(length(y_vals)/2);
mid_x_val=x_vals(mid_x_val_ind);
mid_y_val=y_vals(mid_y_val_ind);

sm=1; ts=1;
while sm<=length(y_vals);
   y_val_tmp=y_vals(sm);
   fnd_y_tmp=find(coord_circum(:,1)==y_val_tmp);
   lim_x_tmp=coord_circum(fnd_y_tmp,2);
   fnd_x_tmp=find((x_vals>=lim_x_tmp(1))&(x_vals<=lim_x_tmp(end)));
   x_crd=x_vals(fnd_x_tmp);
   y_crd=ones(1,length(x_crd))*y_val_tmp;
   coord_inner(ts:length(x_crd)+ts-1,:)=[x_crd' y_crd'];
   sm=sm+1;
   ts=ts+length(x_crd);
end

new_coords=[coord_circum
```

```
   coord_inner];

plot(new_coords(:,1),new_coords(:,2),'k.');
new_coords_cm=(new_coords-1)/1000;
elements=delaunay(new_coords_cm(:,1),new_coords_cm(:,2));
close(figure(1))
close(figure(2))
plotgrid2([new_coords_cm(:,1) new_coords_cm(:,2)],elements)
figure
trimesh(elements,new_coords_cm(:,1),new_coords_cm(:,2))
hold

elements_mat=[(1:length(elements))' elements];
new_coords_cm=(new_coords-1)/1000;
```

```
%%%%%%%%%%%%%%%%%%%%%%%%%%%%%%%%%%%%%%%%%%%%%%%%%%%%%%%%%%%%%%%%%%%%%%%%%%%%%%
%%Lung Sound Generation
%%%%%%%%%%%%%%%%%%%%%%%%%%%%%%%%%%%%%%%%%%%%%%%%%%%%%%%%%%%%%%%%%%%%%%%%%%%%%%
%%The following program determines shape functions and stiffness matrix for
%%  triangular elements
n_ord=input('* enter the order of the element, e.g. cubic=3 (max=quintic=5): ');
xi=-1:2/n_ord:1; eta=-1:2/n_ord:1;
%%Order of the Gauss-Legendre integration:
ord_GL_int=n_ord+1;
%%Tabulate the sample and weight values for Gaussian-Legendre integration:
GLsamp=[0; -0.577350; 0.577350; -0.774597; 0; 0.774597; -0.861136; -0.339981;
0.339981; 0.861136; -0.9061798; -0.5384693; 0; 0.5384693; 0.9061798; -0.9324695; -
0.6612094; -0.2386192; 0.2386192; 0.6612094; 0.9324695];
GLweight=[2; 1; 1; 5/9; 8/9; 5/9; 0.347855; 0.652145; 0.652145; 0.347855; 0.236927;
0.478629; 0.568889; 0.478629; 0.236927; 0.171324; 0.360762; 0.467914; 0.467914;
0.360762; 0.171324];
%%(the samples and weights are each in one vector)
%%For first order, use the values in the first row ord_GL_int+0:ord_GL_int*1
%%Second order: rows 2:3  ord_GL_int+0 : ord_GL_int*1+1
%%Third order: rows 4:6   ord_GL_int*2-2 : ord_GL_int*2
%%Fourth order: rows 7:10  ord_GL_int+3: ord_GL_int*2+2
%%Fifth order: rows 11:15  ord_GL_int*2+1: ord_GL_int*3
%%Sixth order: rows 16:21   ord_GL_int+10: ord_GL_int*3+3
%%The maximum order is 6, meaning the maximum element order is quintic, 5th
if (ord_GL_int/2)==round(ord_GL_int/2)
   end_ind_GL=(ord_GL_int*(ord_GL_int/2))+(ord_GL_int/2);
   st_ind_GL=end_ind_GL-(ord_GL_int-1);
elseif ((ord_GL_int/2)~=round(ord_GL_int/2));
   end_ind_GL=(ord_GL_int*((ord_GL_int+1)/2));
   st_ind_GL=end_ind_GL-(ord_GL_int-1);
end
%%For linear triangles only:
N_nodes(1,:)=[xi(1) eta(1)];
N_nodes(2,:)=[xi(2) eta(1)];
N_nodes(3,:)=[xi(2)+xi(1) eta(2)];
N_nodes_ele=N_nodes;
xi=N_nodes(:,1);
%eta=N_nodes(:,2);
NE=length(elements_mat); %# of elements
ND=max(elements_mat(:,end)); %# of nodes
ND_ele=n_ord*3;
D=[1 0
   0 1];
new_coords_cm1(:,1)=new_coords_cm(:,1);
```

```
new_coords_cm1(:,2)=new_coords_cm(:,2);
%%[K] and [C] must be determined, using the direct stiffness procedure
%%Begin by initializing matrices that will contain all element [k] and [c]
%%matrices (respectively), with every ND-th column marking the end of one
%%matrix (the matrices are initialized with zeros):
kx=1;
while kx<=2048;
K_all_new=[]; C_all_new=[]; K_all_ele=[]; C_all_ele=[];
%%Also initialize the K and C matrices:
K_zer=zeros(ND,ND); C_zer=zeros(ND,ND);
p=1; m=1;
K_all_new=zeros(ND,ND); C_all_new=zeros(ND,ND);
while p<=NE;
   pjx=1;
   mm=1;
   while pjx<=length(N_nodes_ele);
      xi_not_ind=[]; eta_not_ind=[]; xi_new=[]; eta_new=[]; xi_point=[]; eta_point=[];
      xi_not_ind=find(xi~=N_nodes_ele(pjx,1));
      eta_not_ind=find(eta~=N_nodes_ele(pjx,2));
      xi_new=xi(xi_not_ind); eta_new=eta(eta_not_ind);
      xi_point=xi(find(xi==N_nodes_ele(pjx,1)));
      eta_point=eta(find(eta==N_nodes_ele(pjx,2)));
      roots_xi=[xi_new]; roots_eta=[eta_new];
      poly_point_xi=poly(roots_xi);
      poly_point_eta=poly(roots_eta);
      point_solv=polyval(poly_point_xi,xi_point)*polyval(poly_point_eta,eta_point);
      coeff(pjx)=1/point_solv;
      mm=1;
      gsy=st_ind_GL;
      while gsy<=end_ind_GL;
         gsx=st_ind_GL;
         while gsx<=end_ind_GL;
            GL_value_y=GLsamp(gsy);
            GL_value_x=GLsamp(gsx);
            GL_wt_y=GLweight(gsy);
            GL_wt_x=GLweight(gsx);

Jacob_x_eval(pjx,mm)=coeff(pjx)*polyval(polyder(poly_point_xi),GL_value_x)*polyval
(poly_point_eta,GL_value_y);

Jacob_y_eval(pjx,mm)=coeff(pjx)*polyval(polyder(poly_point_eta),GL_value_y)*polyv
al(poly_point_xi,GL_value_x);

N_x_eval(pjx,mm)=coeff(pjx)*polyval(poly_point_xi,GL_value_x)*polyval(poly_point_
eta,GL_value_x);
```

```
N_y_eval(pjx,mm)=coeff(pjx)*polyval(poly_point_xi,GL_value_y)*polyval(poly_point_
eta,GL_value_y);
            gsx=gsx+1;
            mm=mm+1;
          end
          gsy=gsy+1;
        end
        if pjx==1;
          poly_point_xi_save=poly_point_xi;
          poly_point_eta_save=poly_point_eta;
        else
        end
        pjx=pjx+1;
    end
    ddr=1;
    gsy=st_ind_GL;
    while gsy<=end_ind_GL;
      gsx=st_ind_GL;
      while gsx<=end_ind_GL;
        GL_value_y=GLsamp(gsy);
        GL_value_x=GLsamp(gsx);
        GL_wt_y=GLweight(gsy);
        GL_wt_x=GLweight(gsx);

%mult(ddr)=coeff(1)*polyval(poly_point_xi_save,GL_value_x)*polyval(poly_point_eta
_save,GL_value_y)*GL_wt_y*GL_wt_x;
        mult(ddr)=GL_wt_y*GL_wt_x;
        ddr=ddr+1;
        gsx=gsx+1;
      end
      gsy=gsy+1;
    end
    XYmat=[new_coords_cm1([elements_mat(p,2:end)],1)
new_coords_cm1([elements_mat(p,2:end)],2)];
    lim=mm-1;
    gm=1;
    ss=1;
    while gm<=lim;
      I_tst=mult(gm)*det([Jacob_x_eval(:,gm)';Jacob_y_eval(:,gm)']*XYmat);
      J_tst=[Jacob_x_eval(:,gm)';Jacob_y_eval(:,gm)']*XYmat;
      B_tst=inv(J_tst)*[Jacob_x_eval(:,gm)';Jacob_y_eval(:,gm)'];
      N_tst=[N_x_eval(:,gm)'; N_y_eval(:,gm)'];
      c_ele(:,ss:gm*ND_ele)=I_tst*N_tst'*N_tst;
      k_ele(:,ss:gm*ND_ele)=I_tst*((B_tst'*D)*B_tst);
      ss=(gm*ND_ele)+1;
```

```
      gm=gm+1;
    end
    pg=1; ms=1;
    k_ele_new=zeros(ND_ele,ND_ele); c_ele_new=zeros(ND_ele,ND_ele);
    lambda=(1/(35300^2));
    while pg<=gm-1;
      if pg==1;
        k_ele_new=k_ele(:,ms:pg*ND_ele);
        c_ele_new=lambda*c_ele(:,ms:pg*ND_ele);
      else
        k_ele_new=k_ele_new+k_ele(:,ms:pg*ND_ele);
        c_ele_new=c_ele_new+lambda*c_ele(:,ms:pg*ND_ele);
      end
      pg=pg+1; ms=ms+ND_ele;
    end
    %Integral=sum(I_tst)
    K_zer([elements_mat(p,2:end)],[elements_mat(p,2:end)])=k_ele_new;
    C_zer([elements_mat(p,2:end)],[elements_mat(p,2:end)])=c_ele_new;
    K_all_new=K_all_new+K_zer;
    C_all_new=C_all_new+C_zer;
    p=p+1;
    m=m+ND;
    K_zer=zeros(ND,ND); C_zer=zeros(ND,ND);
end
X_coords=new_coords_cm1(:,1); Y_coords=new_coords_cm1(:,2);
xm_X=fbm_chol(0.7,321);
xm_Y=fbm_chol(0.7,321);
new_coords_cm1(:,1)=new_coords_cm1(:,1)+xm_X/1000;
new_coords_cm1(:,2)=new_coords_cm1(:,2)+xm_Y/1000;
x2=new_coords_cm1(:,1);
Vfcn_AP_new=polyval(p_AP, x2);
Vfcn_AP_new(1:68)=0; %%BC velocity
y2=new_coords_cm1(:,2);
Vfcn_RL_new=polyval(p_RL,y2);
Vfcn_RL_new(1:68)=0; %%BC velocity
Vfcn_both=sqrt((Vfcn_RL_new.^2)+(Vfcn_AP_new.^2));
theta_vfcn=atan(Vfcn_RL_new./Vfcn_AP_new);
theta_vfcn(1:68)=0;
br_rad=0.225; br_ang=pi/6;
gamma_both=2*pi*Vfcn_both*br_rad*sin(br_ang);
gamma_RL=2*pi*Vfcn_RL_new*br_rad*sin(br_ang);
gamma_AP=2*pi*Vfcn_AP_new*br_rad*sin(br_ang);
pr=1;
theta=[];
while pr<=length(X_coords);
  if X_coords(pr)==0;
```

```
    theta(pr)=0;
  else
    theta(pr)=atan(Y_coords(pr)./X_coords(pr));
  end
  pr=pr+1;
end
theta=theta';
if kx==1;
  theta(1)=0;
  phi_b_both(:,kx)=(1/(2*pi))*gamma_both.*theta;
  phi_a_both(:,kx)=zeros(321,1);%(1/(2*pi))*gamma_both.*theta;
  phi_b_RL(:,kx)=(1/(2*pi))*gamma_RL.*theta;
  phi_a_RL(:,kx)=zeros(321,1);%(1/(2*pi))*gamma_both.*theta;
  phi_b_AP(:,kx)=(1/(2*pi))*gamma_AP.*theta;
  phi_a_AP(:,kx)=zeros(321,1);%(1/(2*pi))*gamma_both.*theta;
else
  phi_a_both(:,kx)=phi_b_both(:,kx-1);
  phi_b_both(:,kx)=phi_c_both(:,kx-1);
  phi_a_RL(:,kx)=phi_b_RL(:,kx-1);
  phi_b_RL(:,kx)=phi_c_RL(:,kx-1);
  phi_a_AP(:,kx)=phi_b_AP(:,kx-1);
  phi_b_AP(:,kx)=phi_c_AP(:,kx-1);
end
%%The time step is (in seconds):
delt_t=0.0001;
H=(C_all_new)+(delt_t^2)*K_all_new;
phi_c_both(:,kx)=(C_all_new*(2*phi_b_both(:,kx)-phi_a_both(:,kx))\H)';
phi_c_RL(:,kx)=(C_all_new*(2*phi_b_RL(:,kx)-phi_a_RL(:,kx))\H)';
phi_c_AP(:,kx)=(C_all_new*(2*phi_b_AP(:,kx)-phi_a_AP(:,kx))\H)';
phi_deriv_2_both(:,kx)=(phi_a_both(:,kx)-
(2*phi_b_both(:,kx))+phi_c_both(:,kx))/(delt_t^2);
phi_deriv_2_RL(:,kx)=(phi_a_RL(:,kx)-(2*phi_b_RL(:,kx))+phi_c_RL(:,kx))/(delt_t^2);
phi_deriv_2_AP(:,kx)=(phi_a_AP(:,kx)-(2*phi_b_AP(:,kx))+phi_c_AP(:,kx))/(delt_t^2);
phi_deriv_1_int1_both(:,kx)=(phi_a_both(:,kx)-phi_c_both(:,kx))/(2*delt_t);
phi_deriv_1_int1_RL(:,kx)=(phi_a_RL(:,kx)-phi_c_RL(:,kx))/(2*delt_t);
phi_deriv_1_int1_AP(:,kx)=(phi_a_AP(:,kx)-phi_c_AP(:,kx))/(2*delt_t);
rho=1.14*0.001; %%this is kg/m^3; convert to g/cm^3 by multiplying by 0.001
pressure_int1_both(:,kx)=-(0.001)*rho*phi_deriv_1_int1_both(:,kx);
pressure_int1_RL(:,kx)=-(0.001)*rho*phi_deriv_1_int1_RL(:,kx);
pressure_int1_AP(:,kx)=-(0.001)*rho*phi_deriv_1_int1_AP(:,kx);
kx=kx+1;
end
```

```
%%%%%%%%%%%%%%%%%%%%%%%%%%%%%%%%%%%%%%%%%%%%%%%%%%%
%%%%%%%%%%%%%%%%%%%%%%%%%%%%%%%%%%%%%%%%%%%%%%%%
%%January Gnitecki, 6721225
%%Lung Sound Transmission and Genetic Algorithm Optimization
%%%%%%%%%%%%%%%%%%%%%%%%%%%%%%%%%%%%%%%%%%%%%%%%%%%
%%%%%%%%%%%%%%%%%%%%%%%%%%%%%%%%%%%%%%%%%%%%%%%%
clear
load pressure_int1_both_crcl_fb10240 -ascii
pmean=mean(pressure_int1_both_crcl_fb10240);
pmean=pmean/1000;
pmean=pmean';
load freq_PSD_ave -ascii
PSD_freq=freq_PSD_ave;
load psd_hlth_2_all -ascii
PSD_h_all_2=psd_hlth_2_all;
load all_RMSnorm_2_hlth_resam -ascii
RMSnorm_h_all_2=all_RMSnorm_2_hlth_resam;
load all_KFD_2_hlth_resam -ascii
KFD_h_all_2=all_KFD_2_hlth_resam;
load all_KFDnorm_2_hlth_resam -ascii
KFDnorm_h_all_2=all_KFDnorm_2_hlth_resam;
ss=4;
%leave one out
PSD_h_leave1_mat=[PSD_h_all_2(:,1:ss-1) PSD_h_all_2(:,ss+1:9)];
RMSnorm_h_leave1_mat=[RMSnorm_h_all_2(:,1:ss-1) RMSnorm_h_all_2(:,ss+1:9)];
KFD_h_leave1_mat=[KFD_h_all_2(:,1:ss-1) KFD_h_all_2(:,ss+1:9)];
KFDnorm_h_leave1_mat=[KFDnorm_h_all_2(:,1:ss-1) KFDnorm_h_all_2(:,ss+1:9)];
PSD_h_leave1_mean=mean(PSD_h_leave1_mat');
PSD_h_leave1_stdv=std(PSD_h_leave1_mat,0,2);
PSD_h_test=PSD_h_all_2(:,ss);
RMSnorm_h_leave1_mean=mean(RMSnorm_h_leave1_mat');
RMSnorm_h_leave1_stdv=std(RMSnorm_h_leave1_mat,0,2);
RMSnorm_h_test=RMSnorm_h_all_2(:,ss);
KFD_h_leave1_mean=mean(((KFD_h_leave1_mat')/10e8)+1);
KFD_h_leave1_stdv=std(((KFD_h_leave1_mat/10e8)+1),0,2);
KFD_h_test=(KFD_h_all_2(:,ss)/10e8)+1;
KFDnorm_h_leave1_mean=mean(((KFDnorm_h_leave1_mat')/10e8)+1);
KFDnorm_h_leave1_stdv=std(((KFDnorm_h_leave1_mat/10e8)+1),0,2);
KFDnorm_h_test=(KFDnorm_h_all_2(:,ss)/10e8)+1;
nind=30; maxgen=10; nvar=3; preci=20; ggap=0.8;
%FieldD for initial values was developed based on preliminary findings
FieldD=[[preci preci preci]
[0.05 10000 1.8]
[0.2 20000 3.2]
[0 0 0]
[0 0 0]
```

```
[1 1 1]
[1 1 1]];
Chrom=crtbp(nind,nvar*preci);
load GAanaly_knew_sv_init_main -ascii
knew_sv=GAanaly_knew_sv_init_main;
load GAanaly_snew_sv_init_main -ascii
snew_sv=GAanaly_snew_sv_init_main;
load GAanaly_tnew_sv_init_main -ascii
tnew_sv=GAanaly_tnew_sv_init_main;
load GAanaly_Pnew_sv_all_init_main -ascii
Pnew_sv_all=GAanaly_Pnew_sv_all_init_main;
load GAanaly_mean_PSDmod_init_main -ascii
mean_PSDmod=GAanaly_mean_PSDmod_init_main;
load GAanaly_mean_PSDmod_dB_init_main -ascii
mean_PSDmod_dB=GAanaly_mean_PSDmod_dB_init_main;
load GAanaly_Dkatz_mod_all_init_main -ascii
Dkatz_mod_all=GAanaly_Dkatz_mod_all_init_main;
load GAanaly_Dkatz_mod_all_resam_init_main -ascii
Dkatz_mod_all_resam=GAanaly_Dkatz_mod_all_resam_init_main;
load GAanaly_RMS_mod_all_init_main -ascii
RMS_mod_all=GAanaly_RMS_mod_all_init_main;
load GAanaly_RMS_mod_all_norm_init_main -ascii
RMS_mod_all_norm=GAanaly_RMS_mod_all_norm_init_main;
load GAanaly_RMS_mod_all_resam_init_main -ascii
RMS_mod_all_resam=GAanaly_RMS_mod_all_resam_init_main
load GAanaly_RMS_mod_all_norm_resam_init_main -ascii
RMS_mod_all_norm_resam=GAanaly_RMS_mod_all_norm_resam_init_main;

np=1;
while np<=30;
  NMSE_KFD_lv1(np)=sum((((Dkatz_mod_all_resam(:,np)/10e8)*10e4)-
((KFD_h_leave1_mean-1)*10e4)').^2)/(27);
  NMSE_PSD_lv1_150(np)=sum((exp(mean_PSDmod_dB(8:16,np)/10)-
exp(PSD_h_leave1_mean(8:16)/10)').^2)/(9);
  NMSE_PSD_lv1_200(np)=sum((exp(mean_PSDmod_dB(8:21,np)/10)-
exp(PSD_h_leave1_mean(8:21)/10)').^2)/(14);
  NMSE_PSD_lv1_450(np)=sum((exp(mean_PSDmod_dB(46:81,np)/10)-
exp(PSD_h_leave1_mean(46:81)/10)').^2)/(36);
  NMSE_KFD_tst(np)=sum((((Dkatz_mod_all_resam(:,np)/10e8)*10e4)-((KFD_h_test-
1))*10e4).^2)/(27);
  NMSE_PSD_tst_150(np)=sum((exp(mean_PSDmod_dB(8:16,np)/10)-
exp((PSD_h_test(8:16))/10)).^2)/(9);
  NMSE_PSD_tst_200(np)=sum((exp(mean_PSDmod_dB(8:21,np)/10)-
exp((PSD_h_test(8:21))/10)).^2)/(14);
  NMSE_PSD_tst_450(np)=sum((exp(mean_PSDmod_dB(46:81,np)/10)-
exp((PSD_h_test(46:81))/10)).^2)/(36);
```

```
  np=np+1;
end
%%%%%%%%%%%%%%%%%%%%%%%%%%%%%%%%%%%%%%%%%%%%
%%%%%%%%%%%%%%%%%%%%%%%%%%%%%%%%%%
%%updating values
%knew_sv(:,1)=knew; snew_sv(:,1)=snew; tnew_sv(:,1)=tnew;
%n=100;
NMSE_KFD_tst_o=NMSE_KFD_tst;
NMSE_KFD_tst_o=NMSE_KFD_tst_o';
NMSE_PSD_tst_200_o=NMSE_PSD_tst_200;
NMSE_PSD_tst_200_o=NMSE_PSD_tst_200_o';
mp=1;
Px=[]; Fx=[];
krt=1;
while krt<=maxgen;
FitnV_KFD=ranking(NMSE_KFD_tst_o);
FitnV_PSD=ranking(NMSE_PSD_tst_200_o);
SelCh_KFD=select('sus',Chrom,FitnV_KFD,ggap);
SelCh_KFD=recombin('xovsp',SelCh_KFD,0.7);
SelCh_PSD=select('sus',Chrom,FitnV_PSD,ggap);
SelCh_PSD=recombin('xovsp',SelCh_PSD,0.7);
SelCh_KFD=mut(SelCh_KFD);
SelCh_PSD=mut(SelCh_PSD);
Vals_new_KFD=bs2rv(SelCh_KFD,FieldD);
Vals_new_PSD=bs2rv(SelCh_PSD,FieldD);
knew=[]; snew=[]; tnew=[];
knew_KFD=[]; snew_KFD=[]; tnew_KFD=[];
knew_PSD=[]; snew_PSD=[]; tnew_PSD=[];
knew_KFD=Vals_new_KFD(:,1); snew_KFD=Vals_new_KFD(:,2);
tnew_KFD=Vals_new_KFD(:,3);
knew_PSD=Vals_new_PSD(:,1); snew_PSD=Vals_new_PSD(:,2);
tnew_PSD=Vals_new_PSD(:,3);
%[NMSE_KFD_tst,
NMSE_KFD_lv1,NMSE_PSD_tst_200,NMSE_PSD_lv1_200]=fnd_mse(knew,snew,tne
w,pmean);
clear N
clear X
clear Rnew
clear Hp
clear Ha
clear R
NMSE_KFD_tst_P=[]; NMSE_KFD_lv1_P=[]; NMSE_PSD_tst_200_P=[];
NMSE_PSD_lv1_200_P=[];
NMSE_PSD_tst_150_P=[]; NMSE_PSD_lv1_150_P=[];
Ep=6.5625e8; %Young's modulus for parenchyma, dyne/cm^2
Ea=142.05426e4; %Young's modulus for air, dyne/cm^2
```

```
Dp=1.050; %Density of parenchyma, g/cm^3
Da=0.00114; %Density of air, g/cm^3
num_ens=5;
st=1;
while st<=length(knew_PSD);
  bb=1;
  while bb<=num_ens;
    R=gprnd(knew_PSD(st),(1:10:2000)/snew_PSD(st),tnew_PSD(st));
    [N(:,bb),X(:,bb)]=hist(R);
    save_R(:,bb)=R';
    max_R=max(R);
    Rnew=R/max_R;
    Hp=abs((Rnew)');
    g=find(Hp>=1);
    Hp(g)=0.95;
    Ha=abs(1-Hp);
    d=find(Ha>=1);
    if ~isempty(d);
      Ha(d)=0.95;
    else
    end
    m=Dp*Hp+Da*Ha;
    K=((Hp./Ep)+(Ha./Ea)).^(-1);
    w=sqrt(K./m);
    beta=2*w;
    t=(((1/10240)/10):((1/10240)/10):10/100);
    s=2; n=2;
    sigtmp=[];
    while (s-1)<=169;
      sigma=[];
      sigtmp1=[]; sigtmp2=[];
      sigtmp1=(((2^(n-s-1))*factorial(n))/factorial(s-1));
      sigtmp2=((besselj((n+s-1),beta(s-1)*t))./(beta(s-1)*t).^(n-s-1));
      sigtmp(s-1,:)=sigtmp1.*sigtmp2;
      sigma=1-sum(sigtmp,1);
      sigma=sigma';
      if (s-1)==1;
        pnew(:,s-1)=0.8*pmean-sigma./K(2);
      else
        pnew(:,s-1)=pnew(:,s-2)-sigma./K(2);
      end
      s=s+1;
      n=n+1;
    end
    Pnew_sv169(:,bb)=pnew(:,169);
    bb=bb+1;
```

```
   end
   Pnew_sv_all(:,((st-1)*num_ens)+1:num_ens*st)=Pnew_sv169;
   st=st+1;
end
Dkatz_mod=[]; P_mod_RMS=[]; P_mod_tmp_all=[]; Dkatz_mod_all=[];
Dkatz_mod_all_resam=[];
PSDmod=[]; P_mod_tmp=[]; PSDmod_dB=[]; mean_PSDmod=[];
mean_PSDmod_dB=[];
dx=1;
sk=1;
nr=1;
stpt=5121;
limw=5;
numpts=45;
while nr<=st-1;%30;
   P_mod_tmp_all=Pnew_sv_all(:,((nr-1)*num_ens)+1:num_ens*nr);
   PSDmod=[]; P_mod_tmp=[]; PSDmod_dB=[];
   dx=1; sk=1;
   while dx<=num_ens;%num_blk;
      P_mod_tmp=P_mod_tmp_all(:,dx);
      num_winds=limw;
      [PSDmod(:,dx),Fmod(:,dx)]=psd(P_mod_tmp(stpt:end),1024,10240,[],512);
      PSDmod_dB(:,dx)=10*log10(PSDmod(:,dx));
      pr=1;
      while pr<=num_winds+(num_winds-1);
         stind=((pr-1)*512+1)+stpt-1;
         endind=((pr+1)*512)+stpt-1;
         RMS_mod_max(pr,dx)=max(abs(P_mod_tmp(stind:endind)));
         P_mod_RMS(sk)=sqrt(mean(P_mod_tmp(stind:endind).^2));
         mm=1;
         while mm<=1024-1;
            newxvalsk=stind:endind;
            newyvalsk=P_mod_tmp(stind:endind);
            pta=[newxvalsk(1) newyvalsk(1)];
            ptb=[newxvalsk(mm+1) newyvalsk(mm+1)];
            distd(mm)=sqrt((pta(1)-ptb(1)).^2+(pta(2)-ptb(2)).^2);
            ptan=[newxvalsk(mm) newyvalsk(mm)];
            distL(mm)=sqrt((ptan(1)-ptb(1)).^2+(ptan(2)-ptb(2)).^2);
            mm=mm+1;
         end
         d=max(distd);
         L=sum(distL);
         n=1024-1;
         Dkatz_mod(sk)=log10(n)/(log10(n)+log10(d/L));
         sk=sk+1;
         pr=pr+1;
```

```
      end
      dx=dx+1;
    end
    mean_PSDmod(:,nr)=(mean(PSDmod'));
    mean_PSDmod_dB(:,nr)=(mean(PSDmod_dB'));
    Dkatz_mod_all(:,nr)=Dkatz_mod';
    Dkatz_mod_all_resam(:,nr)=resample((Dkatz_mod_all(:,nr)-1)*10e8,27,numpts);
    RMS_mod_all(:,nr)=P_mod_RMS';
    RMS_mod_all_norm(:,nr)=RMS_mod_all(:,nr)/max(P_mod_RMS);
    RMS_mod_all_resam(:,nr)=resample(RMS_mod_all(:,nr),27,numpts);
    RMS_mod_all_norm_resam(:,nr)=resample(RMS_mod_all_norm(:,nr),27,numpts);
    nr=nr+1;
end
np=1;
while np<=nr-1;%30;
    NMSE_KFD_lv1_P(np)=sum((((Dkatz_mod_all_resam(:,np)/10e8)*10e4)-
((KFD_h_leave1_mean-1)*10e4)').^2)/(27);
    NMSE_PSD_lv1_150_P(np)=sum((exp(mean_PSDmod_dB(8:16,np)/10)-
exp(PSD_h_leave1_mean(8:16)/10)').^2)/(9);
    NMSE_PSD_lv1_200_P(np)=sum((exp(mean_PSDmod_dB(8:21,np)/10)-
exp(PSD_h_leave1_mean(8:21)/10)').^2)/(14);
    NMSE_PSD_lv1_450_P(np)=sum((exp(mean_PSDmod_dB(46:81,np)/10)-
exp(PSD_h_leave1_mean(46:81)/10)').^2)/(36);
    NMSE_KFD_tst_P(np)=sum((((Dkatz_mod_all_resam(:,np)/10e8)*10e4)-
((KFD_h_test-1))*10e4).^2)/(27);
    NMSE_PSD_tst_150_P(np)=sum((exp(mean_PSDmod_dB(8:16,np)/10)-
exp((PSD_h_test(8:16))/10)).^2)/(9);
    NMSE_PSD_tst_200_P(np)=sum((exp(mean_PSDmod_dB(8:21,np)/10)-
exp((PSD_h_test(8:21))/10)).^2)/(14);
    NMSE_PSD_tst_450_P(np)=sum((exp(mean_PSDmod_dB(46:81,np)/10)-
exp((PSD_h_test(46:81))/10)).^2)/(36);
    np=np+1;
end
mean_PSDmod_dB_P=mean_PSDmod_dB;
Dkatz_mod_all_resam_P=Dkatz_mod_all_resam;
RMS_mod_all_resam_P=RMS_mod_all_resam;
RMS_mod_all_norm_resam_P=RMS_mod_all_norm_resam;
Pnew_sv_all_P=Pnew_sv_all;
%%%%%%%%%%%%%%%%%%%%%%%%%%%%%%%%%%%%%%%%%%%%%%%%
%%%%%%%%%%%%%%%%%%%%%%%%%%%%%%%%%%%%%%%%%%
NMSE_PSD_tst_200_n=NMSE_PSD_tst_200_P';
%[Chrom
NMSE_KFD_tst_o]=reins(Chrom,SelCh_KFD,1,1,NMSE_KFD_tst_o,NMSE_KFD_tst_
n);
```

```
[Chrom
NMSE_PSD_tst_200_o]=reins(Chrom,SelCh_PSD,1,1,NMSE_PSD_tst_200_o,NMSE_P
SD_tst_200_n);
tnew_sv_nK(:,krt)=tnew_KFD;
knew_sv_nP(:,krt)=knew_PSD; snew_sv_nP(:,krt)=snew_PSD;
tnew_sv_nP(:,krt)=tnew_PSD;
NMSE_KFD_tst_P_sv(:,krt)=NMSE_KFD_tst_P';
NMSE_PSD_tst_200_P_sv(:,krt)=NMSE_PSD_tst_200_P';
NMSE_PSD_tst_150_P_sv(:,krt)=NMSE_PSD_tst_150_P';
NMSE_PSD_tst_450_P_sv(:,krt)=NMSE_PSD_tst_450_P';
NMSE_KFD_lv1_P_sv(:,krt)=NMSE_KFD_lv1_P';
NMSE_PSD_lv1_200_P_sv(:,krt)=NMSE_PSD_lv1_200_P';
NMSE_PSD_lv1_150_P_sv(:,krt)=NMSE_PSD_lv1_150_P';
NMSE_PSD_lv1_450_P_sv(:,krt)=NMSE_PSD_lv1_450_P';
krt=krt+1
end

save GAanaly_forES_knew_sv_nP_n knew_sv_nP -ascii -double
save GAanaly_forES_snew_sv_nP_n snew_sv_nP -ascii -double
save GAanaly_forES_tnew_sv_nP_n tnew_sv_nP -ascii -double
save GAanaly_forES_NMSE_KFD_lv1_P_n NMSE_KFD_lv1_P_sv -ascii -double
save GAanaly_forES_NMSE_KFD_tst_P_n NMSE_KFD_tst_P_sv -ascii -double
save GAanaly_forES_NMSE_PSD_lv1_150_P_n NMSE_PSD_lv1_150_P_sv -ascii -
double
save GAanaly_forES_NMSE_PSD_tst_150_P_n NMSE_PSD_tst_150_P_sv -ascii -
double
save GAanaly_forES_NMSE_PSD_lv1_200_P_n NMSE_PSD_lv1_200_P_sv -ascii -
double
save GAanaly_forES_NMSE_PSD_tst_200_P_n NMSE_PSD_tst_200_P_sv -ascii -
double
save GAanaly_forES_NMSE_PSD_lv1_450_P_n NMSE_PSD_lv1_450_P_sv -ascii -
double
save GAanaly_forES_NMSE_PSD_tst_450_P_n NMSE_PSD_tst_450_P_sv -ascii -
double

save GAanaly_forES_mean_PSDmod_dB_P_n mean_PSDmod_dB_P -ascii -double
save GAanaly_forES_Dkatz_mod_all_resam_P_n Dkatz_mod_all_resam_P -ascii -
double
save GAanaly_forES_RMS_mod_all_resam_P_n RMS_mod_all_resam_P -ascii -double
save GAanaly_forES_RMS_mod_all_norm_resam_P_n RMS_mod_all_norm_resam_P -
ascii -double
save GAanaly_forES_Pnew_sv_all_P_n Pnew_sv_all_P -ascii -double
```